Theses and Dissertations

Fall 2012

Hemodynamics and natural history outcome in unruptured intracranial aneurysms

Rohini Retarekar
University of Iowa

Recommended Citation

HEMODYNAMICS AND NATURAL HISTORY OUTCOME IN UNRUPTURED

INTRACRANIAL ANEURYSMS

by

Rohini Retarekar

An Abstract

Of a thesis submitted in partial fulfillment
of the requirements for the Doctor of
Philosophy degree in Biomedical Engineering
in the Graduate College of
The University of Iowa

December 2012

Thesis Supervisor: Professor Madhavan L. Raghavan

ABSTRACT

There is increasing interest in assessing the role of hemodynamics in aneurysm growth and rupture mechanism. Identification of the indicators of rupture risk can prove very valuable in the clinical management of patients. If rupture risk of aneurysms can be estimated, immediate preemptive treatments can be done for the high risk patients whereas others can avoid the risky intervention. Retrospective studies have been performed in the past to filter out indices that differentiate ruptured aneurysms from unruptured aneurysms. However, these differences may not necessarily translate to differences between aneurysms that present unruptured but fork towards growth/rupture and unruptured aneurysms that are invariably stable. In the present study, the hypothesis that hemodynamic indices of unruptured aneurysms when they first presented are predictive of their longitudinal outcome was tested.

A prospective longitudinal cohort study was designed to test this hypothesis. Four clinical centers participated in this study and a total of 198 aneurysms were recruited. These aneurysms were chosen by the physicians to be kept under watchful waiting. Three-dimensional models of aneurysms and their contiguous vasculature generated using the initial scans of patients were used for computational fluid dynamic (CFD) simulations. Both pulsatile and steady flow analyses were performed for each patient. By collating all the prominent hemodynamic indices available in aneurysm literature and developing a few new indices, 25 hemodynamic indices were estimated for each subject. For statistical analysis, it was hypothesized a priori that low wall shear area is different between stable and unstable aneurysms. All other indices were tested in a post-hoc manner.

The longitudinal outcome information of these patients was recorded at the clinical centers and the author was blinded until all analyses were complete. Aneurysms that grew during the follow up period were labeled as "grown" by the radiologists and

otherwise they were called "stable". After the hemodynamic analysis was complete, a non-parametric Mann Whitney U test was performed to determine if any index can statistically differentiate the two groups ("grown" versus "stable"). It was found that none of the indices distinguished the two groups with statistical significance. Comparison of the steady and pulsatile flow analysis suggested that the patient population is stratified in the same order by an index, irrespective of whether the index is computed using a steady or pulsatile flow simulation. Pearson correlation coefficient was obtained between basic geometric indices and hemodynamic indices of this population. No strong correlation was found in between morphology and hemodynamics, suggesting uniqueness of the hemodynamic indices.

This study is the first to analyze intracranial aneurysm hemodynamics of a large longitudinal cohort in a blinded prospective manner. Results of this study are not consistent with the hypothesis that aneurysm blood flow based indices can be used as prognostic indicators of growth.

Abstract Approved: _____

Thesis Supervisor

_____

Title and Department

_____

Date

HEMODYNAMICS AND NATURAL HISTORY OUTCOME IN UNRUPTURED

INTRACRANIAL ANEURYSMS

by

Rohini Retarekar

A thesis submitted in partial fulfillment
of the requirements for the Doctor of
Philosophy degree in Biomedical Engineering
in the Graduate College of
The University of Iowa

December 2012

Thesis Supervisor: Professor Madhavan L. Raghavan

Graduate College
The University of Iowa
Iowa City, Iowa

CERTIFICATE OF APPROVAL

_____

PH.D. THESIS

_____

This is to certify that the Ph.D. thesis of

Rohini Retarekar

has been approved by the Examining Committee
for the thesis requirement for the Doctor of Philosophy
degree in Biomedical Engineering at the December 2012 graduation.

Thesis Committee: _____
Madhavan L. Raghavan, Thesis Supervisor

_____
Krishnan B. Chandran

_____
David Hasan

_____
Sarah Vigmostad

_____
Ching-Long Lin

To My Family

ACKNOWLEDGMENTS

I would first like to express my deepest gratitude to Prof. Raghavan for his thought-provoking guidance, supervision and encouragement in all aspects of this dissertation. As an adviser, he has been a role-model and I can only hope to someday achieve a fraction of his intellectual eloquence.

I would like to thank all my committee members for serving on my dissertation committee. I am grateful to Prof. Chandran for clarifying numerous fundamental blood flow mechanics problems. I am appreciative of Prof. Vigmostad and Prof. Lin for providing valuable suggestions related to computational fluid dynamic simulations. Dr. Hasan provided a clinical perspective on several issues that benefitted this project immensely.

I owe my sincerest thanks to Ben Berkowitz, Ben Dickerhoff, Manasi Ramachandran, Steve Lin, Tatiana Correa and Kevin Johnson for their assistance in different parts of this work. It would have been impossible to undertake this project without their help and hard work.

I am thankful to Dr. Harbaugh, Dr. Rosenwasser and Dr. Ogilvy for sharing the patient data. I would like to thank the NIH for funding this project, Teragrid and University of Iowa for providing the computational resources necessary for this work.

I would like to specially thank Anil for his encouragement and support in all phases of this work. Not only did he gladly discuss my technical concerns, but also motivated me at every step. And last but definitely not the least; I am indebted to my parents and sister for giving me the opportunities that allowed me to pursue my ambitions and for making me believe that no dream is ever too big.

ABSTRACT

There is increasing interest in assessing the role of hemodynamics in aneurysm growth and rupture mechanism. Identification of the indicators of rupture risk can prove very valuable in the clinical management of patients. If rupture risk of aneurysms can be estimated, immediate preemptive treatments can be done for the high risk patients whereas others can avoid the risky intervention. Retrospective studies have been performed in the past to filter out indices that differentiate ruptured aneurysms from unruptured aneurysms. However, these differences may not necessarily translate to differences between aneurysms that present unruptured but fork towards growth/rupture and unruptured aneurysms that are invariably stable. In the present study, the hypothesis that hemodynamic indices of unruptured aneurysms when they first presented are predictive of their longitudinal outcome was tested.

A prospective longitudinal cohort study was designed to test this hypothesis. Four clinical centers participated in this study and a total of 198 aneurysms were recruited. These aneurysms were chosen by the physicians to be kept under watchful waiting. Three-dimensional models of aneurysms and their contiguous vasculature generated using the initial scans of patients were used for computational fluid dynamic (CFD) simulations. Both pulsatile and steady flow analyses were performed for each patient. By collating all the prominent hemodynamic indices available in aneurysm literature and developing a few new indices, 25 hemodynamic indices were estimated for each subject. For statistical analysis, it was hypothesized a priori that low wall shear area is different between stable and unstable aneurysms. All other indices were tested in a post-hoc manner.

The longitudinal outcome information of these patients was recorded at the clinical centers and the author was blinded until all analyses were complete. Aneurysms that grew during the follow up period were labeled as "grown" by the radiologists and

iv

otherwise they were called "stable". After the hemodynamic analysis was complete, a non-parametric Mann Whitney U test was performed to determine if any index can statistically differentiate the two groups ("grown" versus "stable"). It was found that none of the indices distinguished the two groups with statistical significance. Comparison of the steady and pulsatile flow analysis suggested that the patient population is stratified in the same order by an index, irrespective of whether the index is computed using a steady or pulsatile flow simulation. Pearson correlation coefficient was obtained between basic geometric indices and hemodynamic indices of this population. No strong correlation was found in between morphology and hemodynamics, suggesting uniqueness of the hemodynamic indices.

This study is the first to analyze intracranial aneurysm hemodynamics of a large longitudinal cohort in a blinded prospective manner. Results of this study are not consistent with the hypothesis that aneurysm blood flow based indices can be used as prognostic indicators of growth.

TABLE OF CONTENTS

LIST OF TABLES

LIST OF FIGURES

ix

x

xi

CHAPTER 1

INTRODUCTION

Background of Intracranial Aneurysms

Intracranial aneurysm is the abnormal dilation of a blood vessel in brain. If left untreated, the artery can keep bulging and eventually rupture causing subarachnoid hemorrhage. Prevalence of intracranial aneurysm in the general population is estimated to vary between 0.2-9.9% [1-3] with incidence in women being 1.6 times higher than in men[4]. Majority of intracranial aneurysms do not generate symptoms[1]. Owing to their asymptomatic behavior, detection of intracranial aneurysms is either incidental or only after hemorrhage [4]. Exceptions occur, when the aneurysm starts pressing on a nearby nerve and causes symptoms such as severe headaches or double vision. Multiple studies have estimated the annual rupture risk for intracranial aneurysms to be between 0.1 and 5% [4, 5].

Cerebral aneurysms commonly occur in the Circle of Willis (COW). It is a network of arteries that form a ring-like structure in the brain (Figure 1). COW acts as the main circulation center of blood in the brain. Paired internal carotid arteries and vertebral arteries are the four inlets to the COW. Each internal carotid artery divides into the anterior and middle cerebral arteries. The left and right anterior cerebral arteries are connected together by the anterior communicating artery. These arteries constitute the anterior circulation of brain. On the posterior side, the right and left vertebral arteries merge together and form a basilar artery. The basilar artery then bifurcates into the left and right posterior cerebral arteries. The anterior and posterior sides of COW are connected by two posterior communicating arteries that run between the internal carotid arteries and the posterior cerebral arteries. Such a layout of arteries provides an efficient collateral capacity to the COW.
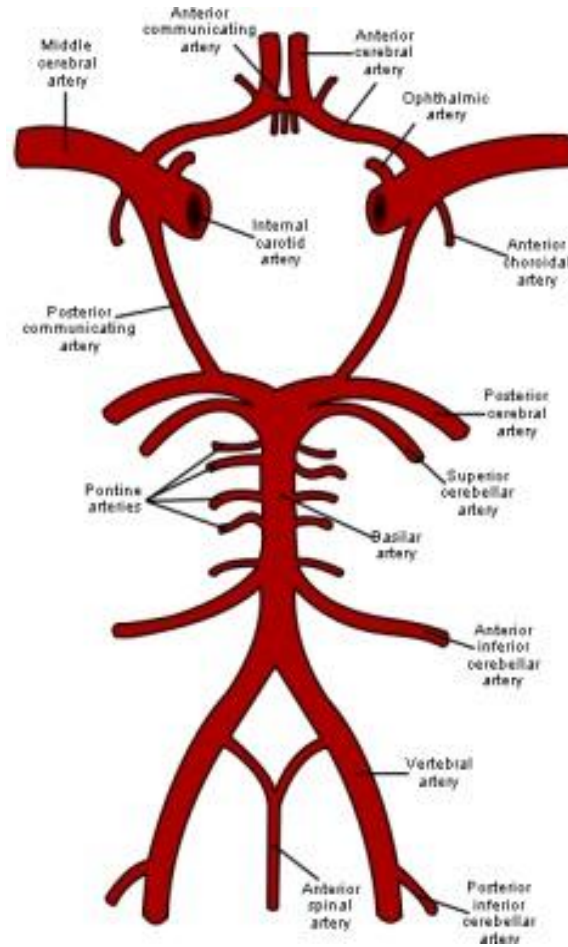
Figure 1: Circle of Willis

Upon diagnosis of an intracranial aneurysm, the two treatment options currently available are: 1. Surgical clipping and 2. Embolization coiling (Figure 2). In the first method, a craniotomy is performed to access the aneurysm by surgically removing a flap of bone from the skull. A clip is then placed at the neck of aneurysm to block any supply of blood into the sac. The second treatment method is a minimally invasive treatment in which the aneurysm is accessed by making a small incision in the femoral artery and then navigating a catheter through the vasculature. Tiny platinum coils are then deployed into

the aneurysm. The goal of this treatment is to pack the aneurysm with coils and thrombus and hence prevent the flow of blood into it.
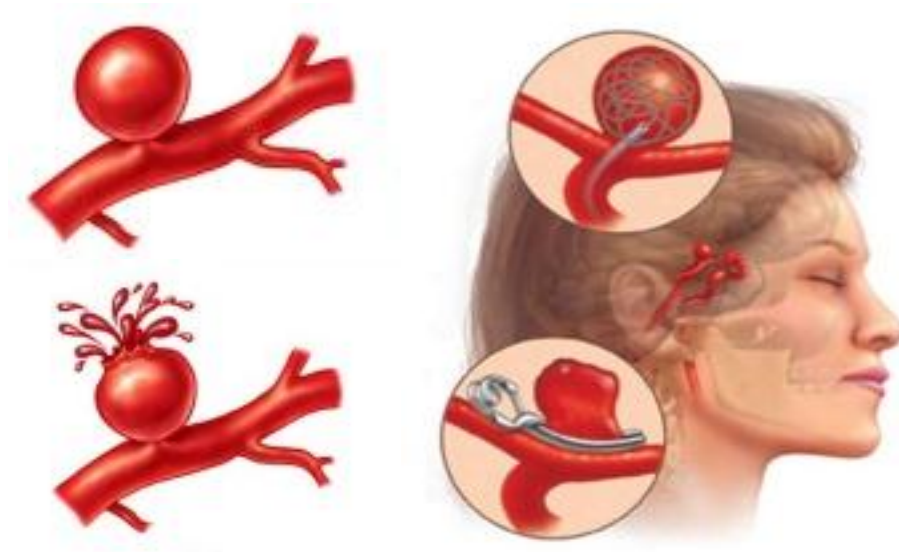
Figure 2: Cerebral aneurysm and the two treatment options

Although the event of an aneurysm rupture is catastrophic and preemptive treatment is the best strategy to reduce mortality rate, the current treatment options carry risks of their own. Mortality and morbidity rates associated with surgical treatment of aneurysms are reported as 2.6% and 10.9% respectively[6]. Investigators of the 'International Study of Unruptured Intracranial Aneurysms (ISUIA)' reported an overall morbidity and mortality rate of 12.6% for open surgical repair and 9.8% for endovascular repair[5]. Since most cerebral aneurysms do not rupture in the lifetime of patients[2, 3], for such patients, the mortality or morbidity risk imposed by clinical intervention exceeds the natural rupture risk of aneurysm. In such a scenario, the ability to accurately predict the rupture risk of an aneurysm can help in preventing the delivery of iatrogenic insults to

patients with stable harmless aneurysms. Such a rupture risk predictor can also help identify growth or rupture prone aneurysms for their immediate preemptive treatment.

<u>Morphology and Wall Tension in Intracranial Aneurysms</u>

Correlation of aneurysm size to its rupture risk has been reported in several studies. The large multicenter study by ISUIA suggested that aneurysms less than 10 mm in diameter have an exceedingly low risk of rupture [3]. In the second phase of their study, the 5 year cumulative rupture rates were reported as 0-2.5% for aneurysms less than 7 mm diameter, 2.6-14.5% for 7-12 mm, 14.5-18.4% for 12-24 mm and 40-50% for aneurysms greater than 25mm [5]. However, rupture incidence of small sized aneurysms (< 7 mm) have been clinically observed and reported [7, 8]. Although the size of aneurysm is deemed important in the clinical decision making process, it is recognized that size is not an independent predictor of rupture risk [1, 4].

Shape of the lesion has also been studied as an indicator of rupture risk. Majority of cerebral aneurysms are saccular in shape [4]. They appear as an out pouching on the arterial wall. It is believed that certain shape characteristics such as presence of multiple lobes on the surface predispose the aneurysm to a higher risk of rupture [4]. Several 2D indices (aspect ratio, size ratio) have been proposed to quantify the shape the aneurysm [9, 10]. However, their effectiveness in predicting rupture is debated [11-15]. Advancement in imaging modalities and image processing techniques has made the 3D quantification of aneurysm shape possible. Our research group proposed several novel shape characteristics [16] and assessed their predictive capabilities within a study population of ruptured and unruptured aneurysms [12]. Non sphericity index, undulation index and ellipticity index were proposed as best predictors of rupture status. However, a prospective study performed with a larger patient population suggested that these metrics do not serve as prognostic indicators of the longitudinal outcome [17].

It is also speculated that the event of rupture occurs when the pressure-induced tension in the aneurysm sac wall exceeds its maximum strength. In-vitro experimental studies have been performed to analyze the behavior of stress-strain curve for aneurysm wall tissue [18, 19]. Several research groups have performed finite element analysis wherein material properties of aneurysm wall are defined using constitutive models of varying degree of sophistication [20, 21]. While Hademenos et al.[20] used a linear elastic model to perform stress analysis on spherical shaped lesions, a nonlinear isotropic model was used to determine stress distribution in a population of idealized axisymmetric aneurysms by Kyriacou et al.[21]. Ma et al.[22] developed a methodology for nonlinear, anisotropic static deformation analysis of patient specific aneurysm population. In their study with 27 aneurysms, ratios between stress components in the stiff and weak fiber directions were significantly higher in the ruptured group than the unruptured group. However, the mean and maximum values of stress and strain were not significantly different in the two groups. Ramachandran et al.[17] studied the role of modeling choices (such as material modeling, geometric modeling, truncation effects and solution schemes) on the stratification of aneurysms. It was found that as long as the boundary conditions and forces remain consistent across the population, modeling choices implemented in the stress analysis do not play a substantial role. In a stress analysis of 198 aneurysms, Ramachandran et al.[17] found no statistically significant difference in the peak wall stress in stable aneurysms versus unstable aneurysms.

<p style="text-align:center">Hemodynamics of Intracranial Aneurysms</p>

It is widely believed that the initiation of an aneurysm is driven by the interplay of multiple factors such as genetic, hemodynamic, structural and metabolic. Experimental and clinical studies have confirmed the presence of intricate hemodynamics at apexes of bifurcations which are common locations of aneurysm formation. Meng et al. [23] surgically created branch points in the common carotid vessels of 6 canine models to

analyze the phenomenon of aneurysm initiation. Two distinct patterns of vascular remodeling were observed: 1.) Formation of intimal padding as a result of hyperplasia 2.) Destructive remodeling in the form of a shallow groove found in the acceleration region. The groove resembled an early stage aneurysm formation. The study speculated that high spatial gradients of WSS can cause this destructive remodeling of vasculature. WSS is the frictional force exerted by the flow of viscous blood against the luminal vessel wall. The endothelial cell lining at the vessel is capable of sensing this shear stress and it has been observed that an abnormal increase in WSS can lead to alterations in endothelial phenotype or even endothelial damage [24, 25].

However, role of hemodynamics in the rupture mechanism of an aneurysm is still unclear. Currently, two contradictory hypotheses are proposed to explain the phenomenon of aneurysm rupture: high flow theory and low flow theory[24]. The high flow theory attributes the enlargement or rupture of an aneurysm to the presence of an elevated WSS. According to this theory, destruction of endothelium due to intensification of WSS causes overexpression of Nitric oxide and hence a non-physiological arterial tone. As the equilibrium between blood pressure and internal wall stress forces is disturbed, wall remodeling is initiated which paves the way for further degeneration [24]. On the other hand, the low flow theory focuses on the reduction in WSS inside the aneurysm sac due to flow stagnation. Presence of an abnormally low WSS is proposed as the underlying mechanism responsible for degeneration of wall via the apoptotic cell cycle [26, 27]. Influence of other hemodynamic factors such as impingement zone, vortex formation, energy transmission etc. on the growth and rupture of an aneurysm is poorly understood and needs further analysis.

Patient specific computational modeling has enabled a qualitative [28-30] as well as quantitative [15, 27, 31-33] description of the nature of blood flow pattern inside an aneurysm. Cebral et al.[28, 31] analyzed the hemodynamics in a large population of intracranial aneurysms and found that ruptured aneurysms in their population possessed

unstable flow patterns, concentrated inflow streams, lower viscous dissipation ratios, larger shear concentration and elevated maximum wall shear stress. Their results back the theories that attribute aneurysm rupture to high flow effects. There is another pool of studies that seem to tell a different story [15, 27, 32]. Results of these studies indicate that ruptured aneurysms have lower mean WSS and large portions of these aneurysms are covered under abnormally low WSS.

Determination of correlation between local aneurysm growth and areas of low WSS was sought by Jou et al. [34] and Boussel et al. [35]. Jou et al. studied 2 similar sized, untreated fusiform basilar aneurysms longitudinally and observed that while one of them grew significantly in the 2 year period, the other remained unchanged. In their study, the maximum growth in the growing aneurysm coincided with the region where WSS was less than $0.1 \ N/m^2$. Boussel et al. analyzed the hemodynamics in 7 untreated intracranial aneurysms and estimated the relationship between the mean local displacement and inverse of time-averaged WSS. They observed a trend of increasing growth at surface patches that experience low WSS throughout the cardiac cycle. Although these two studies underscore the importance of hemodynamics in aneurysm growth, their sample sizes do not warrant confidence.

Clearly, no effort has been made in testing whether the hemodynamics of an unruptured aneurysm when it is first clinically diagnosed is indicative of its longitudinal growth risk on a large patient population.

Motivation and Overview

The hypothesis motivating the current work is that hemodynamics based indices can be used as prognostic indicators of rupture risk in cerebral aneurysms. Indicators of rupture risk can be of significant help in the clinical management of patients. Physicians can benefit from these determinants and provide emergent medical care to patients with aneurysms at high rupture risk, while refrain other patients from the risky intervention.

Given the significant role of hemodynamics in the initiation of aneurysms, it is logical to believe that hemodynamic indices can be used as prognostic indicators of rupture risk in intracranial aneurysms. Moreover, the nature of blood flow inside an aneurysm is influenced by its size, shape and location. Therefore, hemodynamic quantification of an aneurysm can provide biophysical indices that integrate the effect of its size, shape and location. The main objective of this dissertation was to determine whether hemodynamic indices of intracranial aneurysms can be used to predict their longitudinal growth or rupture risk. The hypothesis was tested on a cohort of 198 aneurysms that presented unruptured and were placed for follow up under the watchful waiting strategy. The watchful waiting strategy is an approach in which patients are followed up at regular intervals instead of an immediate intervention.

Several studies have analyzed the hemodynamics in cerebral aneurysms with the main objective of determining blood flow parameters that can discriminate between ruptured and unruptured aneurysms [15, 27, 28, 31, 32]. However, these parameters may not necessarily differentiate between unruptured aneurysms that fork towards growth or rupture and those that remain stable. Also, these studies stand on the premise that shape of the aneurysm does not change after the incidence of rupture, which may or may not be true. Few studies have tested the correlation between hemodynamics and aneurysm growth longitudinally, but, on small patient populations [34, 35]. The current study is the first to test the predictive capabilities of hemodynamic indices in differentiating longitudinal outcome (stable versus growth/rupture) on a large population in a prospective manner. This study is also unique in the sense that it is the first to analyze hemodynamics in small aneurysms. Previous studies that have analyzed hemodynamics in patient populations were primarily composed of large aneurysms. However, the real dilemma that doctors face is for clinical management of aneurysms that are smaller than 7 mm. The present study consists of predominantly small aneurysms (< 7 mm). Unlike most of the previous studies, the patient population in this study was recruited at multiple

centers to eliminate selection bias. Also, the image data collected from these centers were from multiple modalities to render realism to the data collection procedure.

The second objective of this study was to assess the role of modeling choices that are employed in a CFD simulation of blood flow. Using CFD techniques to simulate the transient nature of blood flow is an efficient way of recreating the in-vivo hemodynamic environment. Although physiologically accurate, this incorporation is computationally expensive and demands additional measurements such as the temporal variation in boundary conditions. Hence, if the objective is to stratify a large population of aneurysms according to their hemodynamic behavior, it is reasonable to speculate that a simpler and faster modeling choice of steady flow can prove beneficial. Therefore, in this study, the interpretation of the relative hemodynamic differences in a population of aneurysms obtained from pulsatile flow analysis is compared to that obtained from steady flow analysis. The comparison was first made on an idealized population of aneurysms as a preliminary study and then for the entire patient population.

Several indices have been proposed by research groups to capture the behavior of blood flow inside an aneurysm. However, no effort has been made to perform an exhaustive analysis with all the prominent hemodynamic indices. Therefore, the third objective was to collate and compile the hemodynamic indices that have been reported in the literature so far. Also, a correlation among the hemodynamic and morphologic indices (calculated by Ramachandran et al. [17]) of the patient population was sought to determine the uniqueness of information that these indices provide. Determining whether the flow based indices capture unique hemodynamic characteristics or are many of them redundant has practical implications to prospective studies designed to test the hemodynamics-rupture correlation. Lesser the number of indices, lesser will be the required sample sizes for sufficient statistical power. Alternatively, greater the number of indices, greater the likelihood that such studies will descend into an exercise in data

mining. Further, understanding how these indices relate among themselves can help us better reconcile findings from independent studies.

CHAPTER 2

PRELIMINARY STUDIES

<u>Role of Modeling Choices in CFD Simulation of Blood</u>

<u>Flow</u>

There is increasing interest in assessing what role, if any, that hemodynamics in aneurysm may play in their natural history. It has been proposed that certain characteristics of blood flow in unruptured IAs may provide clues to their eventual outcome – whether they remain stable, grow and/or rupture. While visualizations of simulations may help us understand and gain insights into the nature of flow, to be of practical value (say, as a predictive factor of outcome), such simulations need to be quantified with scalar indices. Ultimately, the main use for such indices is for testing their prognostic value in human subject population. In the literature, most of these indices were computed based on pulsatile flow simulations in patient-specific aneurysms reconstructed from noninvasive volumetric imaging data. Although the simulations of transient blood flow seemingly provide in-depth information of intra-aneurysmal hemodynamics, the simulations are often computationally expensive and demand additional measurements such as the temporal variations in boundary conditions – an area where studies involving large populations inevitably make uniform population-wide assumptions. Moreover, in a large population study, the only patient specific information readily available is the morphology of aneurysm. Consequently, differences in hemodynamics indices within study populations have to merely be reflective of differences in morphological differences such as the angulation of the sac with respect to parent flow, the bottleneck effect at the neck of the sac, etc. Therefore, it is conceivable that if the primary objective is to stratify a population of aneurysms according to their hemodynamic behavior, a simpler and faster method of steady flow simulation can turn out to be as effective as transient flow simulation. Manageable computational cost will

permit ever larger study populations to be accommodated into studies and consequently, greater statistical power in the testing of hypotheses. Of course, a steady flow simulation will not provide temporal information as pulsatile simulations and a comparison of the results will leave the former short. But do the loss of this additional information when employing steady flow simulation have any practical impact – say, in stratifying subjects any differently than that when pulsatile simulations are employed? The objective of this study was to compare steady versus pulsatile flow simulations for a controlled hypothetical population of aneurysms with realistic variation in sac morphology and contiguous vasculature. A manuscript on this study is in review (Retarekar et al., Pulsatile and steady flow modeling for stratification of a population of intracranial aneurysms, ASME, J Biomech. Eng.)

Study Population

Thirty idealized models of cerebral aneurysms and their contiguous vasculature were created in Rhinoceros 3D. Use of additional idealistic models in the study provided a control on the morphological aspect of comparison. The idealized models were created by placing aneurysm sacs in a head and neck arterial network model developed in-house with population averaged dimensions[36] and truncating it to the flow-relevant domains (Figure 3). The entire study population is shown in Figure 4, Figure 5, Figure 6 and Figure 7. Specifically, the 30 sacs were a result of perturbing the following aspects of morphology:

- Location: Internal Carotid Artery (ICA), Anterior Communicating Artery (AComm) and Basilar Artery (Bslar)
- Size Ratio (Diameter of aneurysm/ Diameter of Vessel): 1, 2 and 3
- Shape: Spherical, Prolate Ellipsoid and Oblate Ellipsoid
- Daughter Sac: For spherical ICA aneurysm of size ratio 2, three additional models of daughter sac bearing aneurysms were created. Size of the daughter

sac was chosen to be 40%, 50% and 60% of the aneurysm diameter in the three models.
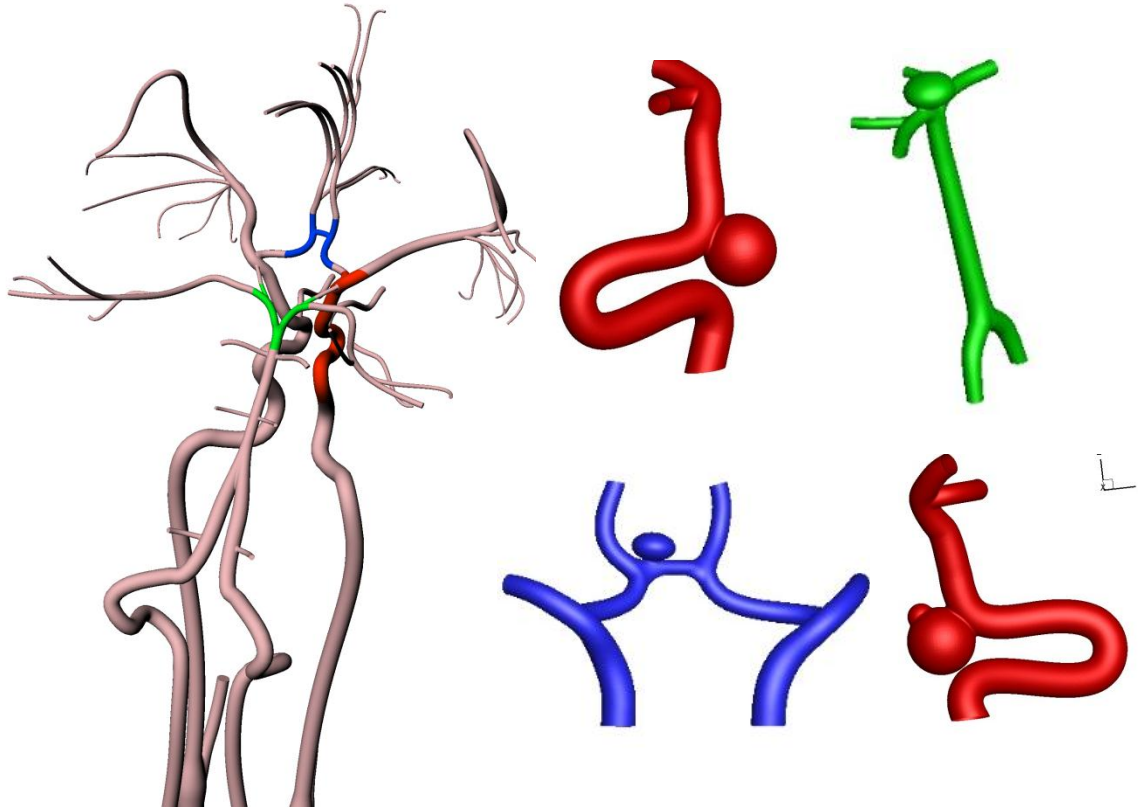
Figure 3: Idealized model of the entire cerebral vasculature (left). Truncated models used for CFD simulations (right)

Meshing

Models were meshed in *Gambit* (Ansys Inc., Lebanon, NH) using triangular surface elements and tetrahedral volume elements. Mesh density for the models varied from 0.97 to 1.48 million tetrahedral elements. Mesh at the aneurysm region was further refined for additional accuracy. Flow simulations were performed in *Fluent* (Ansys Inc., Lebanon, NH). For every model, a transient and a steady flow simulation was performed. Flow waveforms provided by Ford et al.[37] were used to specify the inlet velocity for

the transient analysis (Figure 8).Time averaged values calculated using these waveforms were specified in the steady flow analysis. Outflow boundary condition was specified by using flow rate values published in literature. The outlet boundary condition accounted for the flow carried away by the smaller vessels which were not included in the models [38].   Table 1 provides the flow rate values used in this study for flow division. Blood was assumed to be an incompressible, Newtonian fluid. Rigid wall assumption was made. Effect of gravity was neglected in all the simulations. In the transient cases, solution data from the third cardiac cycle was used for post processing so as to ensure numerical stability. All numerical simulations were performed at the NCSA supercomputing center via the Teragrid project [39].

Table 1: Flow rate values for outflow boundary condition

Artery	Flow Rate
Anterior Cerebral Artery (ACA)	1.4 ml/s
Middle Cerebral Artery (MCA)	2.6 ml/s
Posterior Cerebral Artery (PCA)	1 ml/s
Posterior Communicating Artery (PCOM)	0.1 ml/s
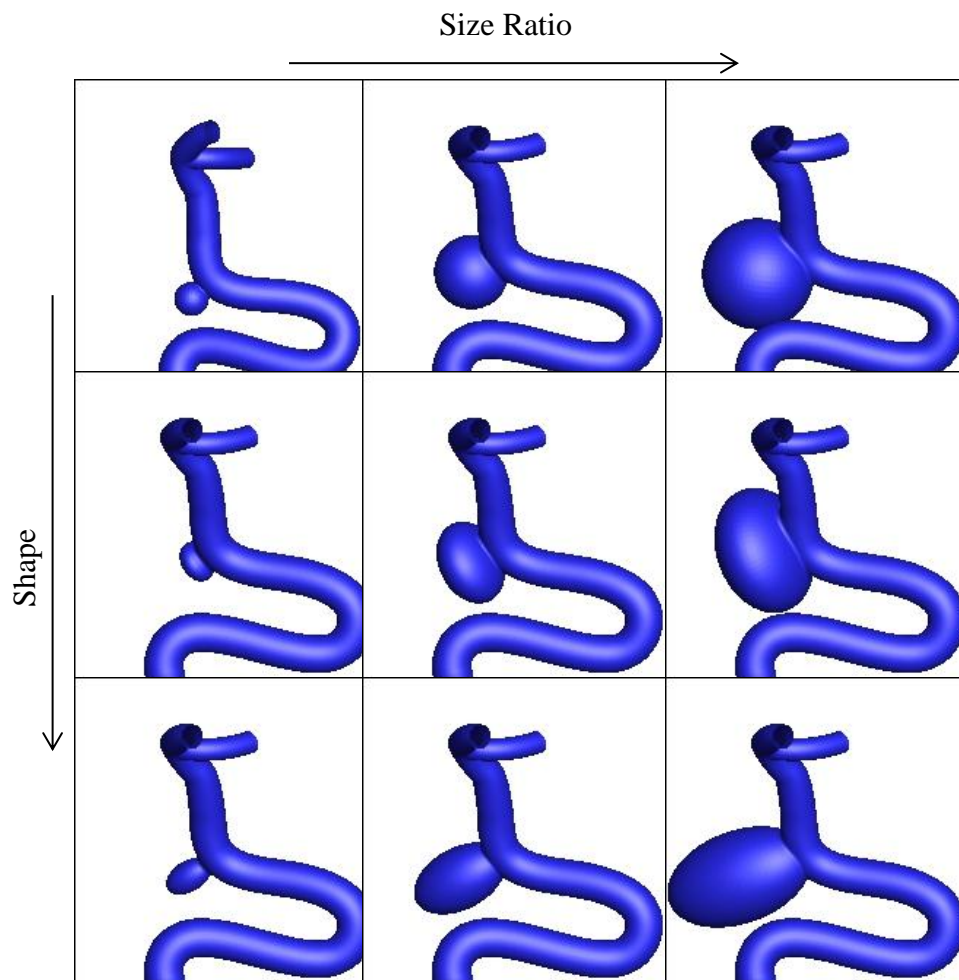
Size Ratio

Shape

Figure 4: ICA models with variation in size ratio and shape
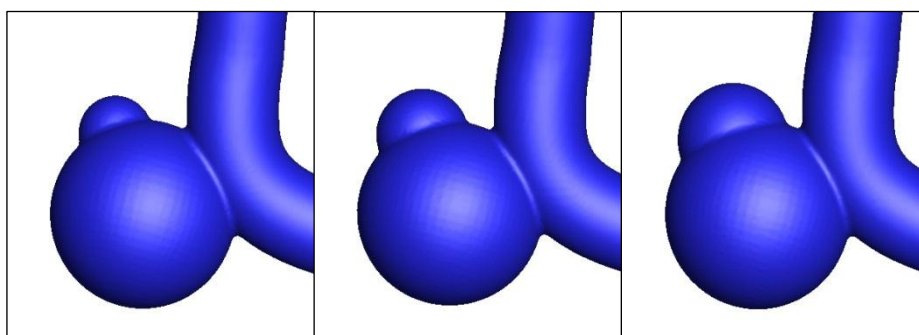
Figure 5: ICA aneurysms harboring daughter sacs
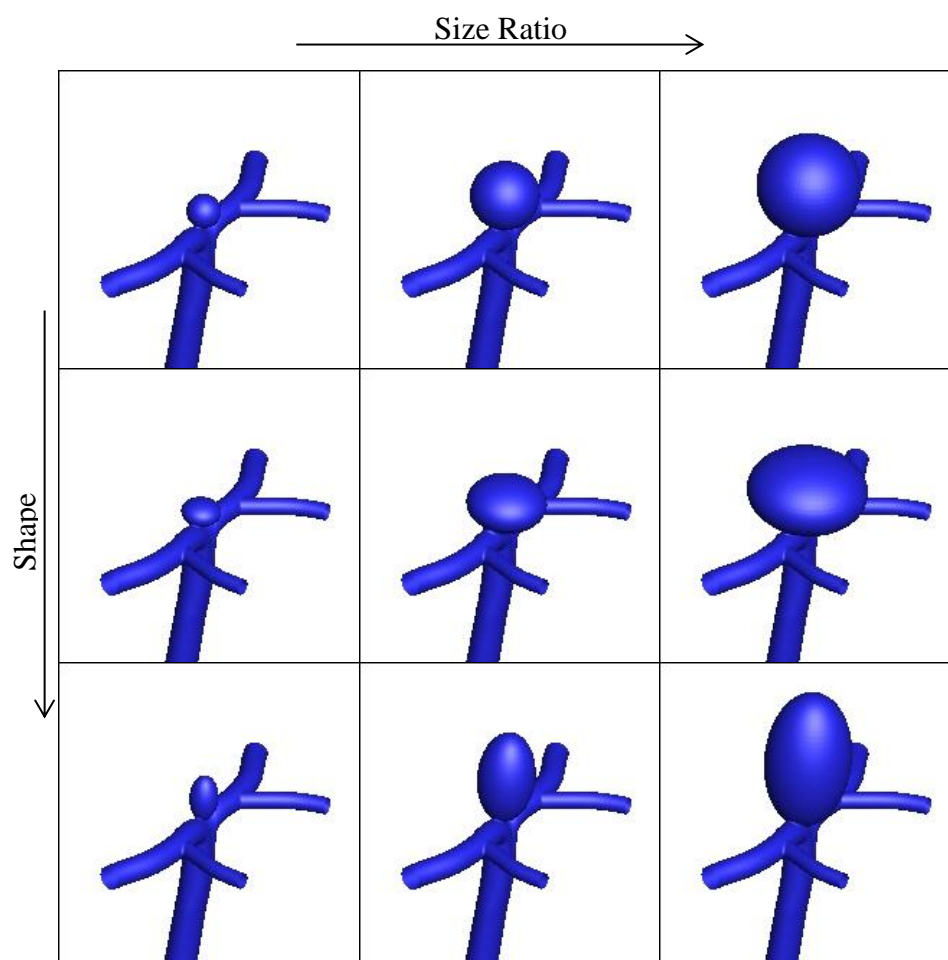
Size Ratio →

Shape →

Figure 6: Bslar models with variation in size ratio and shape
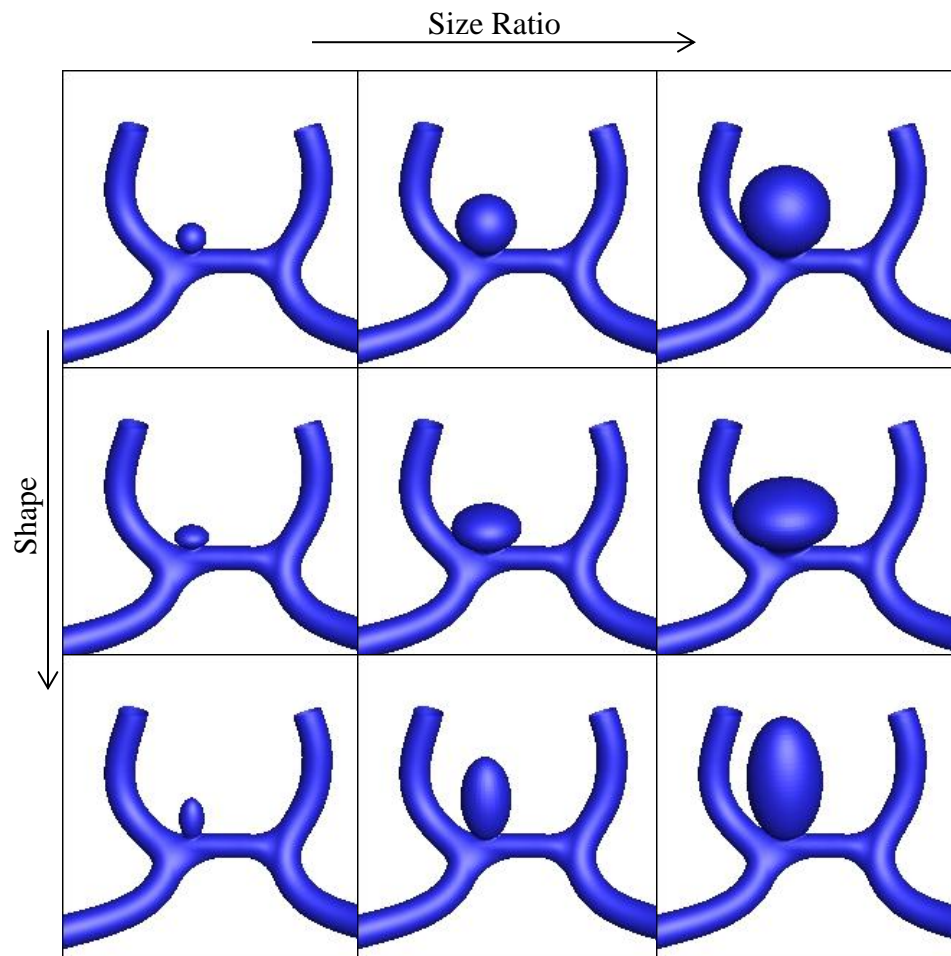
Size Ratio

Shape

Figure 7: AComm models with variation in size ratio and shape
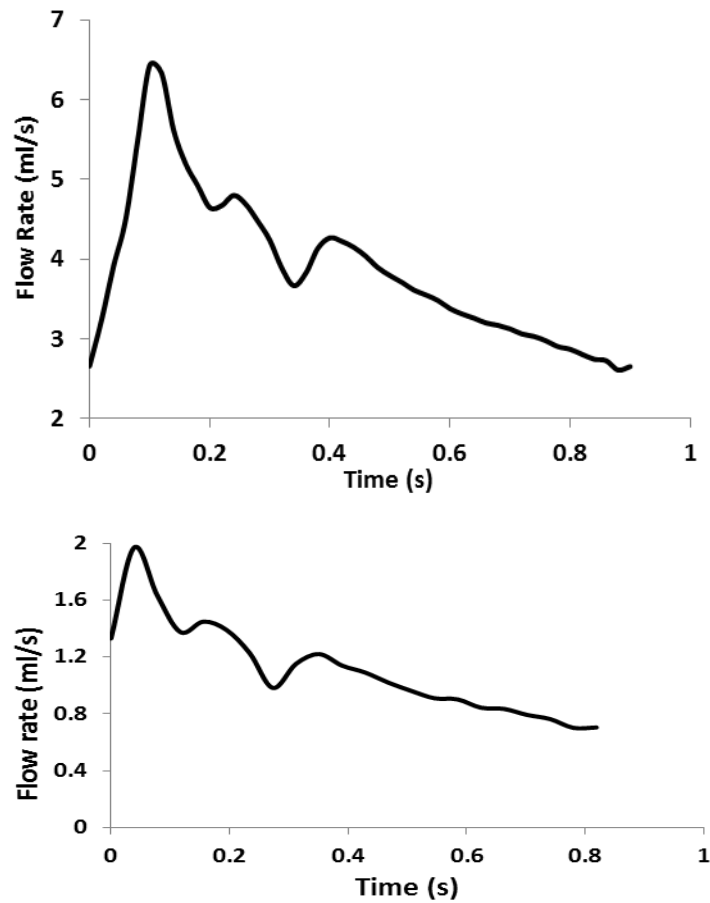
Figure 8: Flow rate waveforms for ICA and vertebral artery

Hemodynamic Indices

Five hemodynamic parameters were chosen to compare the steady and pulsatile flow simulations:

<u>Wall Shear Stress</u>: WSS has long been proposed as a mechanobiological driver of wall remodeling [26]. The spatial mean WSS in the sac region was calculated: $\tau = \mu \dfrac{dU}{dy}$ where τ is the shear stress, μ is the viscosity of blood, U is the flow velocity and y is the distance to wall.

Kinetic Energy (KE): As blood enters the aneurysm, an energy loss occurs by virtue of its inertial effects. It was quantified by calculating the scalar integral of the kinetic energy per unit mass over the aneurysm volume.

Vortex Core (VC): Using the velocity gradient tensor, this index captured the percent volume of aneurysm that is occupied by vortical flow. Traditionally, researchers have used "Number of Vortices" to capture the flow disturbance in an aneurysm. However, the subjectivity involved in the calculation of number of vortices makes it susceptible to user-sensitivity. Therefore, in this study, a different method [40] was used to quantify the presence of a vortex. The Eigen values of the velocity gradient tensor (λ_1, λ_2 and λ_3) were used to extract the vortex core in an aneurysm.

$$\underbrace{\frac{\partial S}{\partial t} + (v.\nabla)S}_{\text{Irrotational Straining}} + \underbrace{S^2 + \Omega^2}_{\text{Rotational Effect}} = -\frac{1}{\rho}\nabla(\nabla p) + \underbrace{\frac{\eta}{\rho}\nabla\nabla^2 v}_{\text{Viscous Dissipation}}$$

- **S**, **Ω** – symmetric and antisymmetric part of velocity gradient tensor
- p, η and ρ – pressure, viscosity and density
- **v** –velocity vector

Presence of minimum pressure is regarded as a criterion for detection of vortices. In the above equation, the first two terms on the left hand side and the last term on right hand side represent the irrotational straining and viscous dissipation caused by pressure gradient. Therefore, the gradient of pressure due to rotational effects can be attributed to the velocity gradient term. Since, the hessian of pressure gives information about the existence of minimum pressure due to vortical motion, the two negative Eigen values of "$S^2 + \Omega^2$" can provide information regarding the presence of vortex core. Hence, the aneurysm volume with $\lambda_2 < 0$ can be used to capture the vortex core in the flow.

Vortex Length (VL): The spread of recirculation region was also calculated by tracking the centerline of the vortex core. Vortex length tracks the centerline of spiraling flow using the critical point theory. Critical points were defined by Chong et al. [41] as 'points where the streamline slope is zero and the velocity is zero relative to an appropriate observer'. According to the critical point theory, the Eigen values and Eigen vectors of

the rate of deformation tensor evaluated at a critical point define the flow pattern about that point. For one real and a pair of complex conjugate Eigen values, the flow forms a spiral-saddle pattern [42]. VL is the length of the vortex centerline and quantifies the extent of recirculation in the aneurysm. Incidentally, Raschi et al. [43] recently reported the use of vortex coreline for cerebral aneurysms whose length is what we propose as a quantitative metric.

Hemodynamic indices are functions of velocity and geometry primarily. Therefore, it is reasonable to speculate that if velocity at each node in the aneurysm shows a linear relationship between steady and pulsatile simulations, majority of the indices would do so as well. Hence the nodal velocity distribution in the entire aneurysm volume was also compared between steady and transient simulations.

Statistical Analysis

Hemodynamic indices computed from steady flow simulations were compared to their pulsatile counterparts (peak systolic time point, end diastolic time point and time-averaged value) using three statistical metrics. The Pearson product-moment correlation coefficient ($-1 \leq r \leq 1$) was used as a measure of the strength of linear dependence between the two approaches based on each index. When r=1, one method consistently scales up or scales down the indices within a study population compared to the other method (that is, the results from one method may be obtained from the other with a constant scale factor). The Spearman's rank correlation coefficient ($-1 \leq \rho \leq 1$) was used as a metric of the similarity in rank between two analysis – i.e., how they rank (and hence stratify) the aneurysms in the study population based on a given index. If the two analyses render an identical ranking order for the aneurysm population, then $\rho = 1$. Slope of the best-fit linear regression (with intercept =0) was used as the third comparison metric in this study ($-\infty \leq k \leq \infty$). If the value of an index calculated from pulsatile flow analysis is identical to its steady counterpart, then k =1. The Pearson's correlation

assesses the level of numerical redundancy between estimates from two analyses. The Spearman's correlation assesses the impact any existing redundancies will have in clinical trial-type studies where hypotheses on rupture risk induced by abnormal hemodynamics are tested.

Results

The simulations converged in all the cases and all hemodynamic indices proposed above were computed. WSS distributions and flow patterns were found to be near identical between steady flow simulations versus time-averaged pulsatile flow simulations (see Figure 9 for representative illustrations). All indices but VC showed a linear relationship between steady flow-based and pulsatile flow-based estimations with a very strong correlation and near-identical ranking (see Figure 10 and Figure 11). Correlation of nodal velocities in the aneurysm showed a near linear relationship between the steady and pulsatile simulations. The correlation coefficient was found to be above 0.9 is all but 5 cases. The R-squared value computed for each model is plotted in the graph shown in Figure 12.

Discussion

The aim of this study was to assess if it is possible to get the same stratification of a population of patient-specific aneurysms based on the aneurysmal hemodynamic environment using steady flow simulation as would be obtained from pulsatile flow simulation when population-wide assumptions are inevitably made about inlet and outlet flow conditions and material properties. At the outset, steady flow simulation may seem to be a dubious substitute for pulsatile flow simulation since we know the flow is indeed pulsatile and temporal variations do exist within a cardiac cycle. Indeed, if we are trying to understand aneurysmal flow phenomenon, pulsatile flow is indispensable. But, if we are trying to distinguish, stratify or rank patient-specific aneurysms based on their flow characteristics – and this is often the case in many reported studies[15, 28, 31, 32, 35, 44,

45] – let us be careful not to confuse what we know happens with what we can reliably learn from modeling it. Two key issues need to be considered in that context. One, we often tend to know little to nothing about the boundary conditions (inlet velocity profiles, outlet impedances) on a patient-specific basis. This forces us to make population-wide assumptions on such conditions (e.g., on temporal variation of inlet velocity and outlet impedance) making pulsatile flow modeling more of an unknown devil than steady flow modeling. And two, what we seek from these studies is not the actual results (such as value of WSS_{ave}), but rather how they differ among patients being evaluated. If the only measured difference between these patient-specific simulations is in the geometry and not in other aspects of the simulation, then the differences among patients in indices attained from pulsatile flow simulations may not (perhaps even should not) be different whether it is based on steady or pulsatile flow conditions. Some reported findings are indeed consistent with this assertion. Geers et al.[46] compared steady-state to transient simulations of two patient specific intracranial aneurysms by conducting experiments examining the effect of flow rate waveform. Their study reported that the hemodynamic environment information obtained from steady state simulation was similar to that obtained from a transient simulation. Cebral et al. [31] in their study with 210 patient specific cerebral aneurysms found that indices based on steady flow simulations distinguished ruptured from unruptured groups as effectively as pulsatile flow simulations. Results reported here are consistent with the above mentioned studies.
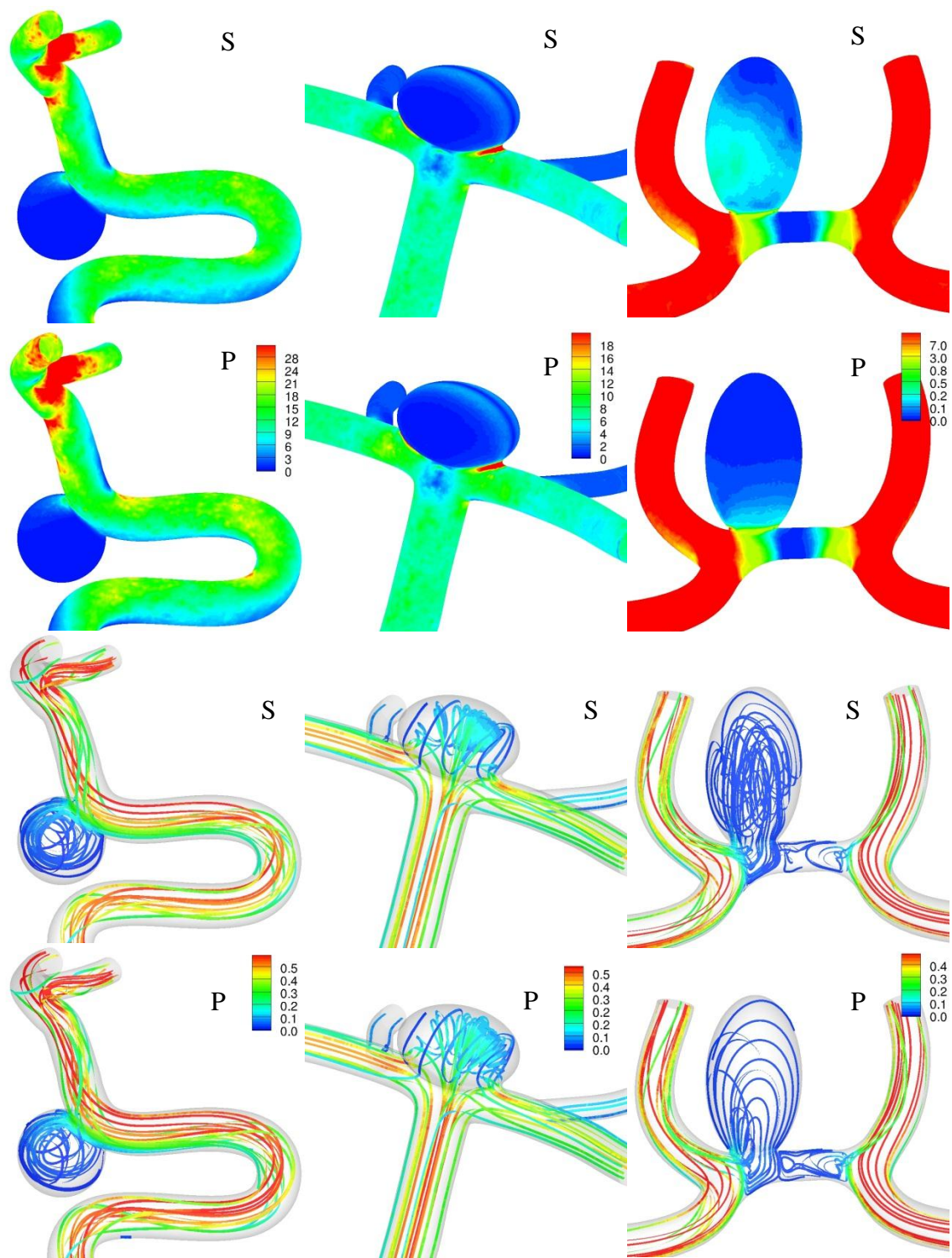
Figure 9: WSS and flow distribution from steady (S) and pulsatile (P) simulations for 3 representative cases
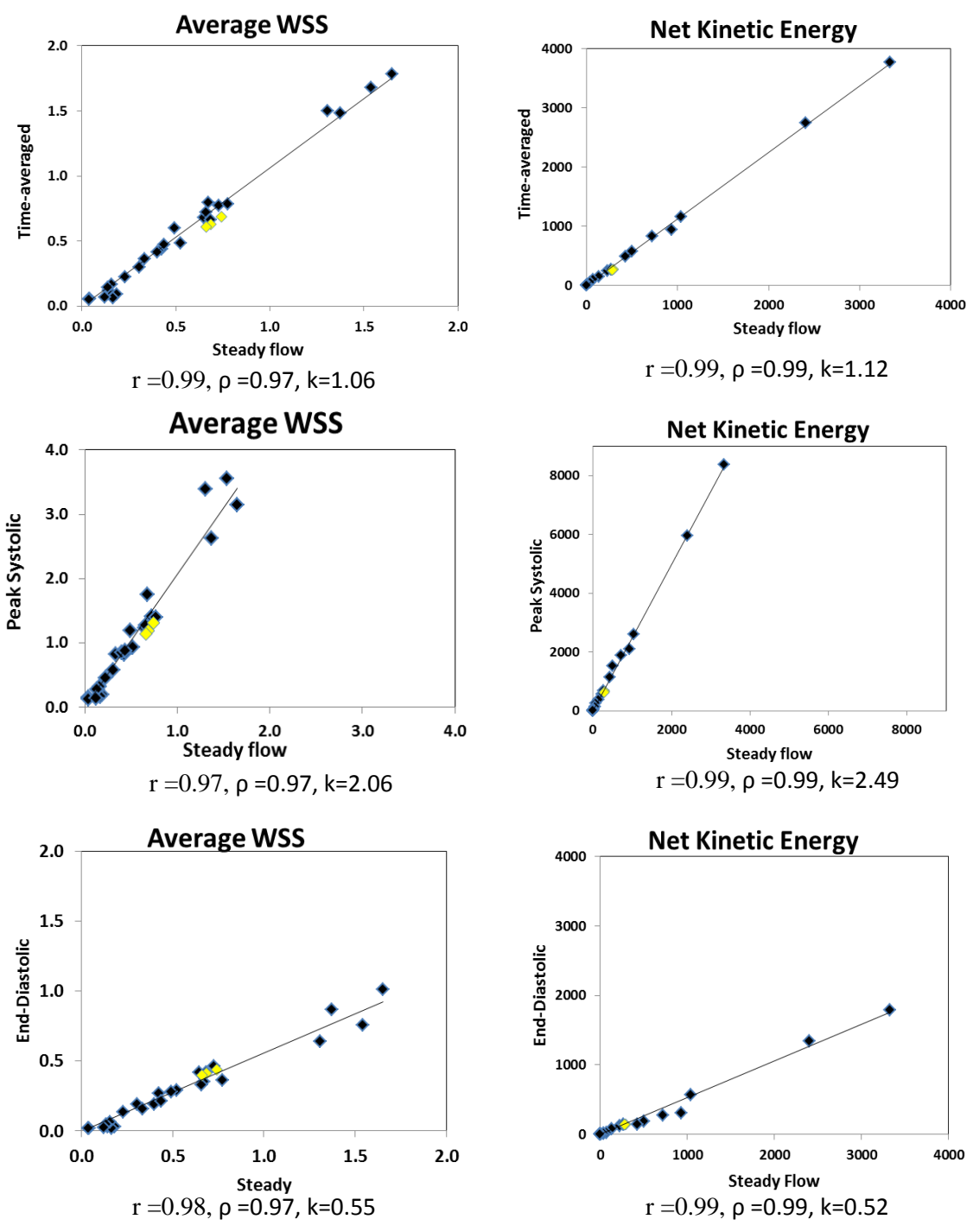
Figure 10: Correlation between steady and pulsatile flow simulations for WSS and KE. Yellow markers refer to aneurysm models with daughter sacs
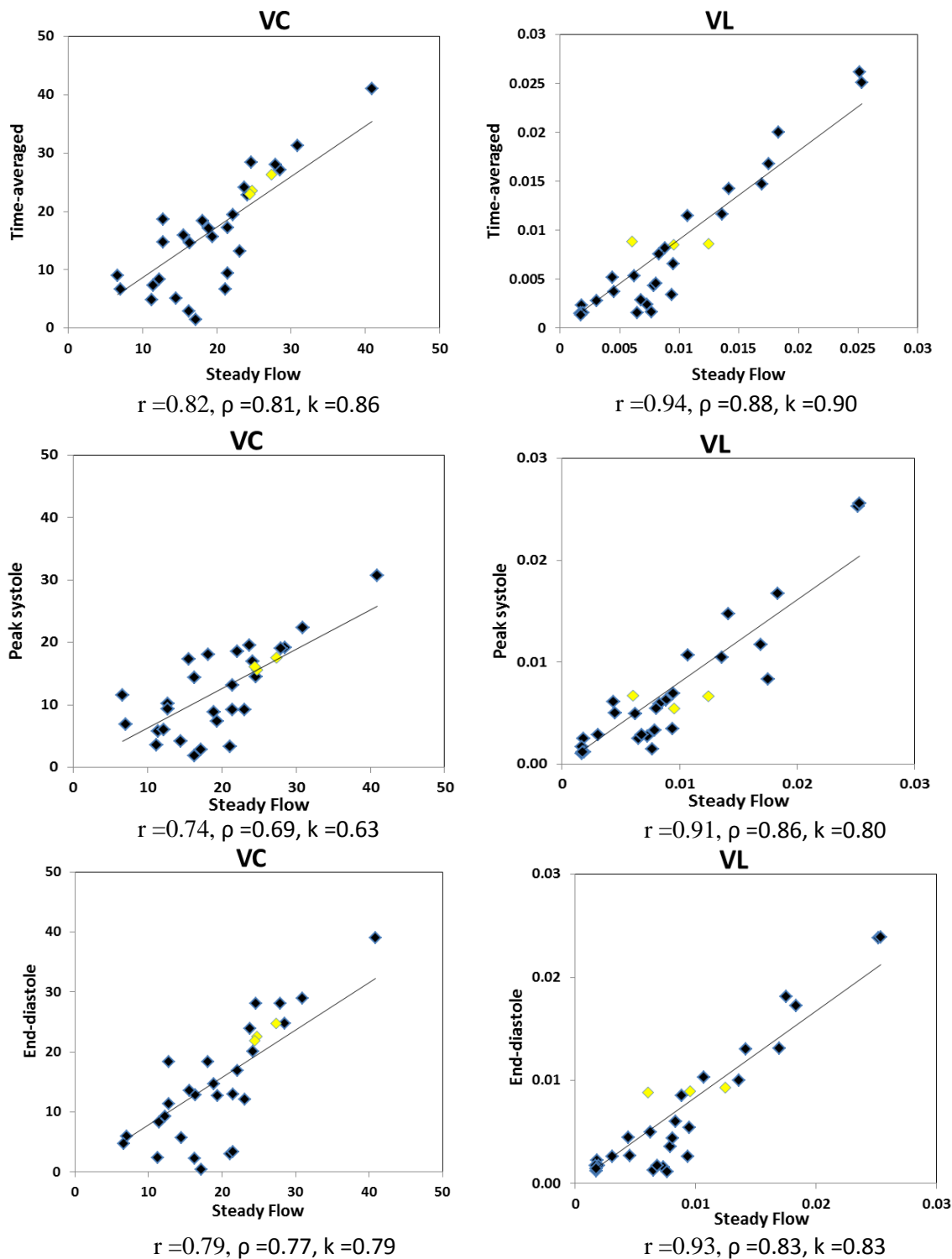
Figure 11: Correlation between steady and pulsatile flow simulations for VC and VL. Yellow markers refer to aneurysm models with daughter sacs
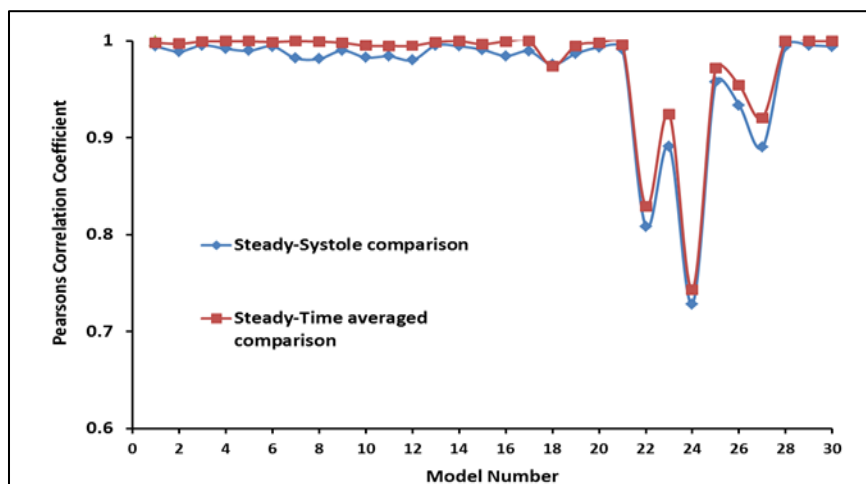
Figure 12: Pearson correlation coefficient comparing the nodal velocity distribution in aneurysm sacs from steady and pulsatile flow simulations

On occasion, few models did show some apparent differences in WSS and flow distribution (Figure 9, Column 3) but these did not manifest in any significant manner on the stratification itself. VC is the only index that did not show a strong correlation between steady and pulsatile flow simulations. However, it is speculated that this non-linearity in relationship is attributed to VC's sensitivity to noise. When a subjective evaluation was performed, it was found that, in a few cases, VC captured additional regions with no apparent recirculation in the vortex core calculation (Figure 13). Hence, the robustness of this index could not be established in this study.
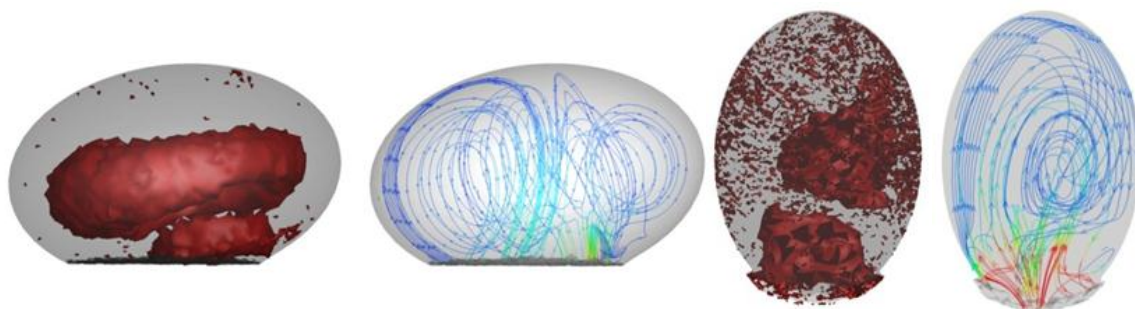
Figure 13: VC in a disc shaped and a rod shaped aneurysm

Out of the two vorticity based indices, vortex length came out as a better index to capture extent of recirculating flow in the aneurysms. Given its one-dimensional nature, it was found to be less prone to noise (Figure 14) and was chosen to be used in the longitudinal study for patient population.
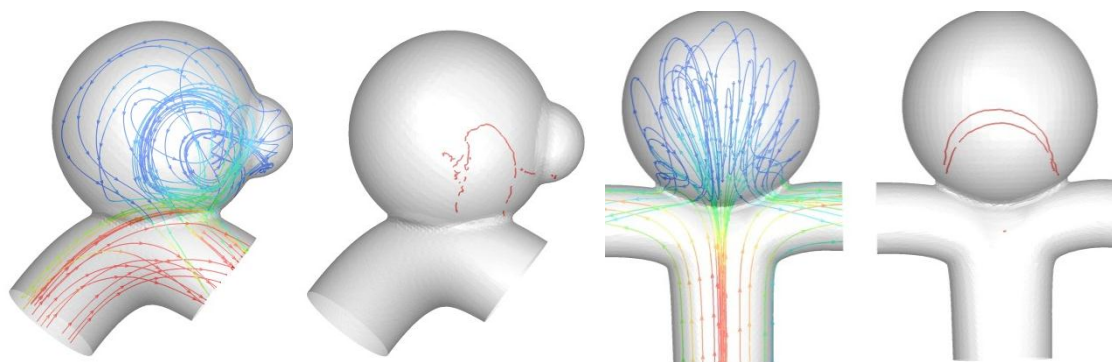
Figure 14: Vortex corelines capturing regions of recirculation

Results of this study clearly indicate that irrespective of whether steady flow overestimates, underestimates or equals pulsatile flow analysis, it does so with significant consistency rendering a near linear relationship. This is logically explained by the fact

that hemodynamics based stratification is but a physically grounded proxy for distinguishing aneurysms based on morphology – which is really the only measured piece of information that is known to be different between the aneurysms in this and even in many patient population studies. However, to ensure that the occasional outliers do not affect the stratification of the patient population and to test whether the hypothesis holds true in patient specific cases, both steady and pulsatile simulations were performed in the longitudinal cohort study.

Collation of Hemodynamic Indices

Simulations of blood flow in intracranial aneurysms (IA) have been reported for populations of human subjects [9, 15, 27, 28, 31-33, 35]. Aneurysmal hemodynamics may be and has been quantified in the literature by numerous indices. These indices have been found to distinguish ruptured aneurysms from unruptured ones and hence proposed as potentially indicative of rupture risk. To be useful, the indices need to be used to stratify large study populations and tested against known outcomes. However, first, it is important to collect and compile the various global quantitative indices that capture the spatially and temporally variant flow characteristics. The objective of this study was to collect and summarize all reported indices of IA hemodynamics with improvements to their definitions where necessary.

A literature survey was performed to determine the indices that have been used to characterize cerebral aneurysm hemodynamics. Where necessary, the existing definitions of indices were modified and additional new ones were developed. The indices were then organized within groups depending upon the nature of blood flow through the aneurysm they attempt to quantify.

WSS based indices

WSS has long been proposed as a mechanobiological driver of wall remodeling [26]. To be effective as a prognostic indicator however, this spatially and temporally varying

quantity should be reduced to an index. The following WSS related indices have been reported in the literature:

1. Temporally averaged, spatial mean WSS in the sac region [15], WSS_{ave}

$$\tau = \mu \frac{dU}{dy}$$

$$WSS_{ave} = \left(\frac{1}{A}\right) \int \tau . dA$$

   where μ is the viscosity, U is velocity, y is distance from wall and A is area.

2. Temporally averaged, spatial maximum WSS in the sac region [15], WSS_{max}

3. Temporally averaged, spatial 99th percentile WSS in the sac region, WSS_{99}. When large study populations are involved, this index may capture the essence of WSS_{max}, while avoiding the pitfalls of localized spikes due to model artifacts if any [47]

4. Low wall shear area, LSA: Under the premise that abnormally low WSS may promote aneurysmal growth [35], and is therefore undesirable, the surface area covered by low WSS has been proposed as an index. However, what constitutes 'abnormally low' is not consistent between investigators. Whereas Jou et al. and later Xiang et al. defined 'abnormally low WSS' as less than 10% of mean parent vessel wall shear stress [15, 32], Cebral et al. defined 'abnormally low WSS' as less than 1 standard deviation (SD) of the near vessel (Figure 15) wall shear stress [31]. Of the two, the latter definition better accounts for the spread of WSS in the parent vessel while prescribing what is 'abnormally low' (for e.g., for aneurysms at the siphon of the ICA, the parent vessel WSS likely spans a rather wide range such that even 10% of the mean may not be justifiably judged to be 'abnormally low'). However the SD based definition does suffer from the limitation that it is parametric (i.e., requires a normal distribution) and may result in negative values for 'abnormally low WSS' when the SD is higher than the mean, a not-so-uncommon occurrence in some parent vessels. We submit that the best alternative

is to use a non-parametric approach while accommodating the spread of WSS in the parent vessel. Hence, we define abnormally low WSS as less than the 15.87[th] percentile (the non-parametric equivalent of mean-SD in a normal distribution) of WSS in the near vessel area.

$$LSA = (A_l/A_a) * 100$$

where A_l is the aneurysm area under abnormally low WSS and A_a is total aneurysm area.
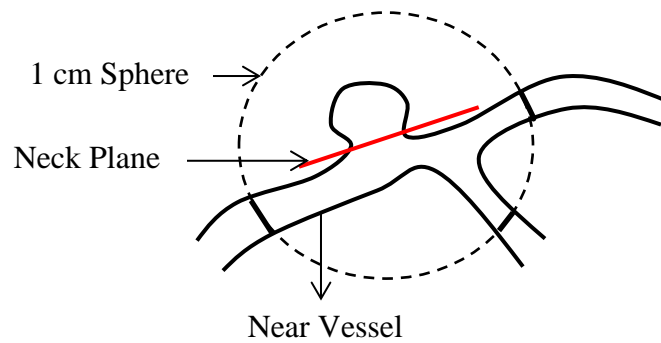
Figure 15: Schematic depicting the near vessel region

5. Low shear concentration index (LSCI) is a new index we define here as the ratio of the average (temporal and spatial) shear stress in the low shear area (see definition for LSA above) over that in the entire aneurysm sac. This new definition is a modified version of low shear index defined by Cebral et al. [31]. LSI was defined as the 'relative amount of the total shear force applied in regions of abnormally low WSS'. The physical meaning of such an index and the mathematical definition proposed for it in their report are unclear to us and hence this modified definition.

$$LSCI = (\frac{F_l}{A_l})/(\frac{F_a}{A_a})$$

$$F_l = \int_{A_l} |\tau| . dA$$

$$F_a = \int_{A_a} |\tau| . dA$$

6. High shear area (HSA): We propose a high shear area index as the area of aneurysm that is exposed to wall shear stress above 84.13th percentile (A_h). Cebral et al. [31] had originally used a high shear area for calculating SCI (defined below), but defined it as the area of regions exposed to shear stress that is higher than mean+SD of WSS in the near vessel region. Our choice of 84.13th percentile for delineating what is 'high' is that it is the non-parametric equivalent of mean+SD in a normal distribution under the same rationale as that for defining 'abnormally low' under LSA.

$$HSA = A_h/A_a$$

7. Shear concentration index (SCI): SCI, defined by Cebral et al.[31] is the ratio of the average (temporal and spatial) shear stress in the high shear area (see definition for HSA above) over that in the entire aneurysm sac. SCI is simply the high shear counterpart to LSCI.

$$SCI = (\frac{F_h}{A_h})/(\frac{F_a}{A_a})$$

$$F_h = \int_{A_h} |\tau| . dA$$

$$F_a = \int_{A_a} |\tau| . dA$$

8. Mean, Maximum and 99th percentile WSS spatial gradient (WSSG): Xiang et al. [15], proposed mean WSSG to capture spatial non-uniformity in WSS. We include the maximum and 99th percentile WSSG in the aneurysm sac under similar rationale as with its WSS counterpart. Respectively, these indices are WSSG$_{ave}$, WSSG$_{max}$ and WSSG$_{99}$. In the Cartesian coordinate system, WSSG is given as:

$$WSSG = \sqrt{\left(\frac{\partial \overrightarrow{\tau_x}}{\partial x}\right)^2 + \left(\frac{\partial \overrightarrow{\tau_y}}{\partial y}\right)^2 + \left(\frac{\partial \overrightarrow{\tau_z}}{\partial z}\right)^2}$$

9. Mean Oscillatory shear index (OSI_{ave}) proposed by Xiang et al. [15] captures the temporal directional change of WSS during the cardiac cycle reduced to a global index by spatial averaging. OSI_{ave} quantifies the temporal disturbance in flow in an aneurysm sac.

$$OSI_{ave} = 0.5 * \left(1 - \frac{\left|\int_0^T \tau.dt\right|}{\int_0^T |\tau|.dt}\right)$$

Energy based indices

As blood flows into the aneurysm, an energy loss occurs by virtue of its inertial and viscous effects and may be quantified by indices proposed by Cebral et al.[31]

1. Kinetic Energy Ratio (KER): This index quantifies the amount of kinetic energy in the aneurysm relative to the contiguous vasculature.

$$KER = \frac{\frac{\int_{V_a} \rho v^2 dV}{V_a}}{\frac{\int_{V_{nv}} \rho v^2 dV}{V_{nv}}}$$

where v is the velocity magnitude, ρ is the density of fluid, V_a is the volume of aneurysm sac, V_{nv} is the volume of the near vessel region.

2. Viscous Dissipation Ratio (VDR): Viscous dissipation is the rate at which the work done against viscous forces is irreversibly converted into internal energy. This index measures the ratio of viscous dissipation in the aneurysm normalized by the viscous dissipation in the near vessel region.

$$VDR = \frac{\frac{\int_{V_a} 2(\frac{\mu}{\rho})(\varepsilon_{ij}\varepsilon_{ij})dV}{V_a}}{\frac{\int_{V_{nv}} 2(\frac{\mu}{\rho})(\varepsilon_{ij}\varepsilon_{ij})dV}{V_{nv}}}$$

where μ is the viscosity, ρ is the density and ϵ_{ij} is the strain rate tensor.

Pressure differential based indices

Pressure in the wall regions is the loading on it that may drive its remodeling and/or rupture. We define in this context, the temporally averaged spatial mean (DP_{ave}) and spatial maximum (DP_{max}) difference in pressure between the aneurysm and near vessel. While physically intuitive, caution is warranted with use of these indices because pressure computations in CFD analyses, especially with the use of constant pressure outlet conditions, are not necessarily reliable [48, 49].

Intra-sac flow based indices

The nature of blood flow inside the aneurysm sac is determined by the sac morphology and how it relates to its contiguous vasculature. The following indices quantify key aspects of such flow:

1. Inflow concentration index (ICI): Defined by Cebral et al. [31], this quantifies the degree of concentration of inflow jet entering the sac relative to the parent vessel.
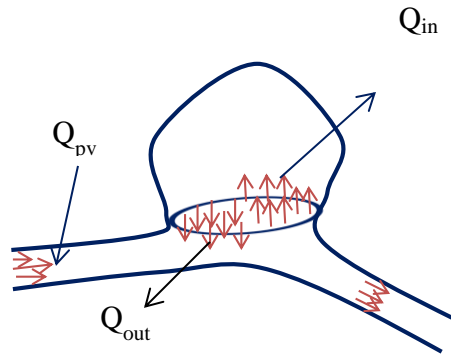
Figure 16: Velocity vectors at the aneurysm neck plane. Arrows pointing towards aneurysm indicate inflow.

$$ICI = \frac{\frac{Q_{in}}{Q_{pv}}}{\frac{A_{in}}{A_n}}$$

where Q_{in} is the inflow into the aneurysm, Q_{pv} is the flow rate in the parent vessel, A_{in} is the neck area with inflow velocities and A_n is the total neck area

2. Residence time (RT): We define here, RT as the average of the time spent by all particles entering the aneurysm. To calculate this index, time-averaged streamtraces may be plotted in the aneurysm sac. Using the velocity and distance information from the streamtraces, the time spent by an average particle may be calculated.

3. Vortex length (VL): As blood flows into the aneurysm, it undergoes recirculation, swirling and exhibits 3-D vortices. Traditionally, vorticity information is obtained from a representative cross sectional plane. However, this method is subjective and might prove erroneous if the vortices inside the aneurysm are out of plane. As proposed in section 2.1.3, VL is a new index to quantify the spread of the recirculation region. Vortex length tracks the centerline of spiraling flow using the critical point theory. Critical points were defined by Chong et al. [41] as 'points where the streamline slope is zero and the velocity is zero relative to an appropriate observer'. According to the critical point theory, the Eigen values and Eigen vectors of the rate of deformation tensor evaluated at a critical point define the flow pattern about that point. For one real and a pair of complex conjugate Eigen values, the flow forms a spiral-saddle pattern [42]. VL is the length of the vortex centerline and can be used to determine the extent of recirculation in the aneurysm. Incidentally, Raschi et al.[43] recently reported the use of vortex coreline for cerebral aneurysms whose length is what we propose as a quantitative metric.

While we have included almost all indices proposed in the literature, some exceptions are worth noting:

- Normalizations of WSS and WSSG based indices with respect to their near vessel averages have been proposed by Xiang et al. [15]. In our longitudinal study, we did

not propose normalization with parent vessels for these indices because the depth of existing literature on WSS-related vessel wall pathology may permit their direct interpretation. But we concede it may be a prudent alternative considering that most other indices proposed above are indeed normalized with respect to the near vessel region.

- Qian et al. [33] proposed energy loss as an index. They calculated it as the difference in energy loss between inlet and outlet points in the near vessel region with and without the aneurysm. That quantity is not included here, as KER likely already quantifies the predominant kinetic energy portion of energy loss.

- Baharoglu et al. [44] proposed shear jet zone size and velocity jet distance to tip as indices of aneurysm in-flow jet characteristics. They are indices of the location (distance from neck or dome) of the median value for WSS and for inflow velocity respectively. However, since the neck point and dome point for an arbitrarily-shaped aneurysm is difficult to define; we did not propose them here. As our ability to characterize sac morphology improves, these indices may yet become objectively calculable.

- And finally, while pulsatile flow simulations result in temporally varying quantities, in the literature, the above indices are calculated after temporal averaging. However, some exceptions exist. Shojima et al. [27] and Jou et al. [32] used peak systolic and end-diastolic instances for calculating indices.

CHAPTER 3

METHODS

Data Collection and Study Population

Scan information of 198 intracranial aneurysms were obtained for this study. The aneurysms belong to patients that are placed under "*watchful waiting*" by doctors. The four clinical centers that participated in recruiting patients for this study are: The Penn State Hershey Medical Center (PSHMC), Thomas Jefferson University Hospital (TJUH), Harvard University- Massachusetts General Hospital (MGH) and The University of Iowa Hospitals and Clinics (UIHC).
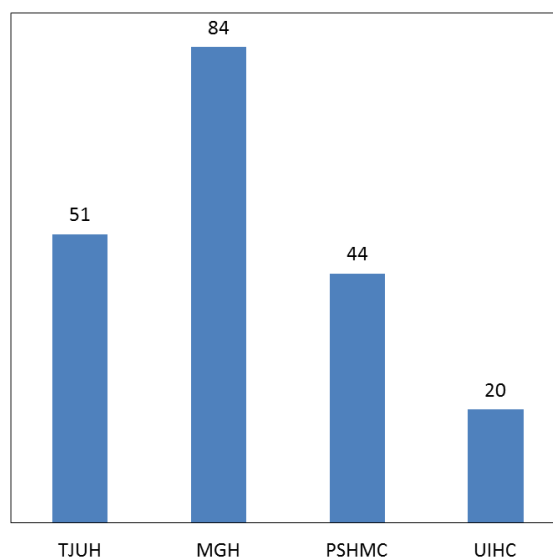
Figure 17: Distribution of study population among the clinical centers

Data from the first scan of patients was obtained from the clinical centers in three different imaging modalities: Computed Tomography Angiography (CTA), Time-of-Flight Magnetic Resonance Angiography (TOF-MRA) and Contrast-Enhanced MRA (CE-MRA). In those cases when the first scan was not available, the second closest scan

was obtained. CTA scanning was the most common modality in this population (78%), followed by MRA-TOF (18%) and then CE-MRA (4%).

About 364 patients were recruited in this study and depending on the quality of image data, 198 intracranial aneurysms were chosen for the analysis. Along with the scan, additional relevant information about the patient such as smoker or non-smoker, single or multiple aneurysms, fusiform or saccular shape etc. were provided. Majority of aneurysms in this population were clinically diagnosed to be located at the anterior location (Figure 18).
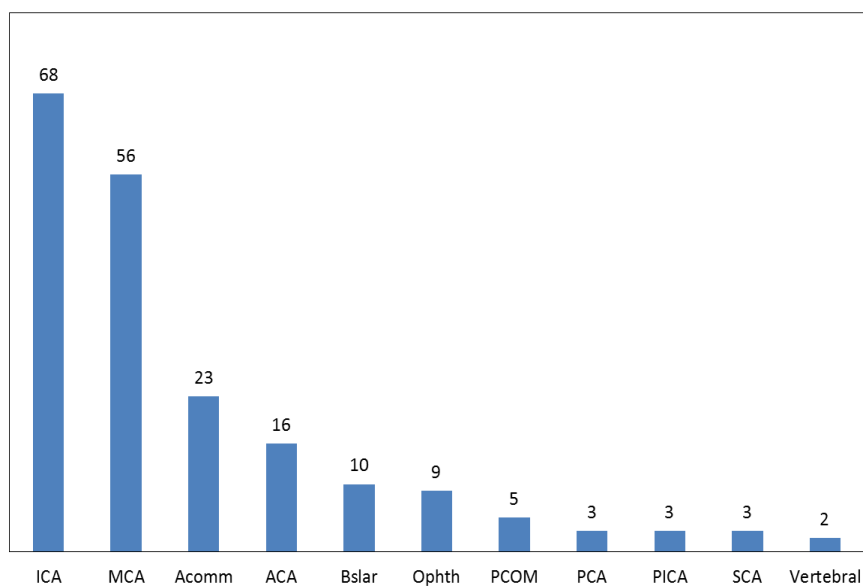
Figure 18: Distribution of aneurysm population according to location. (Ophth - Ophthalmic Artery, PICA -Posterior Inferior Cerebellar Artery and SCA- Superior Cerebellar Artery)

Of the 198 intracranial aneurysms, 132 were single aneurysms while 66 were part of a multiple constellation. The multiple aneurysms belonged to 57 unique patients, out of which 2 possessed what are called aneurysms pairs (aneurysms growing from the same site of an artery [50]). The study subjects were followed up for an average of 607 days. At each follow up, aneurysms were labeled as "stable" or "grown" by the radiologists

after examination of their angiograms or maximum intensity projections. This clinical assessment was performed by making size measurements on the current scan and then comparing it to the notes from the previous scan. Follow up information of each patient was recorded at the respective clinical center and the investigators were blinded from the outcome status until the hemodynamic analysis was complete.

Image Processing and 3D Reconstruction

Image segmentation and reconstruction of 3D models was performed by four investigators in the Biomechanics of Soft Tissue Lab: Benjamin Dickerhoff, Manasi Ramachandran, Steve Lin and Tatiana Correa. For all 198 aneurysms, DICOM images of the 3D scan were archived. The level set segmentation techniques[51] implemented in the Vascular Modeling Tool Kit (VMTK) were used in this process. The level set initialization methods [52] that were used for reconstructing the contiguous vasculature and aneurysm are 'colliding fronts' and 'fast marching' respectively. The 'colliding fronts' initialization type consists of placing two seeds on the image. Two fronts are then propagated from the seeds and the region where they collide is the initial deformable model. The other initialization method, fast marching, involves placement of one seed point at the center of aneurysm and a set of targets on the outer boundary. The initial deformable model in this case is generated by propagating a front from the seed point until the first target is met. Both the initial deformable models are evolved using a set of parameters to form a smooth continuous surface. Finally, the segmented aneurysm model is merged with the contiguous vasculature model. For a detailed description of the segmentation protocol, please refer to the PhD dissertation of Manasi Ramachandran [17].

Computational Fluid Dynamic Simulations

CFD is a branch of science that uses numerical methods and algorithms to simulate the flow of a fluid in a given domain. It has been used extensively to predict the

flow of blood in the human vascular system. The governing equations that describe the flow field in a given domain are the Continuity and Navier Stokes equation. These equations are based on the fundamental laws of conservation of mass and conservation of momentum respectively[53].

CONTINUITY EQUATION: $\frac{D\rho}{Dt} + \rho\nabla.\vec{V} = 0$

NAVIER-STOKES EQUATION: $\frac{\partial\vec{V}}{\partial t} + (\vec{V}.\nabla)\vec{V} = -\frac{1}{\rho}\nabla p + \vec{g} + \frac{\mu}{\rho}\nabla^2\vec{V}$

where ρ is density of fluid, $\vec{V}$ is velocity vector, p is pressure, $\vec{g}$ is gravitational force and μ is viscosity of fluid. Availability of morphometric information, material properties and appropriate boundary conditions are essential factors for a CFD simulation.

Geometric Modeling

The computational domain for blood flow simulations comprised of the aneurysm and its contiguous vasculature. In order to recreate the physiological flow patterns inside the aneurysm, the entire available region of vasculature was included in the hemodynamic simulations. Only in cases when a deviation was observed in the reconstruction of downstream vessels from the image data, the geometry was truncated so as to get rid of the anomaly. If a deviation of the upstream parent vessel or aneurysm surface was observed, a second reconstruction was performed to obtain the accurate geometry. Planar openings were generated on the smoothed models for prescribing the boundary conditions. The clipping boxes, used to generate the planar openings, were selected to lie perpendicular to the arterial axis.

Meshing of the models was performed using VMTK and *Gambit* (Ansys Inc., Lebanon, NH). Each model was truncated by VMTK's clipping box. The inlet was then extended by adding a straight cylindrical tube so as to recreate the fully developed flow condition (explained in detail in Section "Boundary Conditions"). The curvature size function in Gambit [54] was used to obtain finer mesh in regions of larger curvature such

as the aneurysm. Triangular and tetrahedral elements were used to mesh the surface and volume respectively. In order to capture the boundary layer with better accuracy, prism elements were used to mesh the near wall region. Figure 19 shows the entire process of generation of the computational domain. The surface and volume mesh for the aneurysm region of a model are shown in Figure 20.

Three dimensional models used in the blood flow simulations are shown for representative cases in each of the 11 locations in Figure 21, Figure 22, Figure 23 and Figure 24. These images have been scaled such that the viewing distance remains constant for all of them.
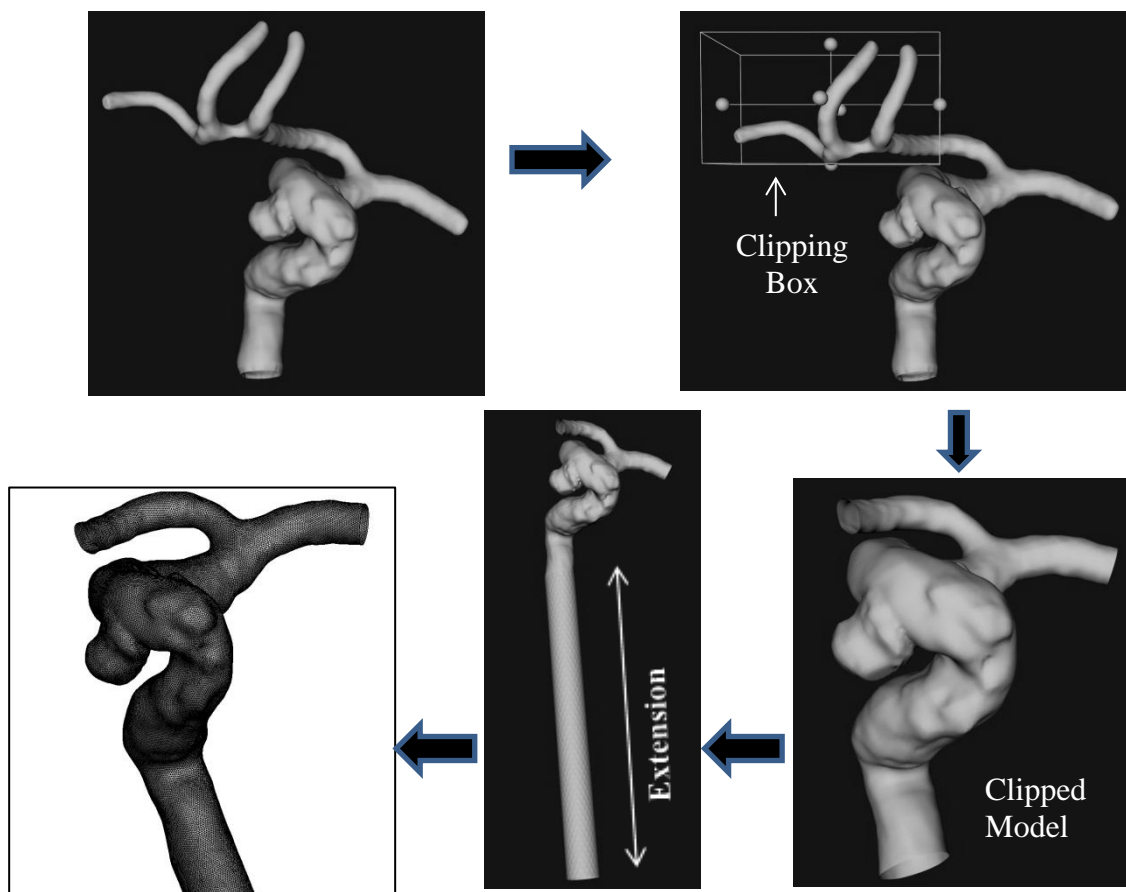
Figure 19: Procedure for meshing the 3D models
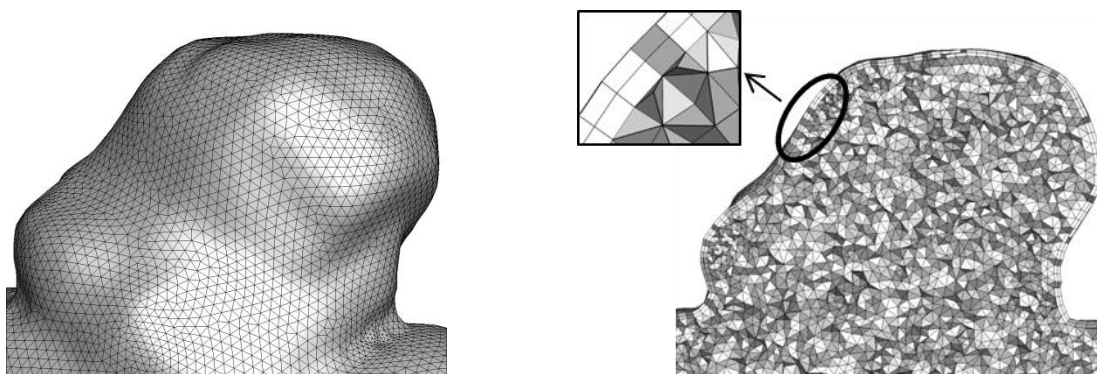
Figure 20: Surface and volume mesh for the aneurysm region. Inset shows the boundary layer
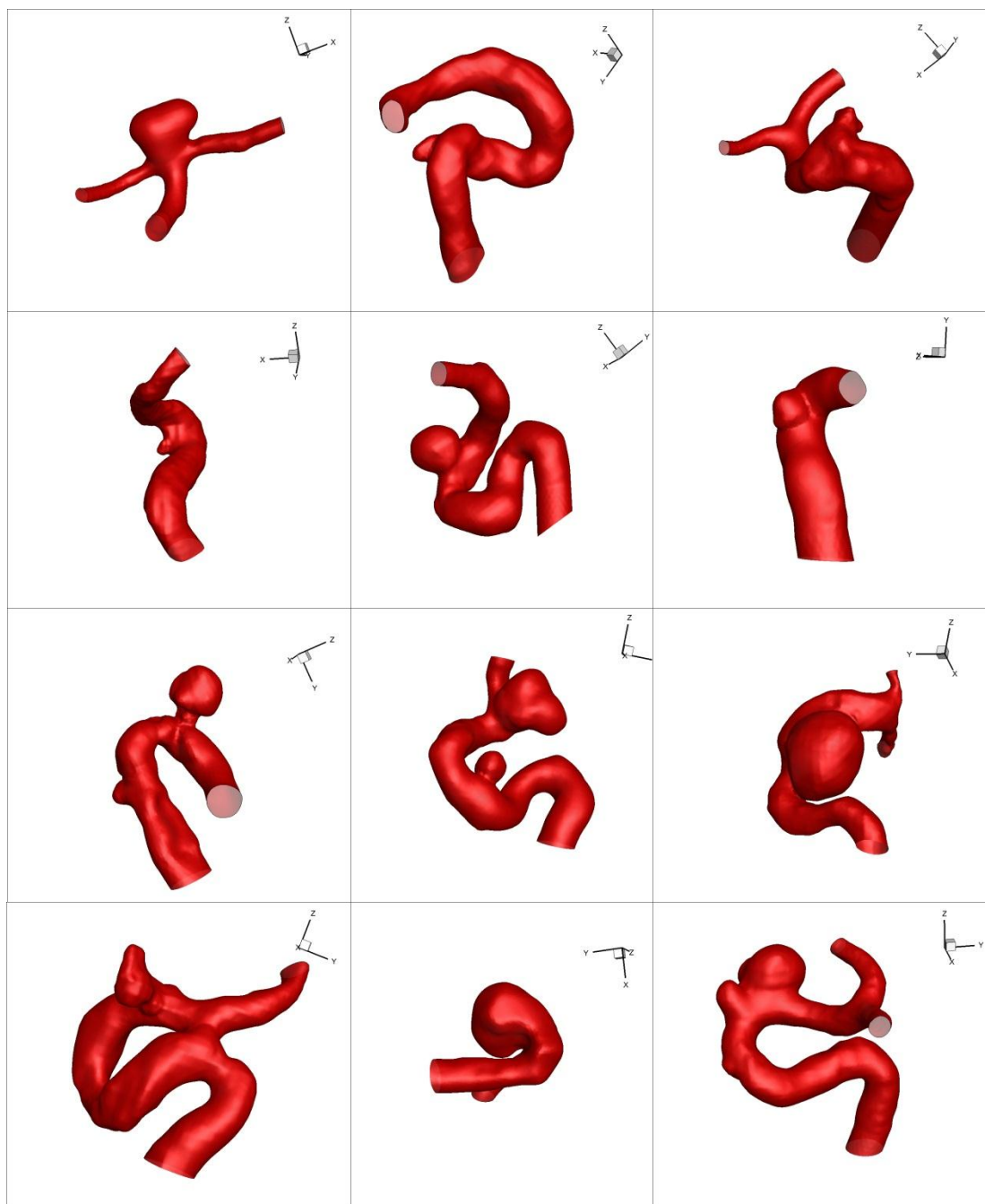
Figure 21: Three dimensional models of aneurysms at ICA.

.
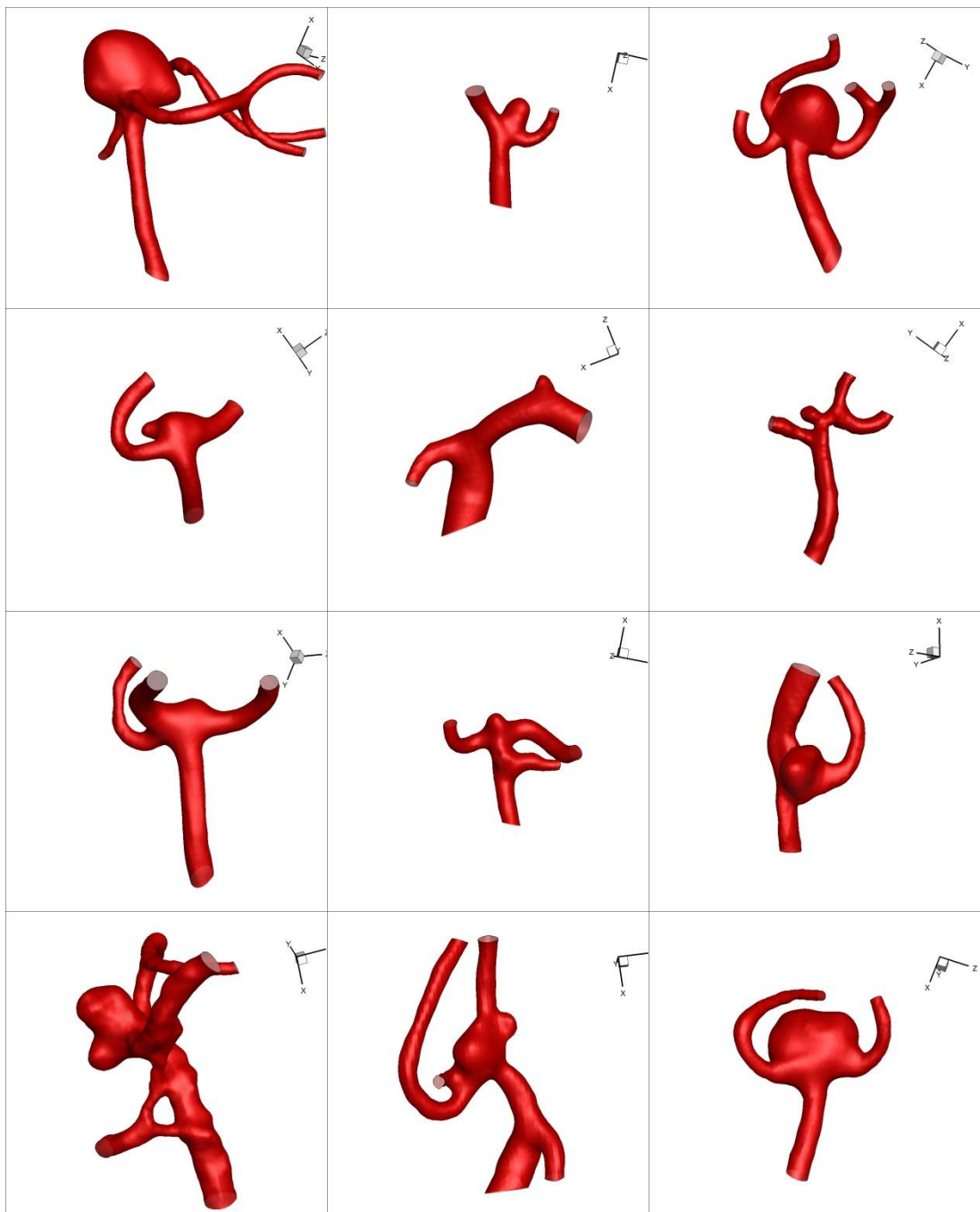
Figure 22: Three dimensional models of aneurysms at MCA.
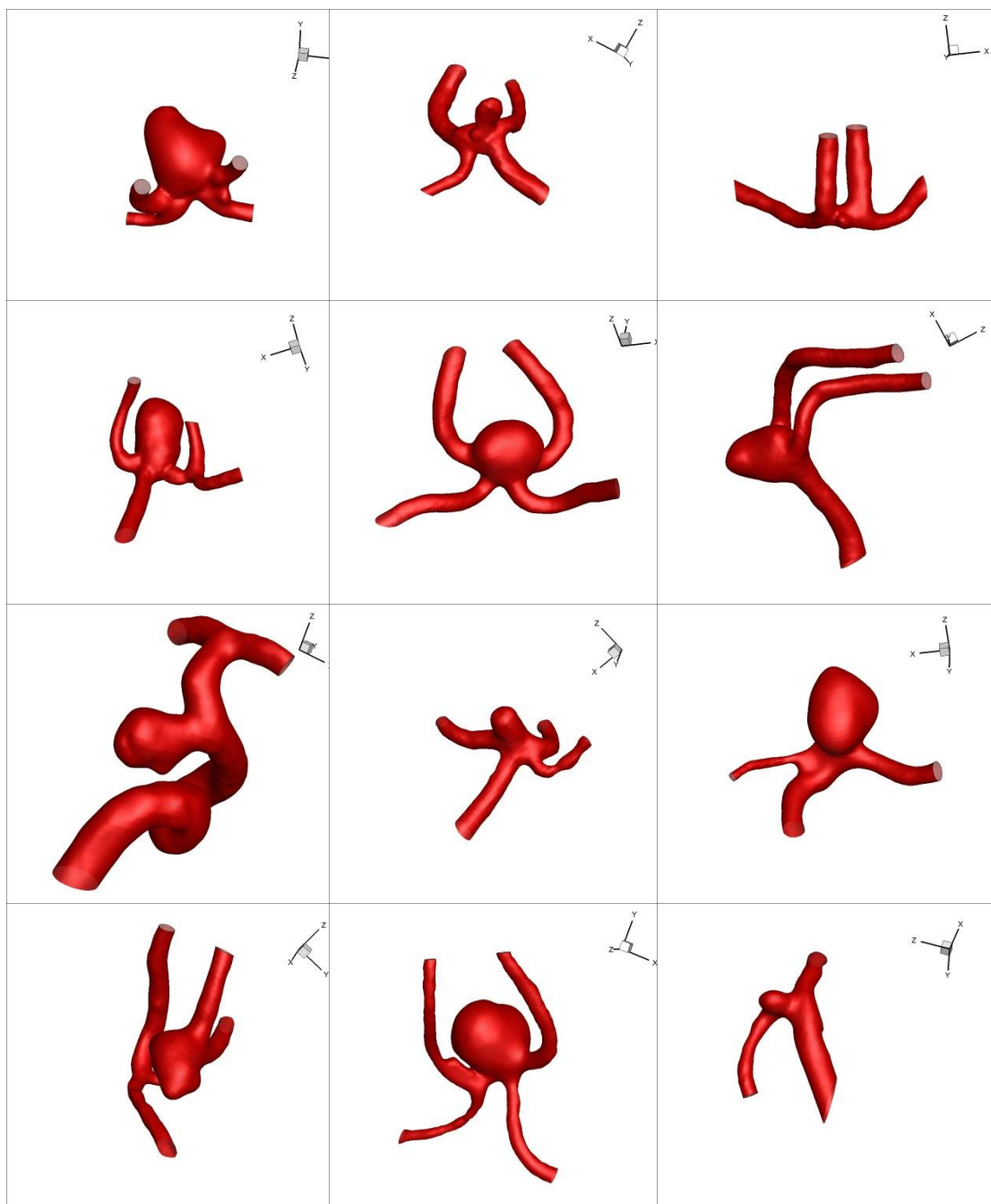
Figure 23: Three dimensional models of aneurysms at AComm and ACA.
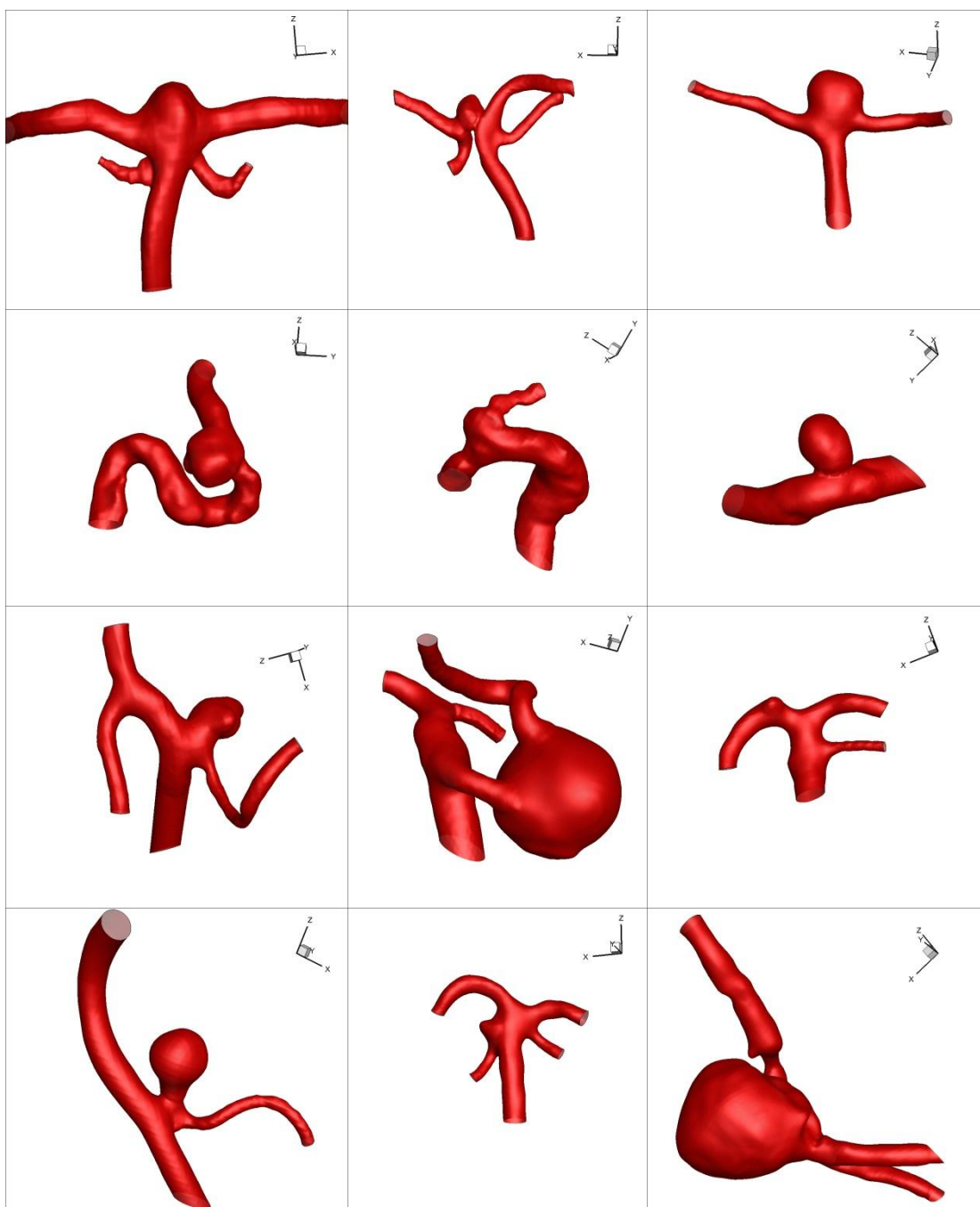
Figure 24: Three dimensional models of aneurysms at Bslar, Ophth, PCOM, PCA, PICA, SCA and Vertebral artery.

Boundary Conditions

Since it is difficult to obtain patient specific flow information for such a large population, in the present study, population averaged flow conditions were used. In order to specify velocity waveforms at the inlets, descriptive statistics of the internal carotid waveform presented by Ford et al.[37] were fitted to Fourier series using a Matlab program. The velocity waveform was then represented as:

$$v(t) = (\frac{1}{A}) * (Q_0 + \sum_{i=1}^{15} a_i \cos(i * 2\pi * f) + \sum_{i=1}^{15} b_i \sin(i * 2\pi * f))$$

$$f = (0.9 - t)/0.9$$

where A is the cross section area of inlet, Q_0 is the time-averaged flow rate, t is time, a_i and b_i are the Fourier coefficients. The cardiac cycle was assumed to be 0.9 seconds. Parameters for an internal carotid artery flow waveform are listed in Table 2. Note that the time-averaged flow rate mentioned in the table is not equal to population averaged flow rate value (4.6 ml/s). This is because these parameters were computed for the waveform used in idealized ICA models where the input flow accounted for the absence of small vessels. However, in the patient specific study population, the waveform was scaled such that the temporally averaged flow matches the population averaged value reported in literature.

A theoretical solution for the fully developed pulsatile motion of a viscous fluid in a straight circular tube was provided by Womersley [55]. In order to impose a Womersley velocity profile at the boundary, a Fast Fourier Transform is used to extract the frequency content of the flow waveform given the fundamental frequency [56]. This method has been used in several studies [28, 29, 57]. However, implementation of this method is relatively complicated and approximations are unavoidable in cases with non-circular inlet faces. A second method been proposed to minimize entrance effect by adding cylindrical extensions to the inlet and then imposing a flat velocity profile at the

Table 2: Input flow waveform parameters

Parameter	Value	Parameter	Value
Ω	6.97 rad/s	Q_0	3.8908 ml/s
a1	-0.0725	b1	-0.9802
a2	-0.1920	b2	-0.5886
a3	-0.4004	b3	-0.2279
a4	-0.2157	b4	-0.0648
a5	-0.2692	b5	0.0212
a6	-0.0699	b6	0.2039
a7	0.0607	b7	0.0433
a8	0.0140	b8	0.0093
a9	0.0409	b9	-0.0109
a10	-0.0015	b10	-0.0527
a11	-0.0193	b11	-0.0299
a12	-0.0312	b12	-0.0355
a13	-0.0571	b13	-0.0001
a14	-0.0205	b14	0.0283
a15	-0.0070	b15	0.0127
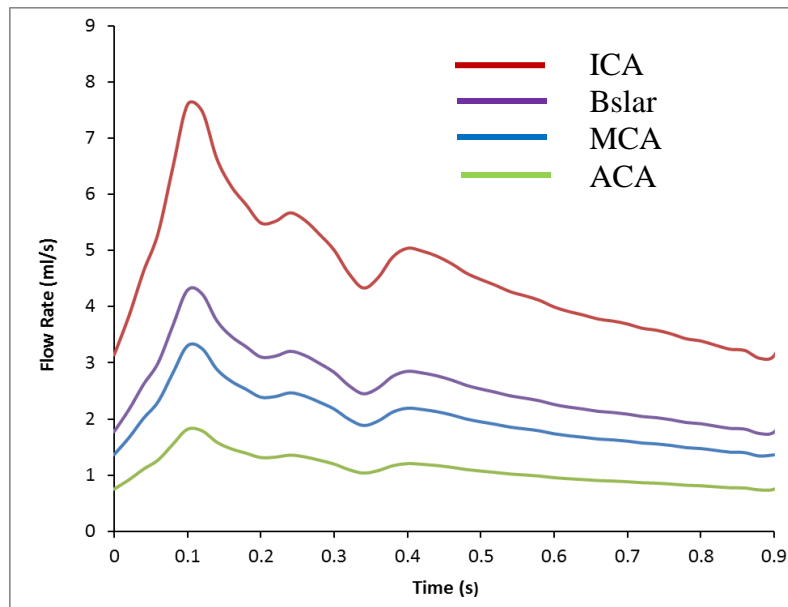
Figure 25: Flow waveforms for inlet vessels

new extended inlet [45, 58]. Due to its ease of implementation, the latter was the method of choice for the current study. The length of cylindrical extensions added to the geometry was 10 times the diameter, as shown in Figure 26. The transient flat velocity profile was specified at the new inlets using a User Defined Function in *Fluent* [59].
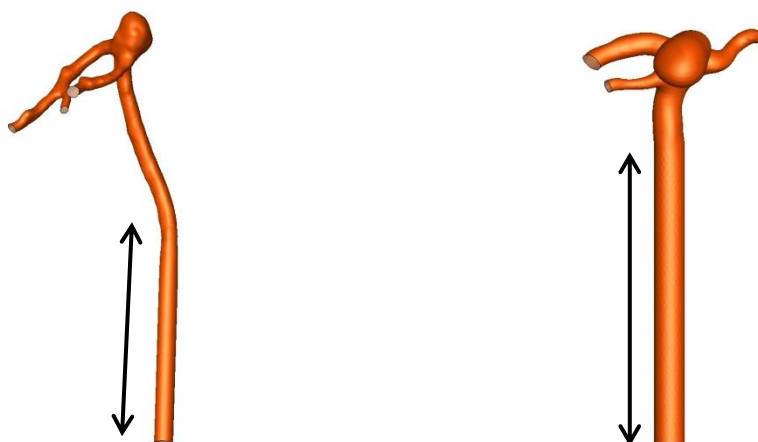
Figure 26: Cylindrical extensions added to the inlets

For each model, a steady flow simulation was also performed. The temporally averaged flow rate value from the pulsatile analysis was used to specify the inlet velocity in steady flow simulations. Presence of the cylindrical extension ensured fully developed flow conditions in the steady simulations as well.

At the outlets, constant pressure boundary condition was applied. Although flow division seems as a better alternate, the population averaged flow rate values for smaller cerebral vessels are not available in literature. Some studies have used the principal of optimal work which says that the mass flow rate in each outlet vessel is proportional to the cube of its diameter [60]. However, this method is sensitive to the geometrical truncation effects and, therefore, has not been used in this study. In cases when a flow reversal was observed at the outlet faces, cylindrical extensions were added to outlets to improve convergence. The outlet boundary condition remained the same for steady flow simulations.

No slip boundary condition was imposed at the vessel wall and a rigid wall assumption was made. Effect of gravity was neglected in all the simulations.

<center>Material Properties</center>

In this study, blood was modeled as an incompressible fluid exhibiting Newtonian rheological property. The density and viscosity of blood were taken as 1060 Kg/m^3 and 0.0035 Pascal-second respectively. Despite the fact that the viscosity of blood changes with the applied shear forces, a Newtonian fluid assumption is deemed reasonable in this study. The reason being that at relatively high rates of shear, the viscosity coefficient approaches a constant value and, therefore in cerebral blood vessels, the non-Newtonian effects are of minor importance[61].

<u>Flow Solver</u>

All CFD simulations were run using the commercial software, Fluent. Owing to the small vessel diameters and low flow, the Reynolds number in the cerebral vasculature falls in the laminar regime [61]. Therefore, the viscous-laminar model was used. Given the incompressible nature of fluid medium, a pressure based segregated algorithm was chosen to solve the continuity and momentum equations[62]. The first order upwind scheme and first order implicit scheme were used for spatial and temporal discretization. The pressure Interpolation was performed using the default standard scheme. To evaluate gradients, the 'Least squares cell-based method' was used. The pressure-velocity coupling was facilitated by using the 'Semi-implicit method for pressure linked equations' scheme. Under relaxation factor of 0.35 and 0.15 were used for pressure and momentum with an absolute convergence criterion $1*10^{-5}$. In the pulsatile analysis, a fixed time step method was used with a time step size of 0.001s. For each time step, 300 iterations were performed and two cardiac cycles were simulated for each case.

Parallel Processing and Supercomputing Cluster

A total of 396 flow simulations were performed in this study, 198 steady and 198 pulsatile. To tackle the computationally intensive nature of this problem, the parallel processing capabilities of *Fluent* were utilized. Using 50 parallel licenses of *Fluent*, the simulations were run on The University of Iowa's supercomputing cluster, Helium. The steady and transient simulation took on average 1 and 10 hours for completion respectively.

The entire process implemented in the computational fluid dynamic simulation of a patient is illustrated in Figure 27.
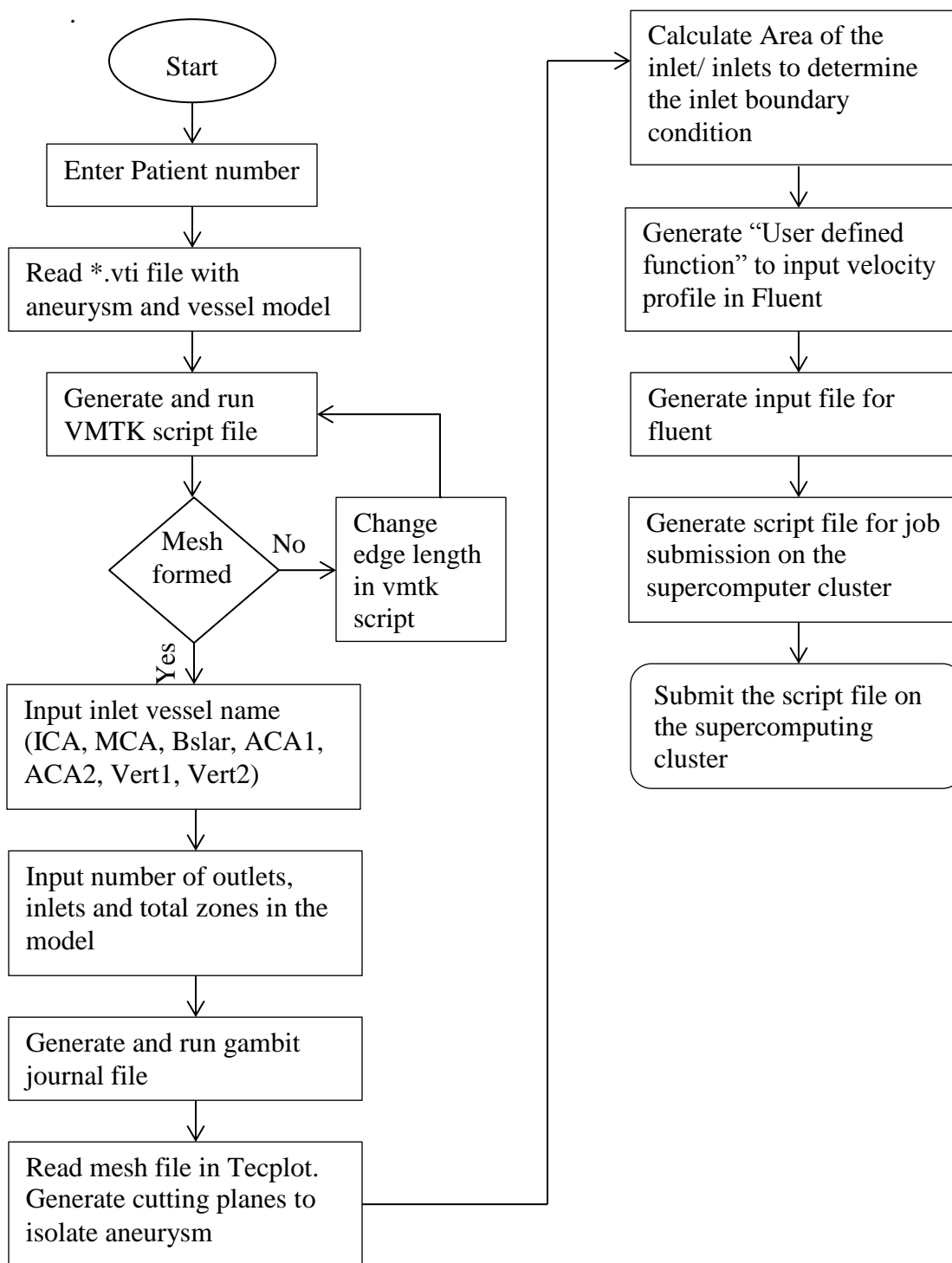
Figure 27: Flow chart outlaying the entire automated method of running a CFD simulation for a patient

Aneurysm Isolation

In order to calculate hemodynamic indices, aneurysms were isolated from the contiguous vasculature using cutting planes. A morphometric analysis has been performed on this study population by Ramachandran[17] and therefore, the neck cutting plane in this study was made consistent with the one used in the morphometric analysis to the extent possible. The neck cutting plane was located at a position where the physician would put a clip during craniotomy. Multiple cutting planes were used to isolate the aneurysm from the adjacent vessels. Figure 28 shows the aneurysms isolated from their contiguous vasculature in four cases.

Hemodynamic Indices

All the hemodynamic indices documented in Chapter 2 were calculated for the 198 aneurysm cases. Matlab programs and Tecplot macros were written by the author for computation of these indices (Figure 29, Figure 30 and Figure 31). The entire process was automated using a matlab code. Steady counterparts of all indices but OSI were calculated for the steady flow simulations.
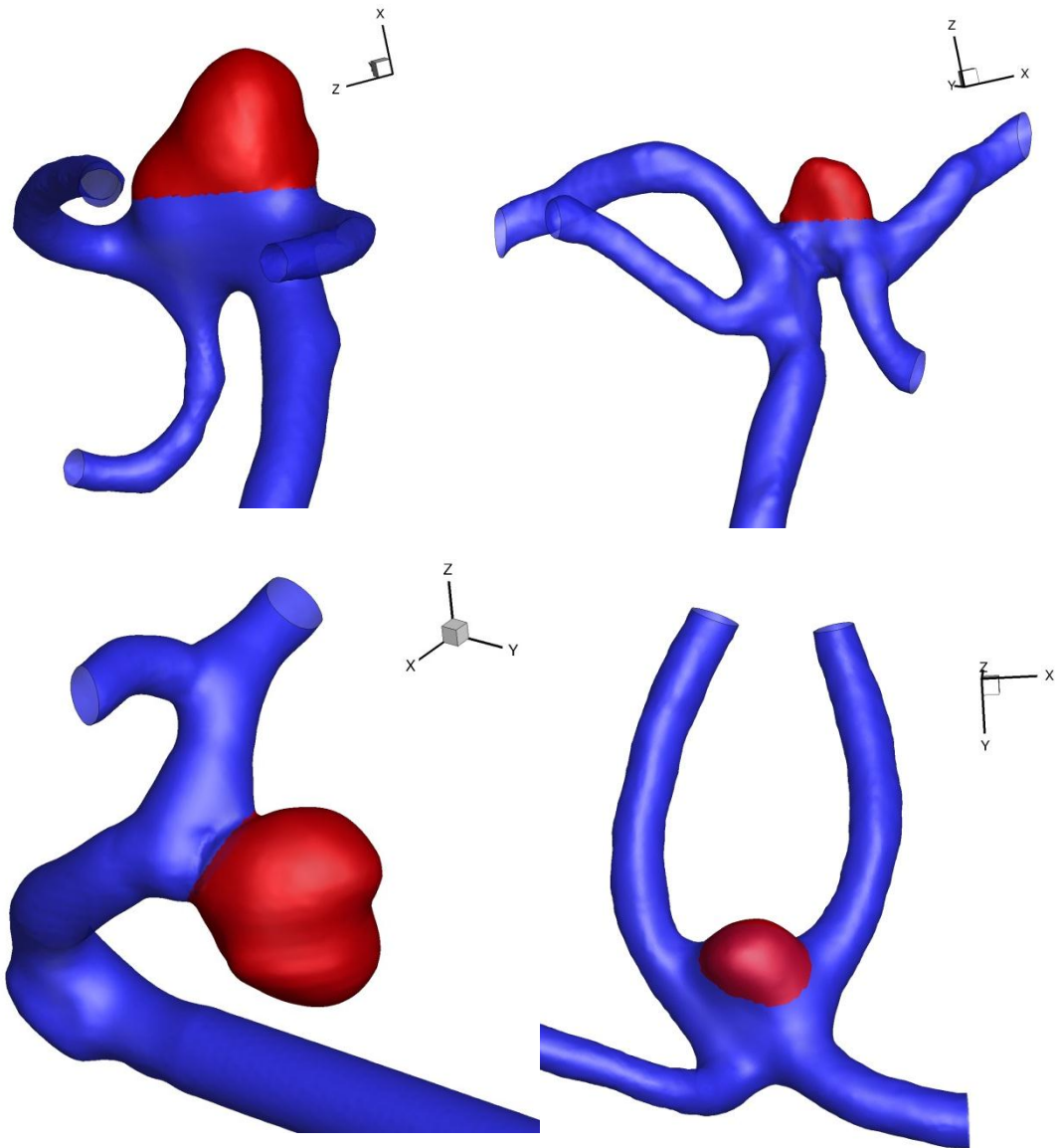
Figure 28: Isolated aneurysms shown in red. Cutting planes were used to perform the isolation
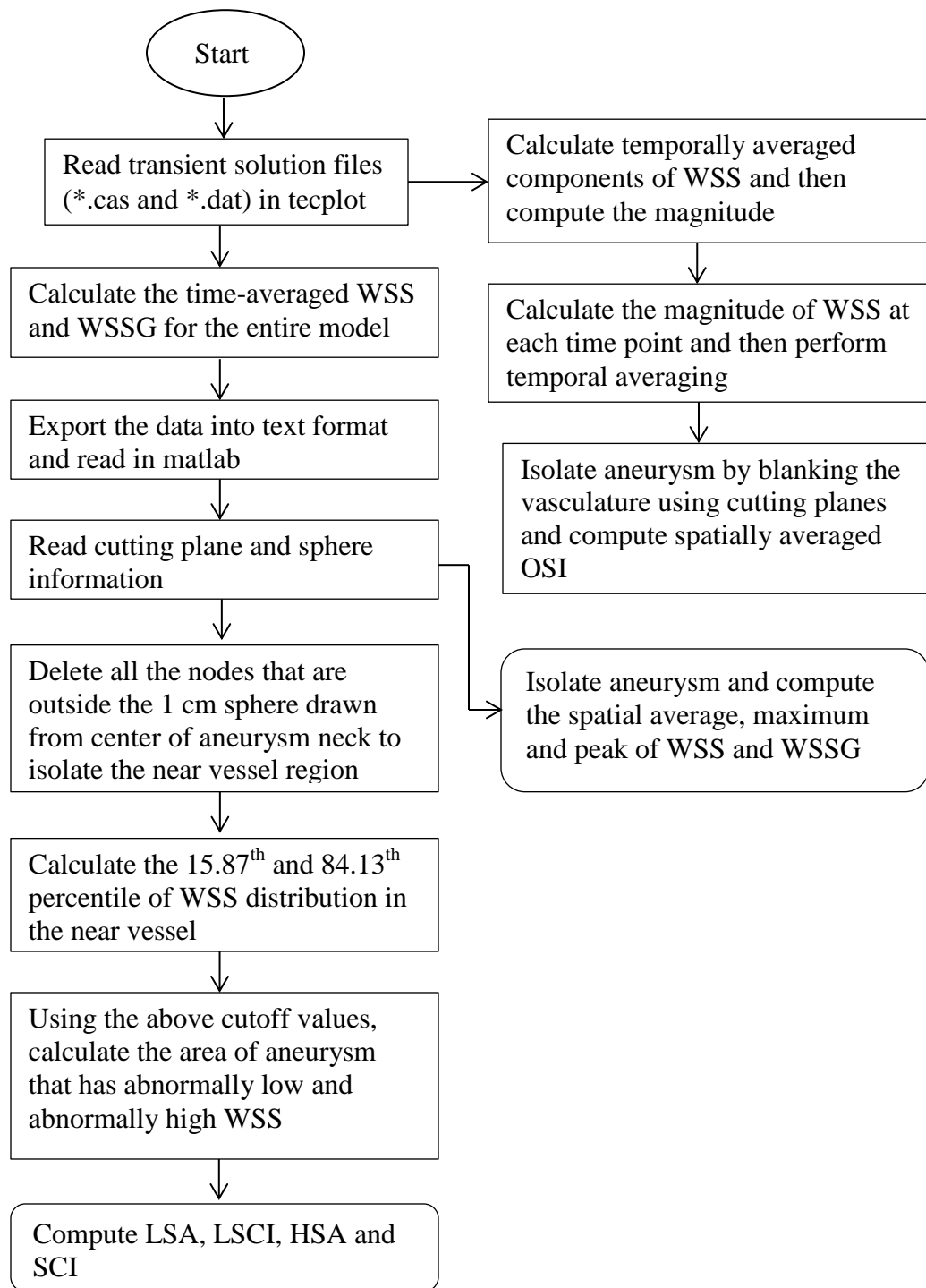
Figure 29: Flow chart explaining the method of calculation of WSS based indices
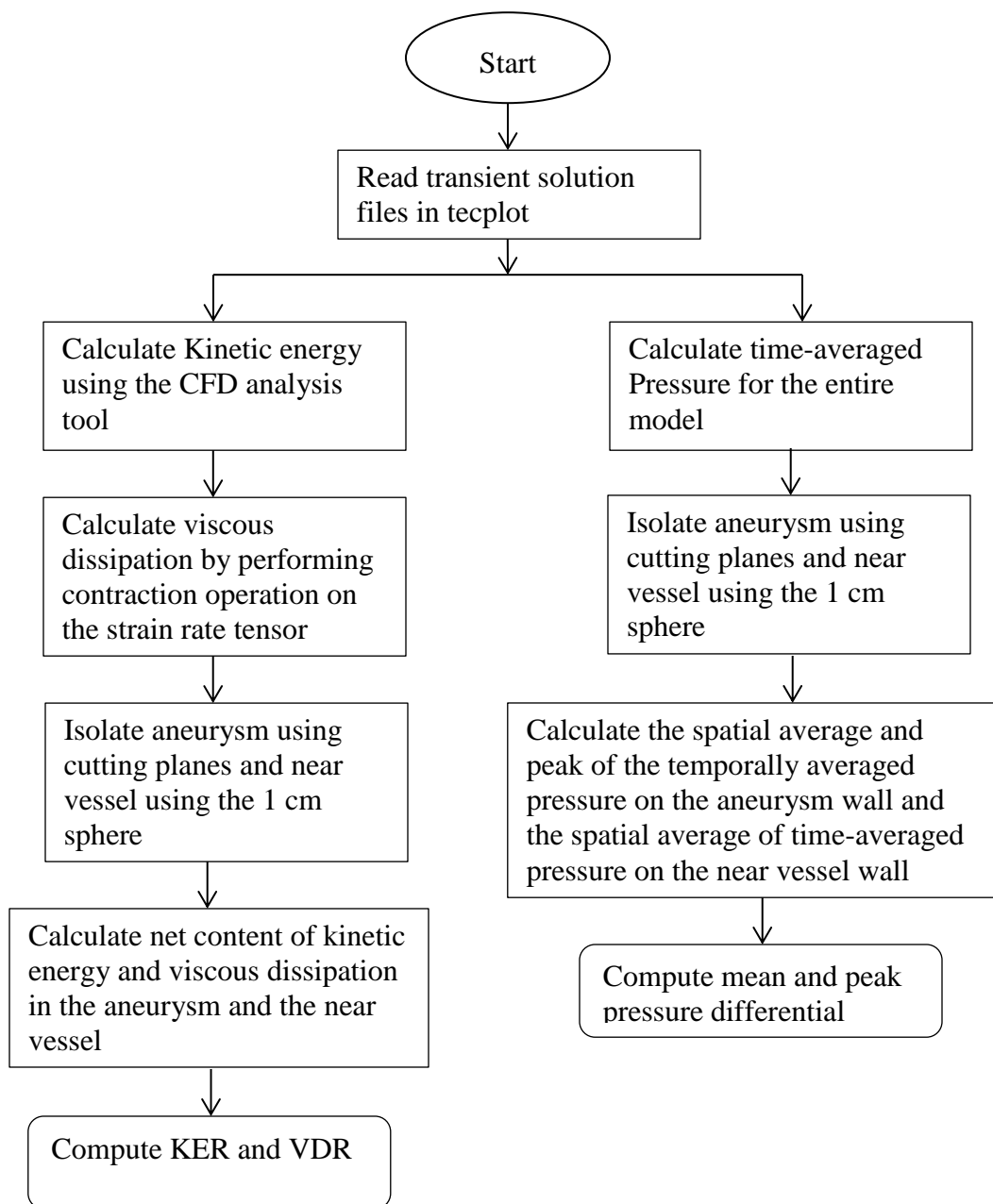
Figure 30: Flow chart explaining the method of calculation of energy and pressure based indices

Extract boundary nodes of the inlet of model

Use diagonally opposite nodes to draw rakes for placing streamtraces at the inlet face

Extract the location and velocity vector for all streamtraces.

Use the cutting plane as gates to isolate the portion of streamtraces that are inside the aneurysm

Isolate the portions of streamtraces that are inside the aneurysm

Using the distance travelled by each streamtrace and its velocity values; calculate the total time spent inside the aneurysm

Start

Read transient solution files in tecplot

Calculate time-averaged velocity in the model

Extract neck plane of aneurysm. Neck Plane: $Ax+By+Cz+D=0$

Normal of the neck plane points towards the aneurysm

Yes

No

Select portion of the neck plane where: $V_xA+V_yB+V_zC < 0$

Select portion of the neck plane where: $V_xA+V_yB+V_zC > 0$

Compute RT by averaging all the times over the number of streamtraces

Extract vortex core using the CFD analysis tool

Isolate aneurysm using Cutting plane and calculate length of vortex core in the aneurysm

Compute VL

Calculate area and flow rate in the selected portion of neck plane

Compute ICI using parent vessel flow rate

Figure 31: Flow chart explaining the method of calculation of intra-sac flow based indices

In this population of aneurysms, few aneurysms pairs were present. These are multiple aneurysms that grow on the same site of an artery. Additionally, an ACA aneurysm had a paired AComm aneurysm where the AComm aneurysm was not a part of this study. In cases where the 1 cm sphere drawn from center of neck plane of first aneurysm, captures some or all of the second aneurysm, the near vessel region was isolated by deleting the entire aneurysm portion from the spherical region (Figure 32). It was done to ensure that the near vessel region captures only the healthy portion of the vasculature.
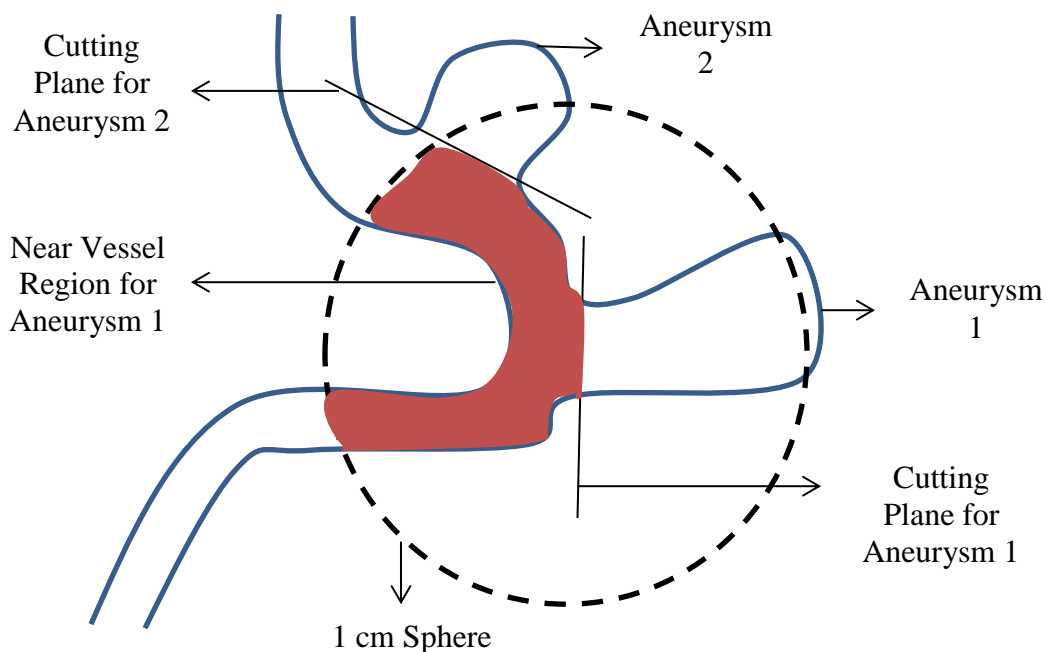
Figure 32: Near vessel region of Aneurysm 1 in the aneurysm pair

User-sensitivity Study

Given the large population scope of this study, involvement of multiple users in the segmentation process is indispensable. In order to assess the impact of uncertainty in

the segmentation process on the estimation of hemodynamic indices, a user sensitivity study was performed.

Ten patients from the cohort population were chosen for this study (3 ICA aneurysms, 2 MCA aneurysms, 1 ACA aneurysm, 1 SCA aneurysm, 1 AComm aneurysm, 1 PCOM aneurysm and 1 Bslar aneurysm). It was ensured that these subjects realistically represent the variations in aneurysm size, shape, imaging modality of the entire population. Three dimensional models were reconstructed for these patients by two users, Benjamin Dickerhoff and Manasi Ramachandran (Figure 33). The neck cutting planes for aneurysm isolation were also chosen by the respective users. Computational fluid dynamic simulations of pulsatile blood flow in these 20 cases were performed using the methods described above. All the hemodynamic indices presented in Chapter 2 were computed for each case.

Pearson correlation coefficient (r), Spearman correlation coefficient (ρ) and slope (k) were used to determine the correlation between the hemodynamic indices of the models reconstructed by the two users (Table 3).
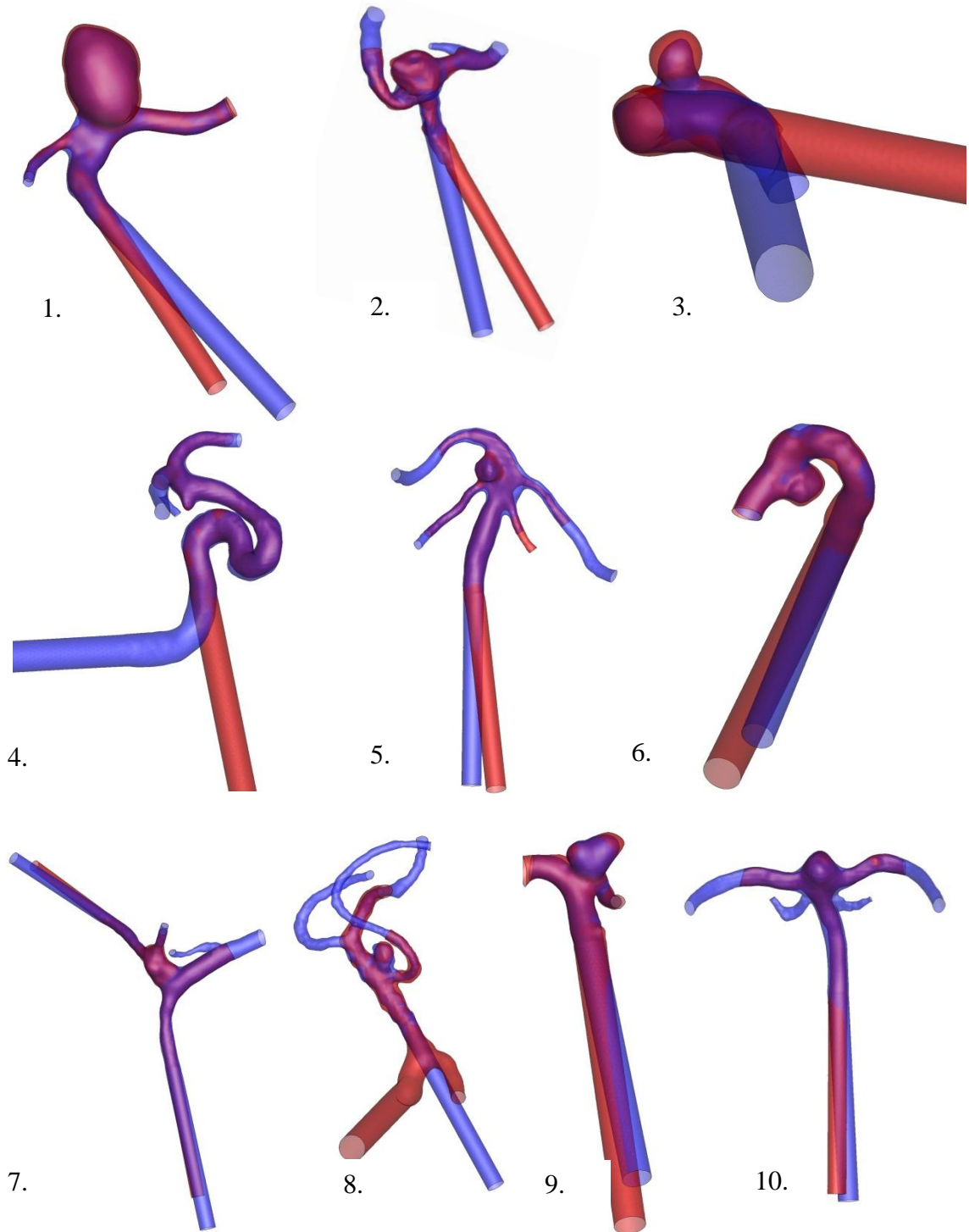
Figure 33: Aneurysms and their contiguous vasculature reconstructed by the two users:
(Blue: User1, Red: User2)

Table 3: Statistical metrics for the indices are reported.[1]

Indices	r	ρ	k	Mean (U1)	Mean (U2)
WSS_{ave}(Pa)	0.542	0.564	0.406	4.703	4.795
WSS_{max}(Pa)	0.574	0.406	1.060	18.803	32.046
WSS_{99}(Pa)	0.884	0.661	1.046	13.683	19.984
LSA (%)	0.817	0.855	0.824	52.463	46.925
LSCI	0.891	0.927	0.691	2.928	2.810
HSA	0.469	0.660	0.397	3.308	2.969
SCI	0.513	-	0.650	3.240	5.435
$WSSG_{ave}$(Pa/mm)	0.715	0.782	0.617	9.136	10.421
$WSSG_{max}$(Pa/mm)	0.580	0.745	0.388	126.360	131.886
$WSSG_{99}$(Pa/mm)	0.848	0.673	1.180	56.791	80.390
OSI_{ave}	0.711	0.297	0.489	0.007	0.006
KER	0.797	0.697	0.781	0.259	0.239
VDR	0.740	0.758	0.503	0.526	0.434
DP_{ave}(mm Hg)	0.660	0.672	0.935	1.357	1.674
DP_{max} (mm Hg)	0.686	0.745	1.224	1.523	1.743
ICI	0.978	0.782	1.425	0.718	0.885
RT (s)	0.988	0.709	1.446	0.089	0.107
VL (mm)	0.937	0.855	0.946	2.319	2.576

---

[1] Mean value of indices for user 1 (U1) and user 2 (U2) are also reported.

Figure 34: Scatter plots depicting correlation for a few indices.

Streamtraces and WSS distribution for models reconstructed by the two users are shown for four cases in Figure 35, Figure 36, Figure 37 and Figure 38. A qualitative analysis revealed that the differences in hemodynamic behavior of the same aneurysm reconstructed by two users could be attributed to differences in truncation lengths, neck plane used for isolation, connection between aneurysm and adjacent vasculature and any user introduced m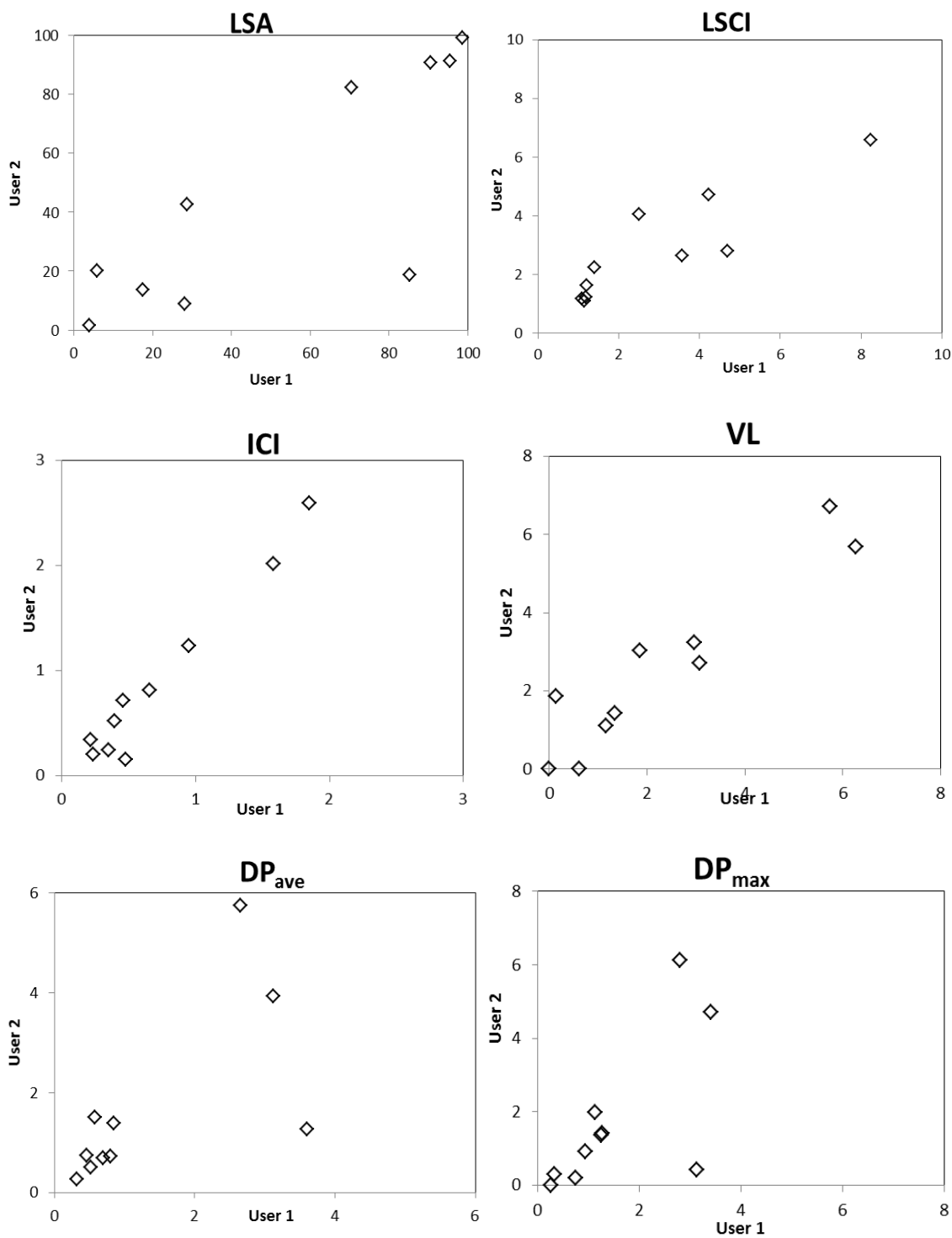odel reconstruction error such as localized vessel narrowing or missing branch vessels. Figure 35 illustrates the differences in flow pattern inside the aneurysm in the presence and absence of SCA proximal to the basilar tip aneurysm. Effect of truncation length on the aneurysmal flow can be observed in Figure 36. In this case, two morphological differences were visible: point of truncation of vasculature and connection between the aneurysm and contiguous vasculature. It is possible that combined effect of these two morphological differences resulted in the significantly different flow patterns and hence different hemodynamic indices (Figure 36). Absence of branch vessels distal to the aneurysm was found to have little impact on the hemodynamics inside the aneurysm (Figure 37).

Although hemodynamic differences were observed in models reconstructed by two users, it was found that indices normalized with respect to parent vessel better correlated the two groups. LSA, LSCI, KER, VDR, DPmax, DPave, ICI, HSA and SCI are the indices that are calculated after normalization with respect to the near vessel. All but three of the normalized indices have r and ρ greater than 0.7. Since 4 out of the 10 patients had an HSA value of 0, their SCI's were indeterminate. It could be the reason that the r and ρ values of HSA and SCI are low. VL and RT, which are purely aneurysm inflow based indices, also correlated the two patient groups strongly (r> 0.9 and ρ>0.7).

Velocity Magnitude (m/s)

0.47
0.42
0.37
0.32
0.26
0.21
0.16
0.11
0.05
0.00

WSS (Pa)

50
44
37
31
25
19
12
6
0

User 2

User 2

User 1

User 1

Figure 35: Streamtraces and WSS distribution in a basilar tip aneurysm model reconstructed by two users.
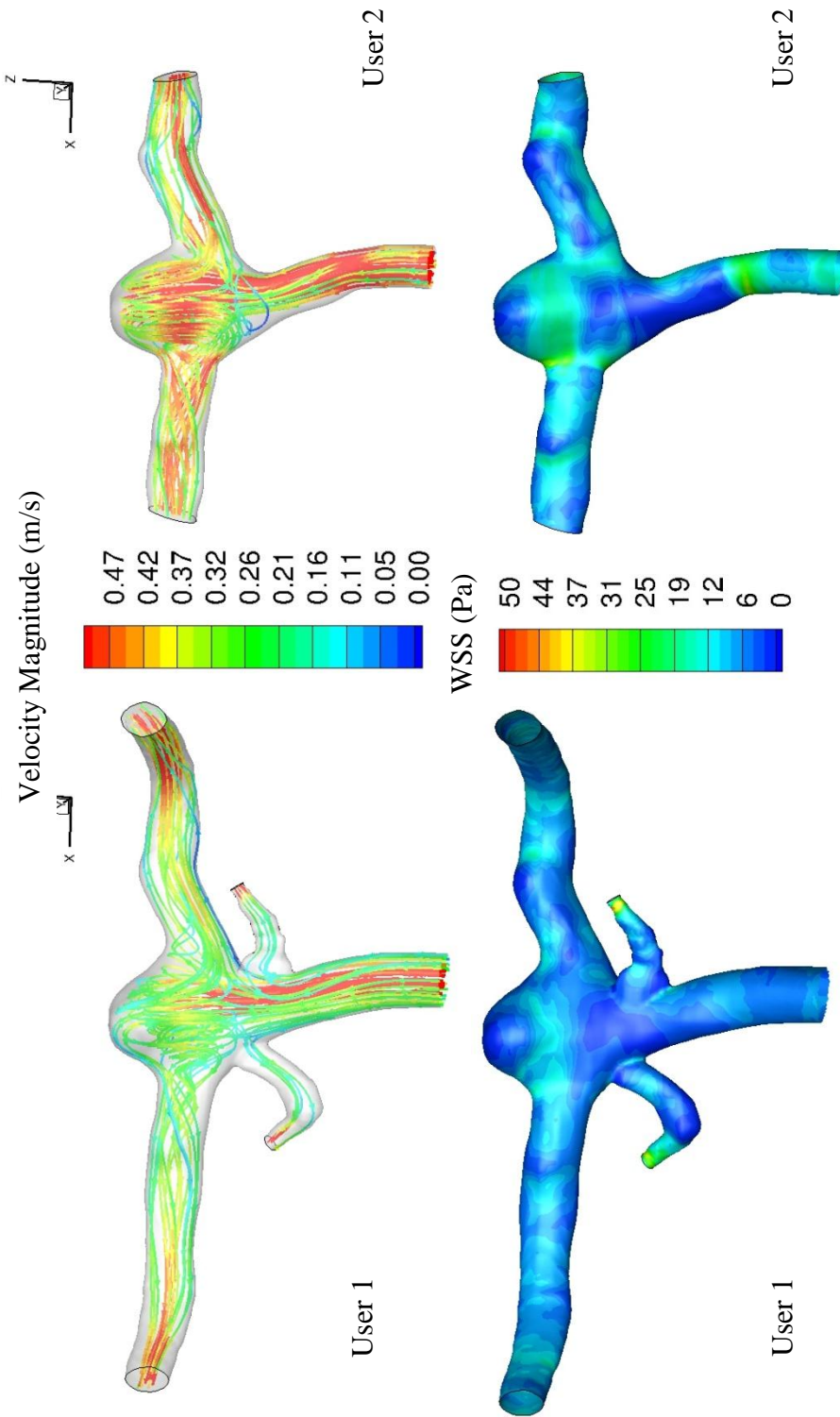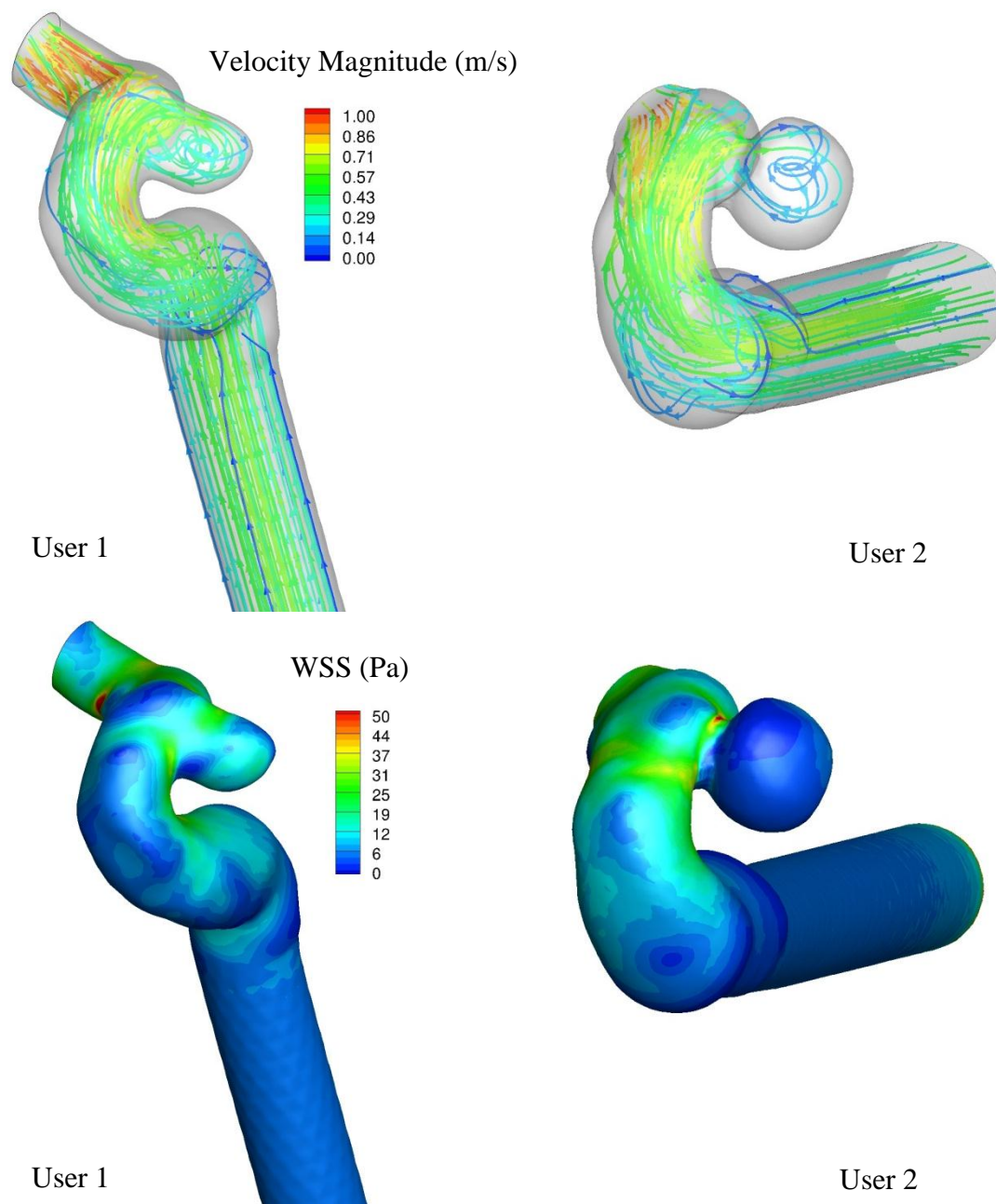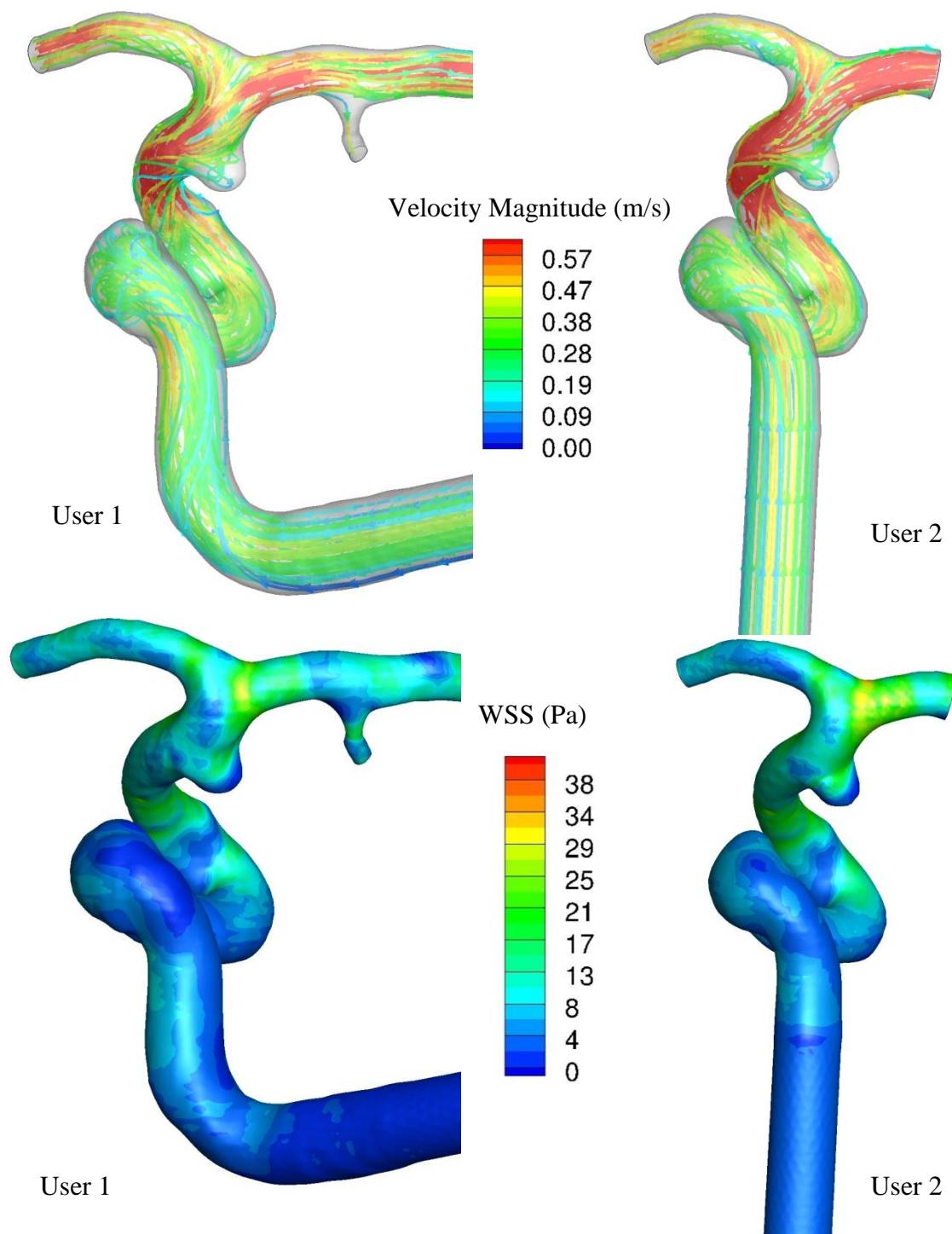
Figure 36: Streamtraces and WSS distribution in ICA aneurysm model reconstructed by two users

Figure 37: Streamtraces and WSS distribution in ICA aneurysm model reconstructed by two users

Velocity Magnitude (m/s)

User 1

User 2
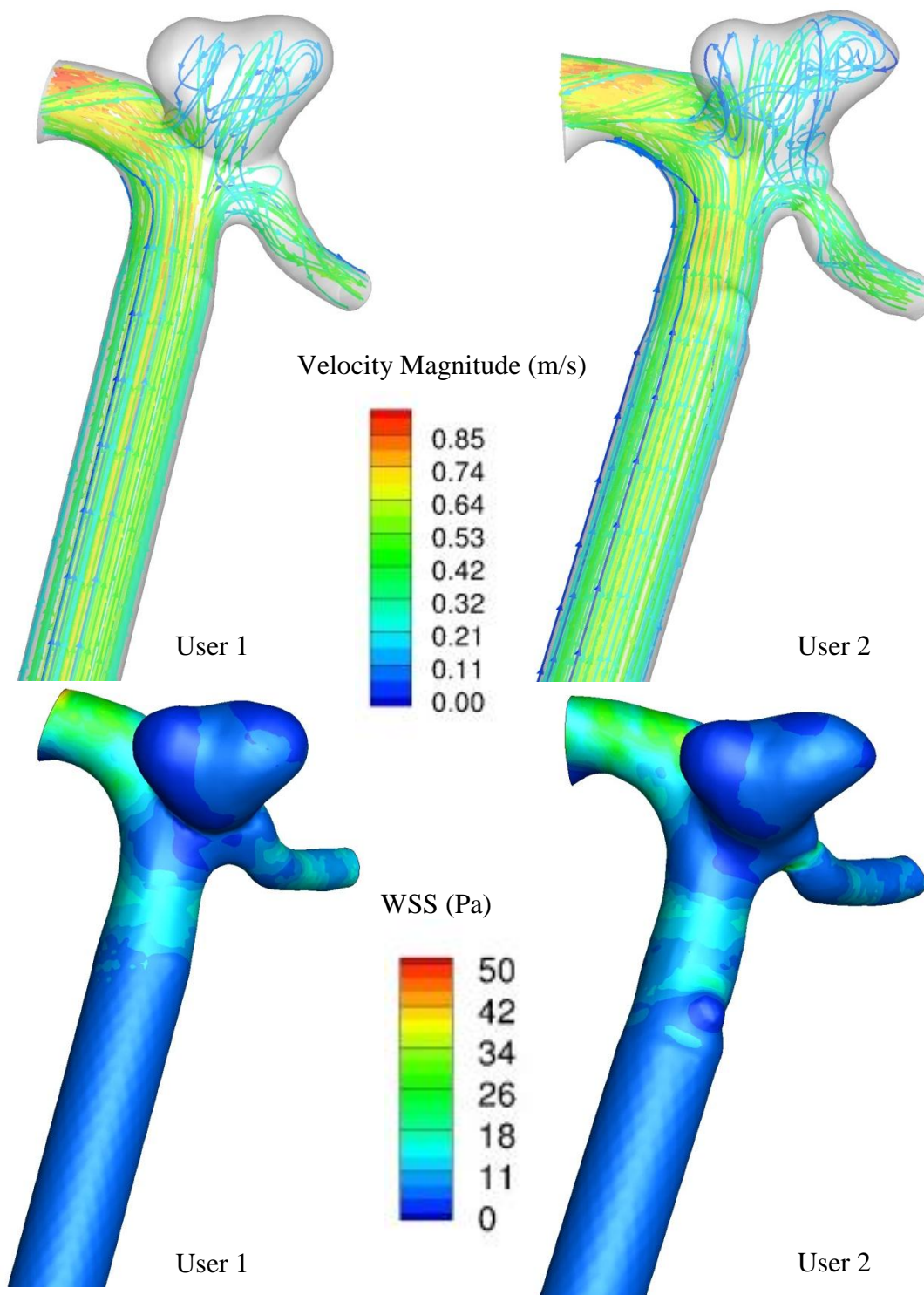
WSS (Pa)

User 1

User 2

Figure 38: Streamtraces and WSS distribution in a PCOMM aneurysm model
reconstructed by two users

In the longitudinal study with 198 aneurysms, although models reconstructed by multiple users were included, the cutting planes were chosen by a single user and kept consistent with the morphometric analysis done earlier on this population by Ramachandran et al. [17]. In order to remove any discrepancies (such as forced vessel narrowing) introduced by the user in the 3D model reconstruction process, the images for the entire patient population were reviewed by the author and an independent user. For cases where such differences were observed between the image data and reconstructed model, the reconstruction process was repeated.

<center>Statistical Analysis</center>

After the hemodynamic analysis was complete on the entire cohort, the follow up information was collected from the clinical centers. Aneurysms were divided into two groups, stable versus growth, depending on their clinical outcome status. Statistical analysis was then performed for all the computed blood flow based indices. However, an a priori hypothesis was specified: Hemodynamic behavior as quantified by LSA will be different in the unstable aneurysms as compared to the stable aneurysms. LSA has been shown to distinguish ruptured aneurysms from unruptured aneurysms in previous studies [15, 32]. Also, LSA was found to be one of the least user-sensitive indices from the user sensitivity study conducted on 10 patients (r and $\rho > 0.8$). Although other indices also correlated the two groups in the user-sensitivity study, LSA was singled out as a key index because it has a physically intuitive meaning and a fixed range (0-100%). The rest of the indices were tested in a post hoc manner. Non parametric Mann Whitney U-tests were performed to test for statistically significant difference between the stable and unstable (growth) groups.

Correlation between steady and pulsatile flow based indices was computed for the patient specific aneurysm population. Pearson product moment correlation coefficient, Spearman correlation coefficient and slope were used as the 3 statistical metrics to

determine the correlation. Correlation between the hemodynamic and basic geometric indices was also tested using the Pearson correlation coefficient.

CHAPTER 4

RESULTS

Longitudinal Study

Of the 198 study subjects that were followed for an average of 607 days, 27 were lost to follow up and 1 could not be located on the angiogram. A total of 170 aneurysms could be classified into the two groups: stable (150) versus grown (20). Out of these 150 stable aneurysms, the inlet outlet arteries of one aneurysm could not be identified and hence it was left out from the hemodynamic analysis. Another subject was found to be miscounted twice by the clinical collaborators and was also excluded from the blood flow analysis. Therefore, statistical analysis of the hemodynamic indices was performed on 148 stable subjects and 20 grown subjects. None of the aneurysms in this population went on to rupture. The study started with 200 aneurysm subjects but it later realized that one of patients was wrongly recruited and 1 not included in the follow up. Among the 198 study subjects that were followed, 53 aneurysms got electively treated during the follow up period. Figure 39 shows the distribution of stable and unstable aneurysms according to location.

Flow simulations converged for all cases but 5 (3 ICA, 1 MCA and 1 Bslar aneurysm model). In these 5 models, the steady flow simulations started diverging and did not meet the convergence criterion of $1*10^{-5}$. Since the transient analyses were fully converged for these cases, they were included in the longitudinal study but were excluded from modeling choice evaluation. The values of hemodynamic indices computed in this study were validated by comparison to results reported in the literature (Table 4). Since some of the indices are either newly proposed or improved upon in this study, their comparison could not be made. Non parametric Mann Whitney U tests were performed for all the indices to test for statistically significant differences between the stable (n1 = 148) and unstable (n2 =20) group. In some subjects, computation of LSCI and SCI

resulted in indeterminate values. Therefore, the sample sizes used in the Mann Whitney u test were reduced to n1 =145 for LSCI and n1 =88 and n2 =12 for SCI. Results from the statistical analysis indicate that LSA which was hypothesized as a predictor of rupture risk in this study was not found to differentiate stable aneurysms from unstable aneurysms in a statistically significant manner. As seen in Table 5, none of the other indices that were tested in a post hoc manner distinguished the two groups with statistical significance.
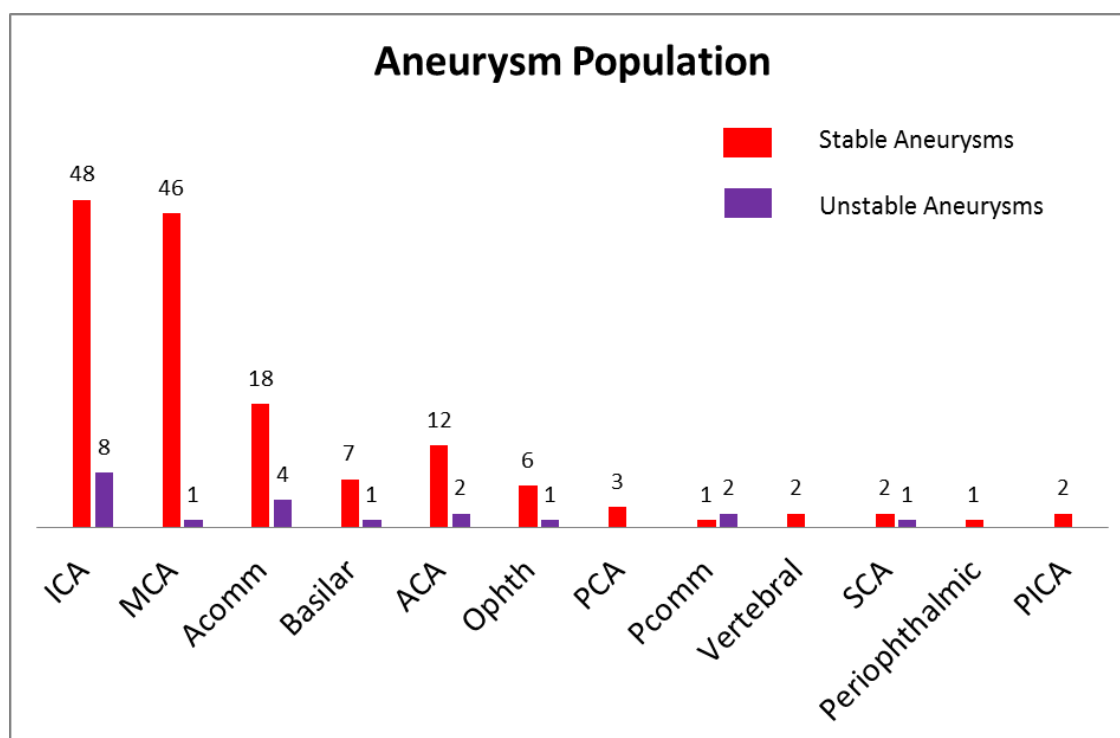

Figure 39: Distribution of stable and unstable aneurysms based on their location in the cerebral vasculature

Table 4: Comparison of the computed hemodynamic indices to literature[2]

Indices	Literature Values	Study Average (198 patients)
ICI	Cebral et al. [31]– Ruptured 1.012, Unruptured 0.66	1.115
WSS_{ave}	Jou et al.[32]–Ruptured 1.9 Pa, Unruptured 2.6 Pa (Diastole), Valencia et al. [63]- 25.3 Pa (Peak Systole), Qian et al. [33] --Unruptured aneurysms – 2.86 +/-0.63 Pa, Takao et al. [64] –Ruptured 5.104 Pa (ICA) 6.139 Pa (MCA) Unruptured 5.189 Pa (ICA) 5.349 Pa (MCA)	6.835 Pa
WSS_{max}	Ma et al.[65] – 24.25 Pa, Cebral et al.[31] –Ruptured 38.4 Pa, Unruptured 27.7 Pa	36.585 Pa
OSI	Takao et al. [64] Ruptured 0.00976 (ICA) 0.0102 (MCA), Unruptured 0.0128, Xiang et al. [15] –Ruptured 0.016+/-0.031, Unruptured 0.0035+/- 0.0044	0.009
LSA*	Xiang et al. [15] –Ruptured 0.38+/-0.31 Unruptured 0.10+/-0.21, Cebral et al. [31] –Ruptured 60 % Unruptured 56%	50.9
KER	Cebral et al. [31] –Ruptured 0.232 Unruptured 0.176	0.253
VDR	Cebral et al. [31] –Ruptured 0.36 Unruptured 0.951	0.441
DP_{ave}*	Ma et al.[65] 0.12 mm Hg	1.693mmHg
DP_{max}*	Ma et al.[65] 0.49 mm Hg	2.253mmHg

---

[2] * indicates that the literature used a different definition to compute the index

Table 5: Median values of indices for the stable and unstable group are presented.[3]

Indices	Median (Stable) n1 =148	Median (Unstable) n2 =20	Mann Whitney U test p-value
WSS_{ave} (Pa)	4.720	4.461	0.789
WSS_{max} (Pa)	24.828	31.7645	0.190
WSS_{99}(Pa)	17.873	19.133	0.345
LSA (%)	**51.739**	**68.997**	**0.488**
HSA (%)	0.132	0.279	0.766
LSCI*	0.489	0.542	0.622
SCI*	3.863	3.723	0.978
$WSSG_{ave}$(Pa/m)	8761	9741	0.591
$WSSG_{max}$(Pa/m)	116700	147925	0.374
$WSSG_{99}$(Pa/m)	53365	72100	0.175
KER	0.188	0.181	0.529
VDR	0.255	0.154	0.733
DP_{ave} (mm Hg)	0.938	0.976	0.939
DP_{max} (mmHg)	1.396	1.295	0.693
ICI	0.798	0.718	0.595
VL (mm)	2.71	2.67	0.920
RT (s)	0.046	0.037	0.838

---

[3] P-values obtained from the Mann Whitney U test are also shown. (* LSCI and SCI used different sample sizes for the statistical test)

Histograms depicting the frequency distribution of a few key indices across the patient populations are shown in the following figures.
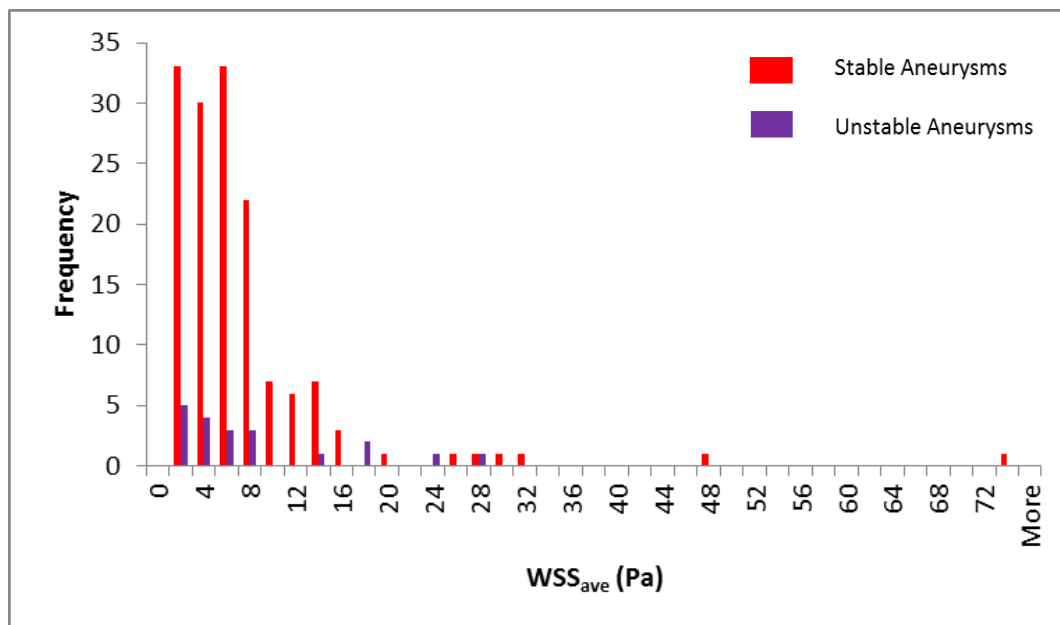

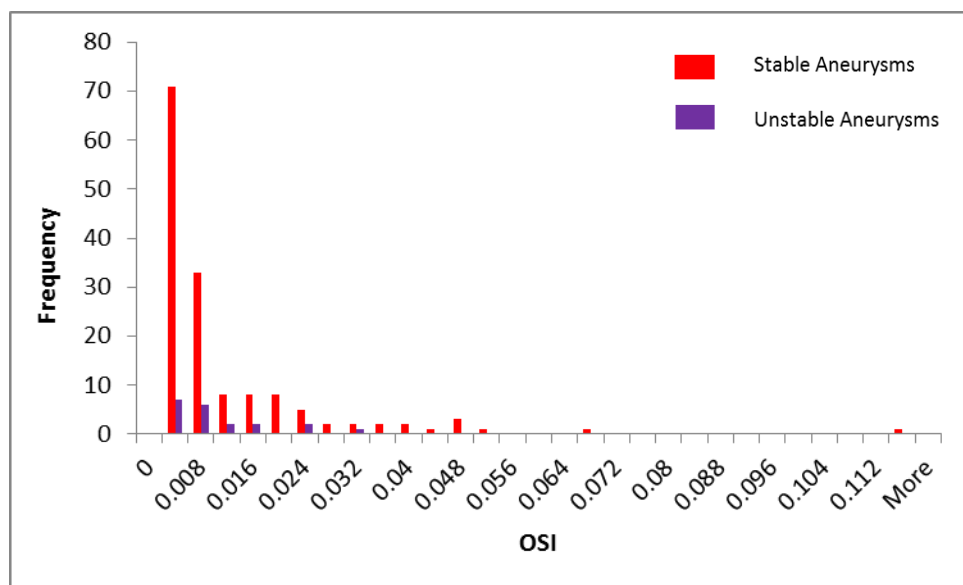Figure 40: Distribution of WSSave across the patient population

Figure 41: Distribution of OSI across the patient population
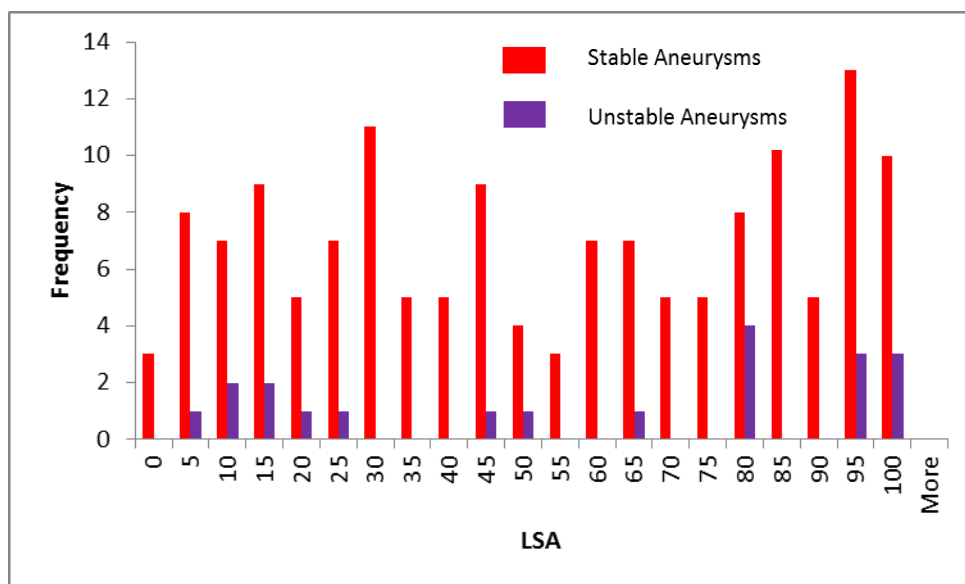
Figure 42: Distribution of LSA across the patient population
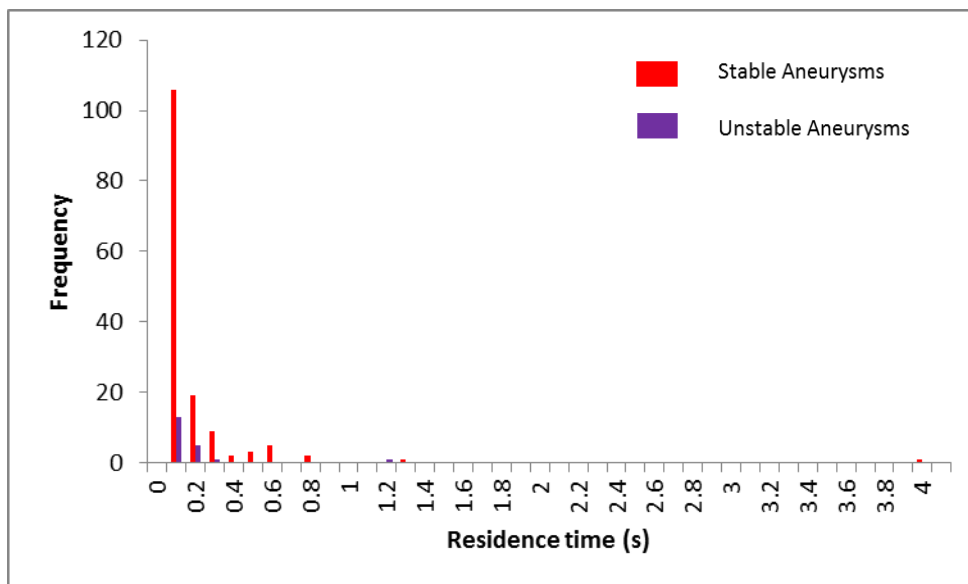
Figure 43: Distribution of residence time across the patient population
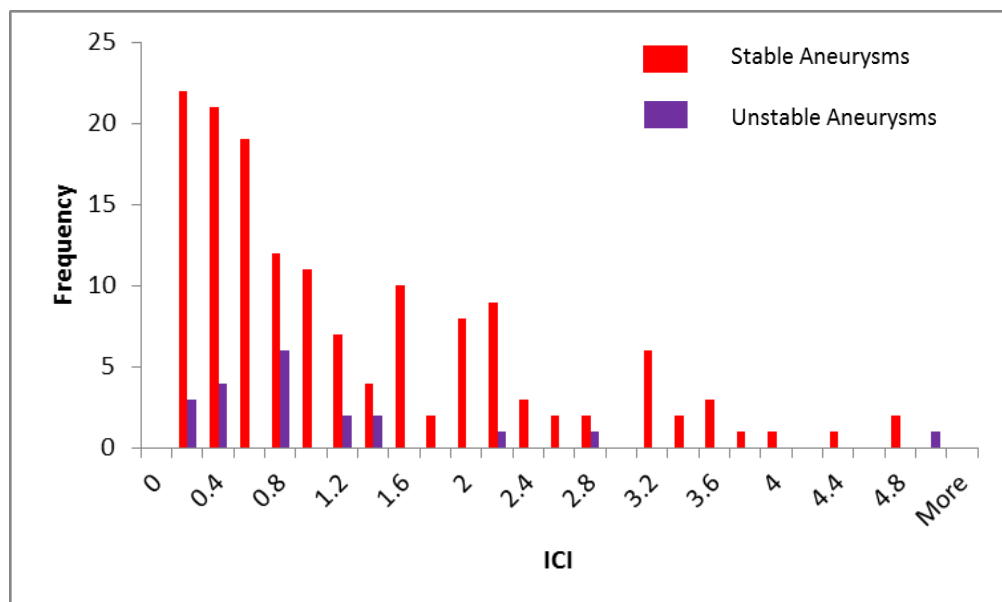
Figure 44: Distribution of ICI across the patient population
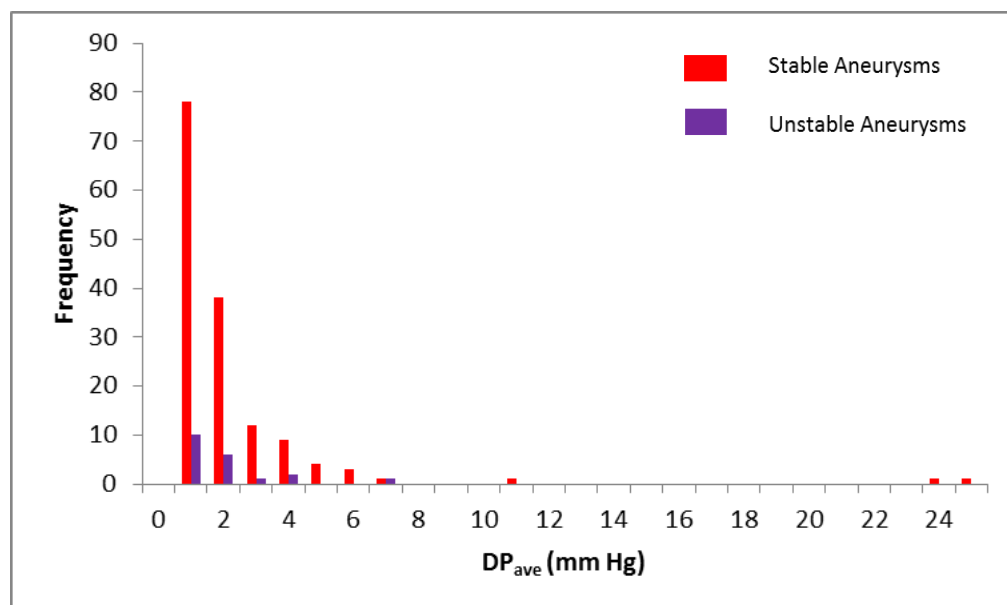
Figure 45: Distribution of DPave across the patient population

<u>Role of Modeling Choices</u>

All the indices showed a linear relationship between steady and pulsatile flow based estimations with a very strong correlation and near identical ranking (Figure 46, Figure 47 and Table 6). WSS distribution along with region of low wall shear area computed by steady and pulsatile flow analysis is shown in Figure 48 for 4 stable and 2 unstable representative cases. Streamtraces depicting the flow patterns estimated by steady and time-averaged pulsatile flow simulations are shown for 4 stable and 2 unstable aneurysms and their contiguous vasculature in Figure 49.
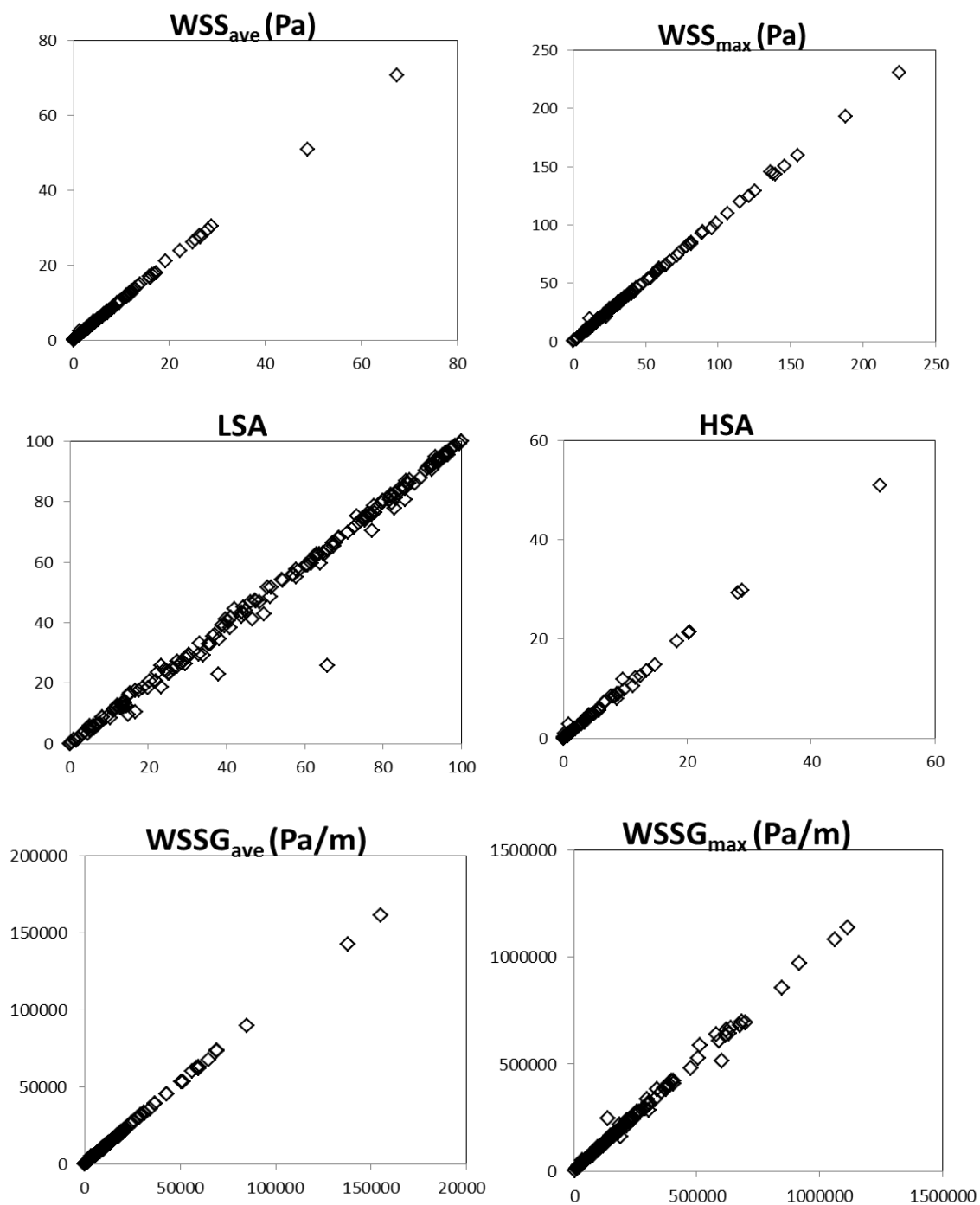
Figure 46: Correlation between steady (x-axis) and time-averaged pulsatile flow (y-axis) analysis for WSS based indices.
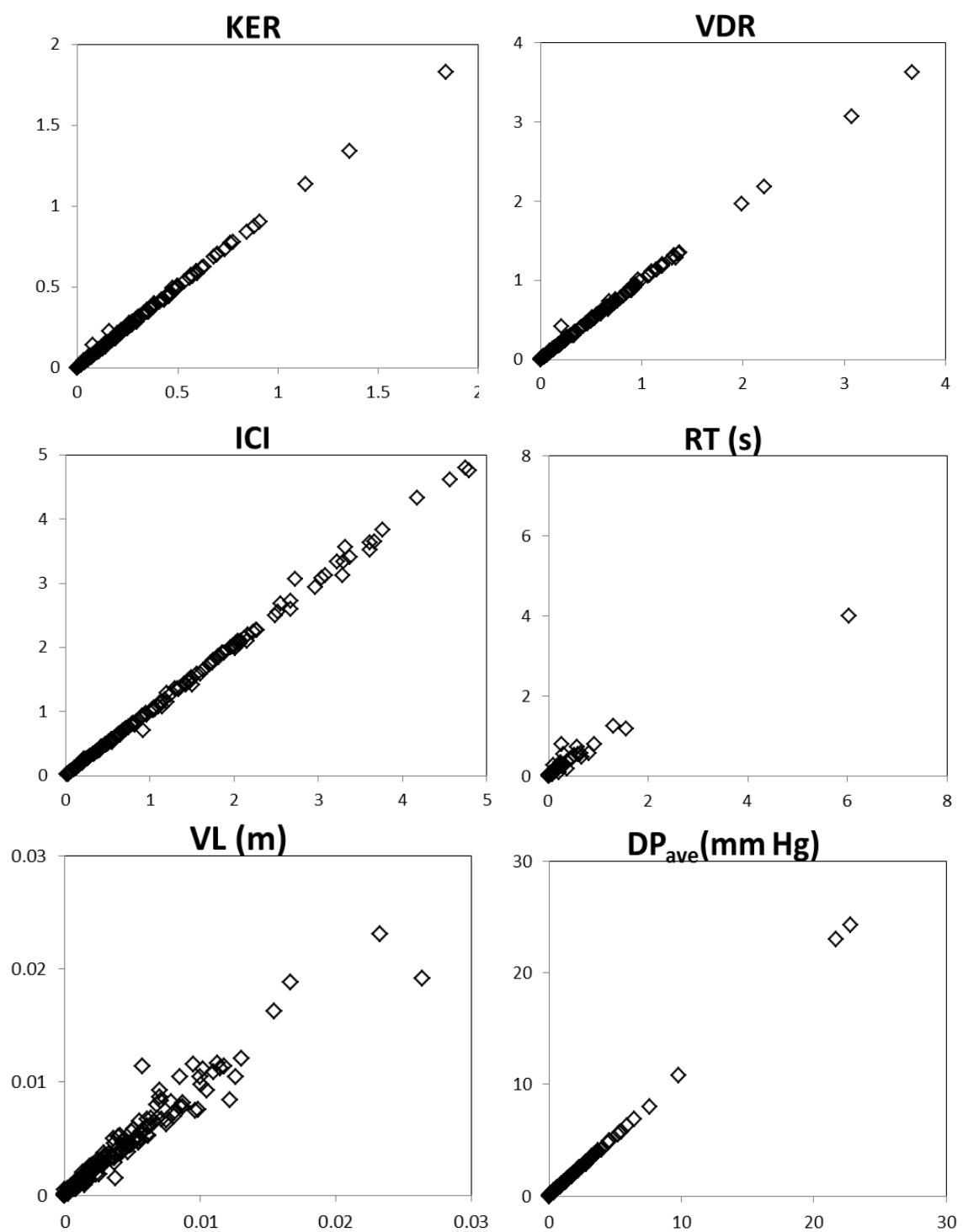
Figure 47: Correlation between steady and time-averaged pulsatile flow analysis for energy, sac flow and pressure based indices

Table 6: Statistical metrics for all the hemodynamic indices[4]

Index	Pearson Correlation (r)	Spearman Correlation (ρ)	Slope (k)
WSS_{ave}	0.9998	0.9992	1.0505
WSS_{max}	0.9997	0.9983	1.0320
WSS_{99}	0.9998	0.9994	1.0395
LSA	0.9948	0.9954	0.9990
HSA	0.9987	0.9908	1.0208
LSCI	0.9931	--*	0.9857
SCI	0.9943	--*	0.9139
$WSSG_{ave}$	0.9998	0.9991	1.0471
$WSSG_{max}$	0.9975	0.9981	1.0236
$WSSG_{99}$	0.9997	0.9991	1.0362
KER	0.9994	0.9983	0.9923
VDR	0.9993	0.9988	0.9874
DP_{ave}	0.9999	0.9995	1.0676
DP_{max}	0.9997	0.9987	1.0690
ICI	0.9991	0.9994	1.0110
VL	0.9713	0.9841	0.9292
RT	0.9752	0.9644	0.6777

---

[4] * indicates that no spearman correlation could be obtained as some subjects had indeterminate values of these indices
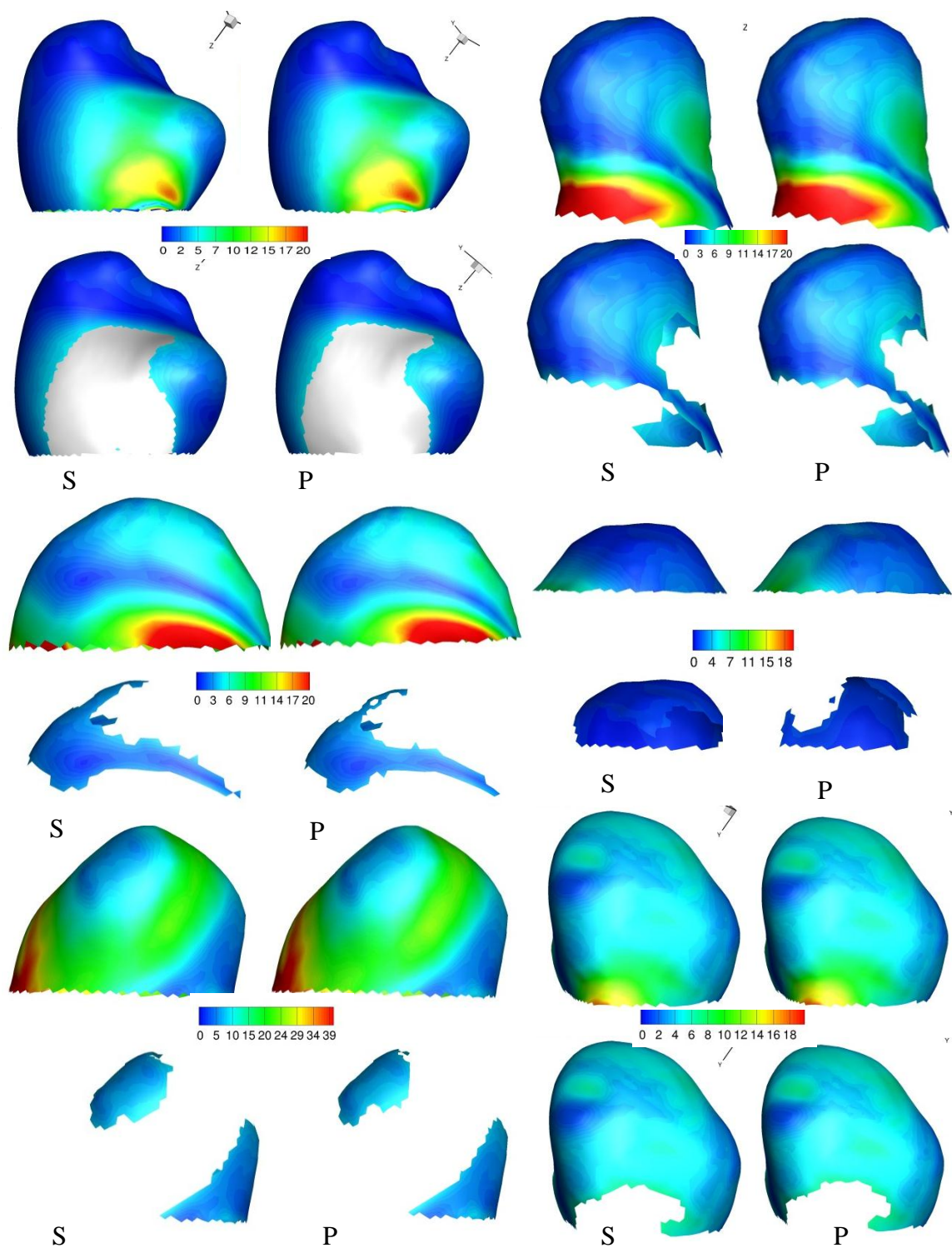
Figure 48: WSS (Pa) and LSA estimated by steady (S) and pulsatile (P) flow analysis for 4 stable (1st and 2nd row) and 2 unstable (3rd row) aneurysms
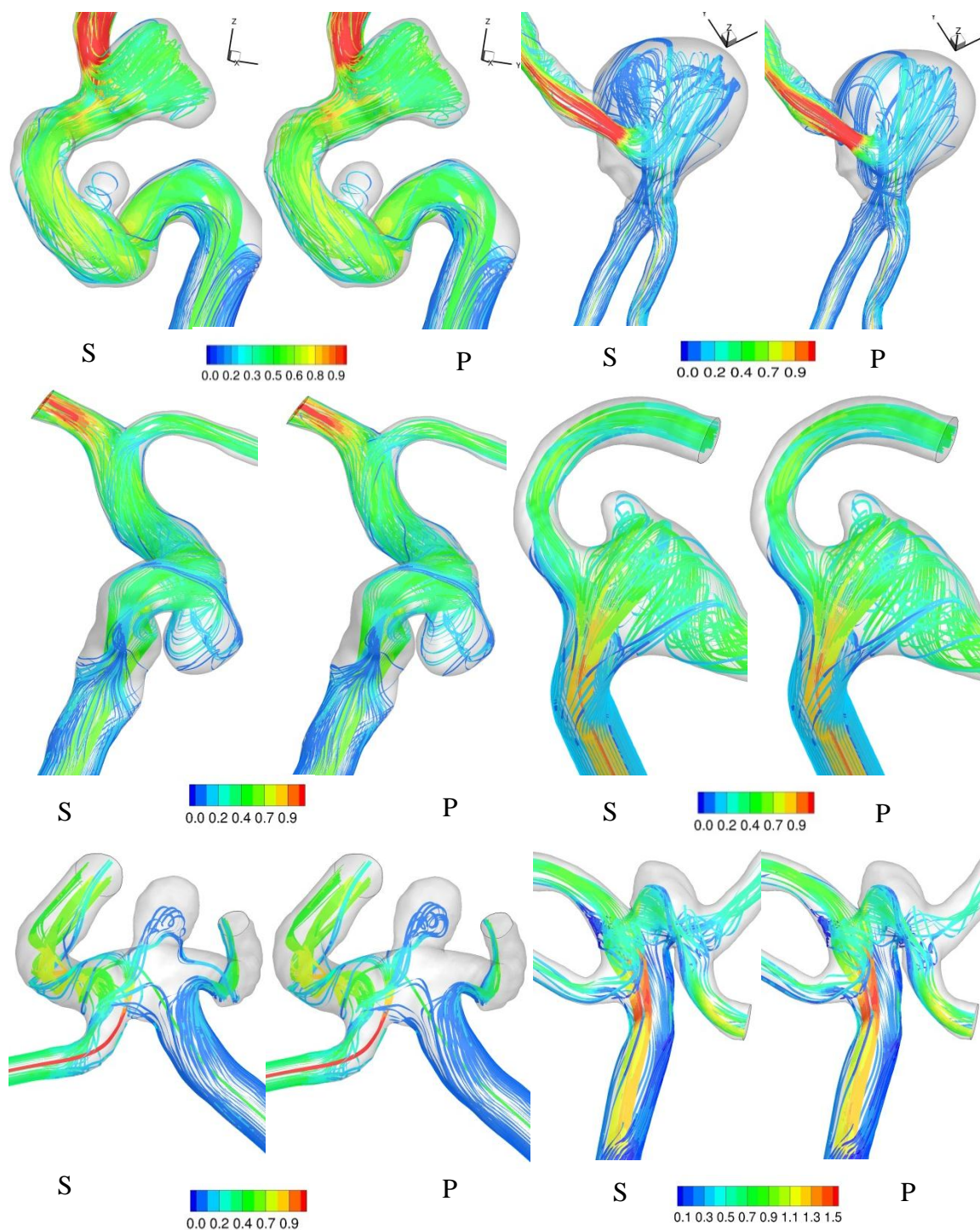
Figure 49: Streamtraces with velocity contours (m/s) computed by steady (S) and pulsatile (P) flow analysis for 4 stable (1st and 2nd row) and 2 unstable (3rd row) aneurysm models

Morphometric - Hemodynamic Correlation

In order to determine the correlation between the hemodynamic and basic morphometric indices (Height -H, Diameter -D_{max}, Surface Area -S and Volume -V), a Pearson correlation coefficient was calculated. The morphometric indices for the patient population were calculated by Ramachandran et al. [17]. It was found that there exists no strong correlation between the geometric indices and the blood flow based indices. Out of the 25 different hemodynamic indices, only VL showed a mild positive correlation to H (r = 0.76) and V (r =0.72).
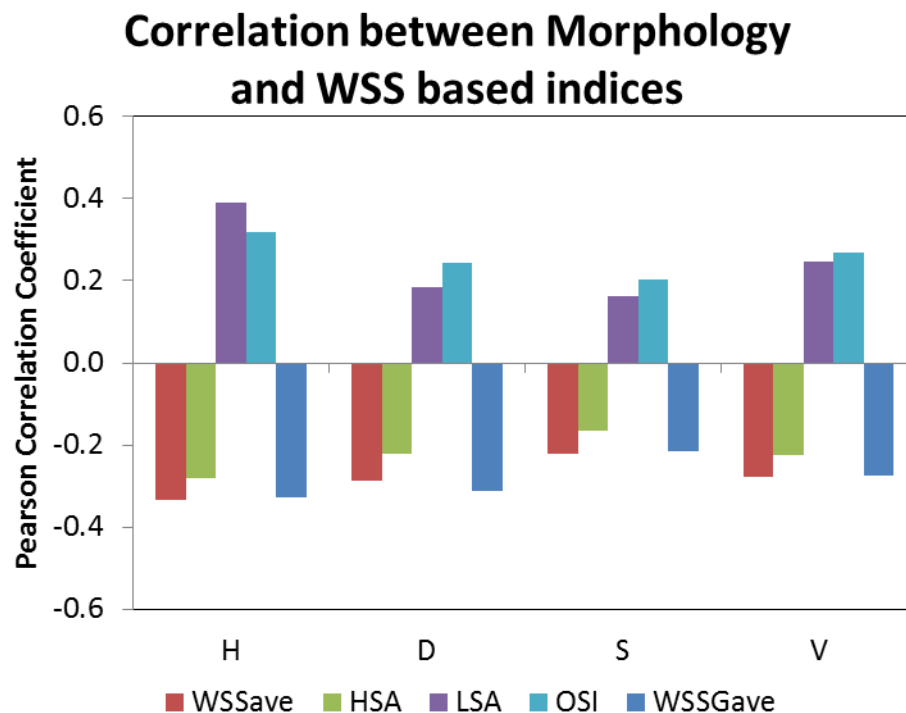
Figure 50: Correlation between the WSS based indices and the geometric indices
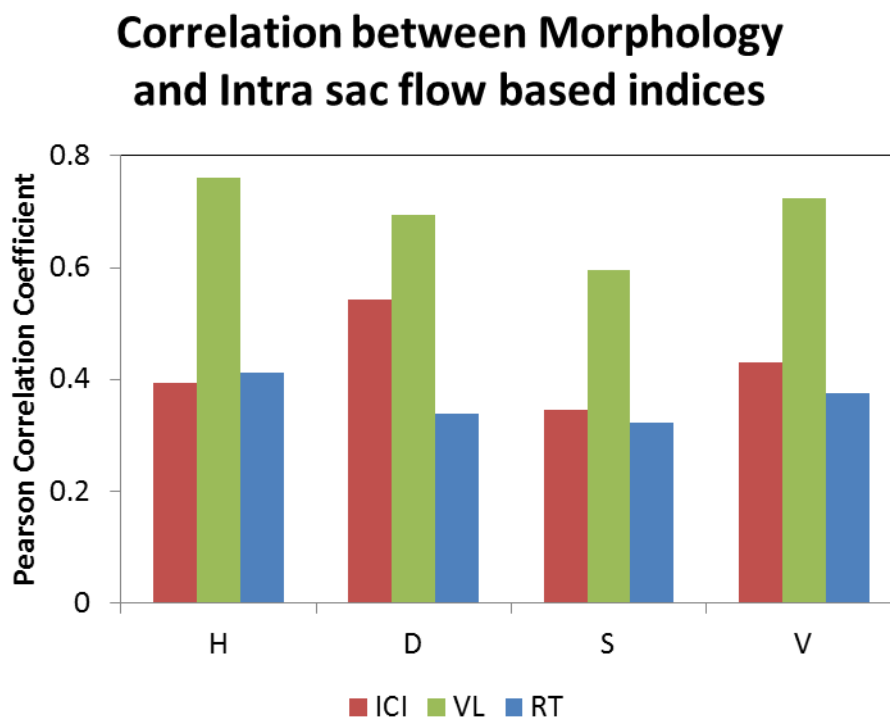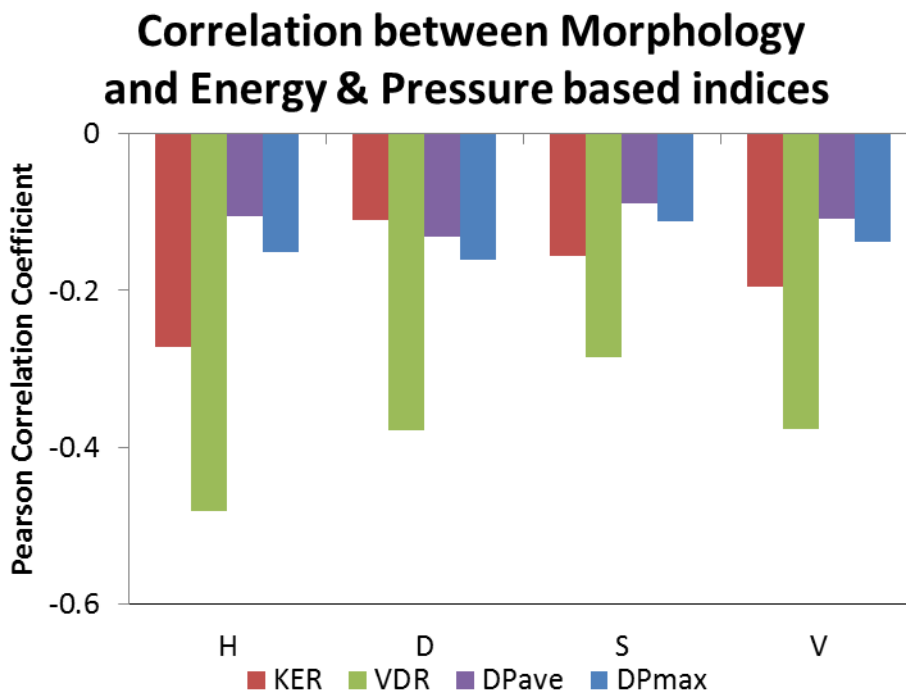
Figure 51: Correlation between Energy and pressure based indices and geometric indices (top). Correlation between intra sac flow based indices and geometric indices (bottom)

Correlations among the hemodynamic indices were also sought. It was found that correlations existed only between indices that are grouped under one category (WSS based, energy based etc.). WSS based indices, LSA and HSA, are the only indices that correlated (outside their group) to energy based indices. However, the correlation between them was weak (Figure 52). The indices that did not correlate to any other index even in their own group are: OSI, ICI and RT.

Correlation between WSS and Energy based indices
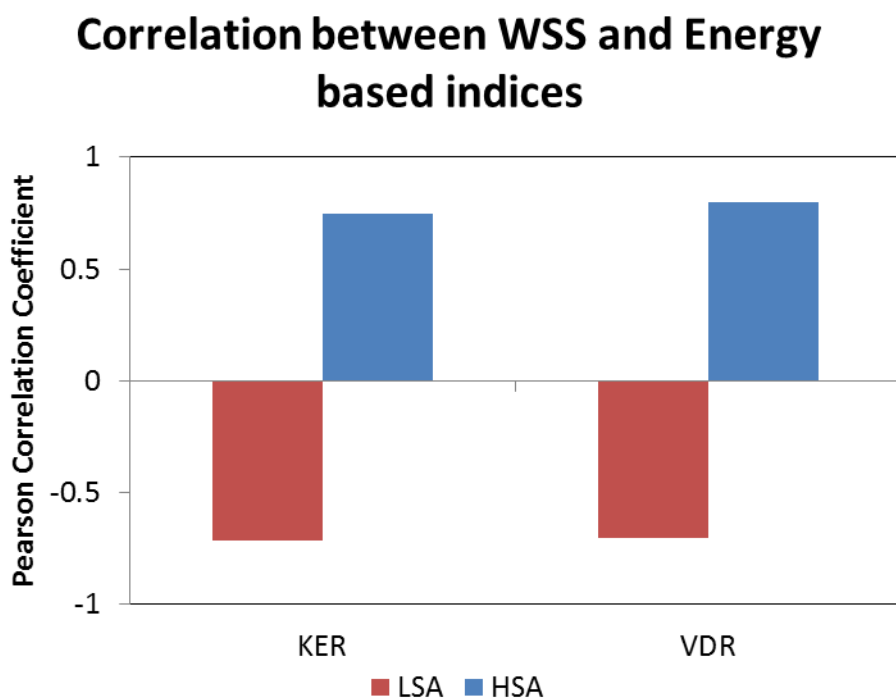
Figure 52: Bar chart depicting weak correlation between abnormal shear area and energy based indices

CHAPTER 5

DISCUSSION

In the current work, the hypothesis that blood flow based indices can be used to predict the longitudinally rupture risk of intracranial aneurysms was tested on a cohort of 198 subjects. Since blood flow behavior has been shown to play a crucial role in the initiation of aneurysms, it is logical to speculate that hemodynamic indices could be used as prognostic indicators of the growth or rupture risk of aneurysms. The implication of such a finding would be a significant improvement in the clinical management of patients diagnosed with unruptured intracranial aneurysms. Quantified blood flow behavior can then be used to distinguish aneurysms that are on a high rupture risk and need an immediate aggressive treatment while the stable aneurysms can be placed on a more relaxed follow up schedule.

In order to test the above-mentioned hypothesis, a unique study was designed. Patients that presented with unruptured intracranial aneurysms and were placed on a watchful waiting strategy by doctors were prospectively recruited for this study. Several research groups have retrospectively studied the relative hemodynamic differences between ruptured and unruptured aneurysm population. However, their results are all based on the assumption that shape of the aneurysm does not change post rupture. Moreover, differences between ruptured and unruptured aneurysms may not necessarily translate to differences between unruptured aneurysms that fork towards growth/rupture and stable unruptured aneurysms. This is especially significant because even though the number of patients presenting with ruptured aneurysms to patients presenting with unruptured aneurysms in a clinical setting is approximately equal, the rupture rate for patients with unruptured aneurysms followed over a course of period is just about 1%. This conundrum suggests that aneurysms which fork towards growth or rupture fall into a different category and hence need to be studied independently. The current study is the

first that directly addresses the dilemma that clinicians face when patients present themselves with unruptured intracranial aneurysms. It is also the first to recruit patients from multiple clinical centers. Involvement of multiple centers allowed for averaging of physician specific selection bias and hence made the study population representative of the general population. Collection of patient images from multiple scanning modalities also added realism to the procedure.

To quantify the intra-aneurysm hemodynamics, the prominent indices published in the literature so far were used for this population. Although retrospective studies have previously quantified aneurysm hemodynamics using several indices, a holistic analysis was lacking. By collating and documenting the prominent indices in the aneurysm hemodynamic literature, the current study captured all the unique blood flow characteristics for this population. Pipelining of the entire mesh generation and the index calculation process provided an efficient way of performing the CFD analysis of the patient specific geometries. Use of a supercomputing cluster for CFD simulation proved as an effective way of saving the computational time for a large population study like this. Assessment of the modeling choices implemented in a CFD simulation provided a simpler, cheaper and faster alternative that can be used in future. The findings of this work are discussed in detail below:

<u>Hemodynamics as a Rupture Risk Indicator</u>

It was hypothesized that blood flow based indices can be used as prognostic indicators of rupture risk in intracranial aneurysms. LSA was singled out as a key hemodynamic index to test this hypothesis. However, LSA was not found to be statistically different in between aneurysms that went on to grow and become unstable and those that remained stable (p =0.488). Rest of the hemodynamic indices that were tested in a post hoc manner did not differentiate stable from unstable aneurysms either. Therefore, results of this study are not consistent with the hypothesis that the

hemodynamics is different in aneurysms that will become unstable compared to those that remain stable and hence are predictive of clinical outcome.

Previous studies that have focused on identifying hemodynamic indices that differentiate ruptured from unruptured aneurysms are mainly based on 2 different schools of thoughts: high flow theory and the low flow theory. Xiang et al.[15] found that the maximum WSS was lower in ruptured aneurysms than unruptured aneurysms. Their results indicated that slow, recirculating and oscillatory flow in the ruptured aneurysms lead to lower values of mean and maximum WSS and high values of OSI. On the contrary, Cebral et al.[31] found that ruptured aneurysms had higher maximum WSS, larger ICI, VDR and SCI than the unruptured aneurysms and hence suggested that concentrated rapid flow activity is correlated to aneurysms rupture status. Although the present study focusses on a different breed of aneurysms, the general hemodynamic behavior of unstable aneurysms did not confine to any one of these two theories. Results of the present study indicate that the mean and median values of WSS_{max} in unstable aneurysm population are higher than those in the stable aneurysm population. Counter intuitively, the LSA was also found to be higher in aneurysms that went on to instability than those that remained stable. However, neither of these differences achieved statistical significance in this study.

In order to qualitatively visualize and compare the hemodynamic environment in unstable aneurysms to those that remained stable, a size and location matched control group was chosen from the stable aneurysms. If a perfect match was not found, then the closest possible match was chosen from the stable group. WSS distribution in representative unstable aneurysms and their control counterparts is shown in Figure 53 and Figure 54. As seen in Figure 53, WSS distribution seems to be higher in the unstable cases as compared to their controls. However, this is not consistently true in the unstable aneurysms in Figure 54. For the Ophthalmic, ACA and SCA aneurysm cases, the adjacent vessels have larger WSS than the vessels in their unstable counterparts but the

aneurysm WSS appears similar. WSS distribution in the unstable ACOM aneurysm
seems to be higher than its control counterpart. When scatter plots comparing WSS_{max}
and LSA in the unstable aneurysms to their stable controls were obtained, the data points
did not consistently lie above or below the 45° line (Figure 55). This is consistent with
the subjective observation that while some unstable aneurysms have higher WSS_{max} and
LSA than their stable control, others have lower values of these parameters than their
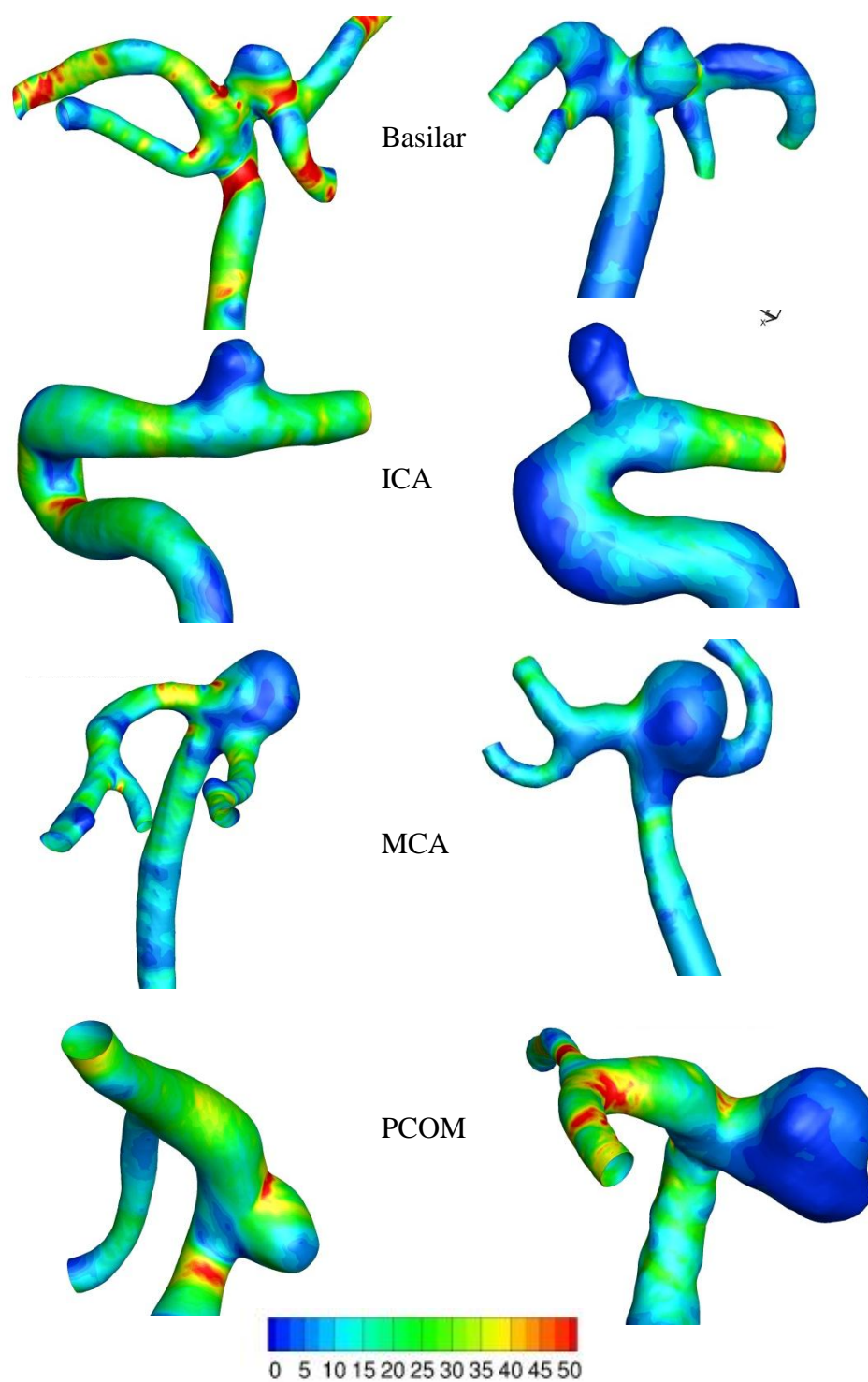stable counterparts.

Figure 53: Time-averaged WSS distribution in unstable aneurysms (left) at Basilar, ICA, MCA and PCOM and their controls (right)
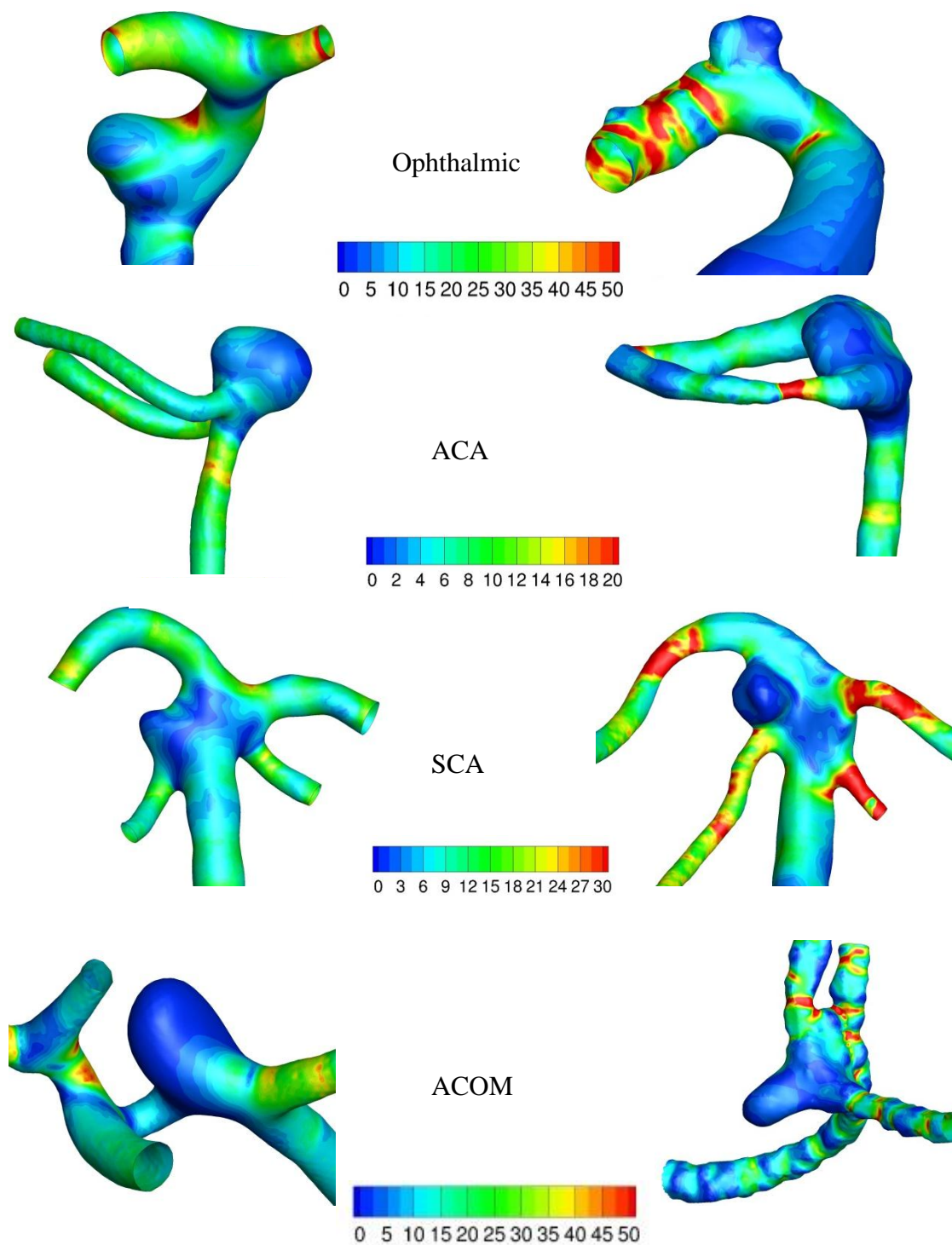
Figure 54: Time-averaged WSS distribution in unstable aneurysms (left) at Ophthalmic, ACA, ACOM and SCA and their controls (right)
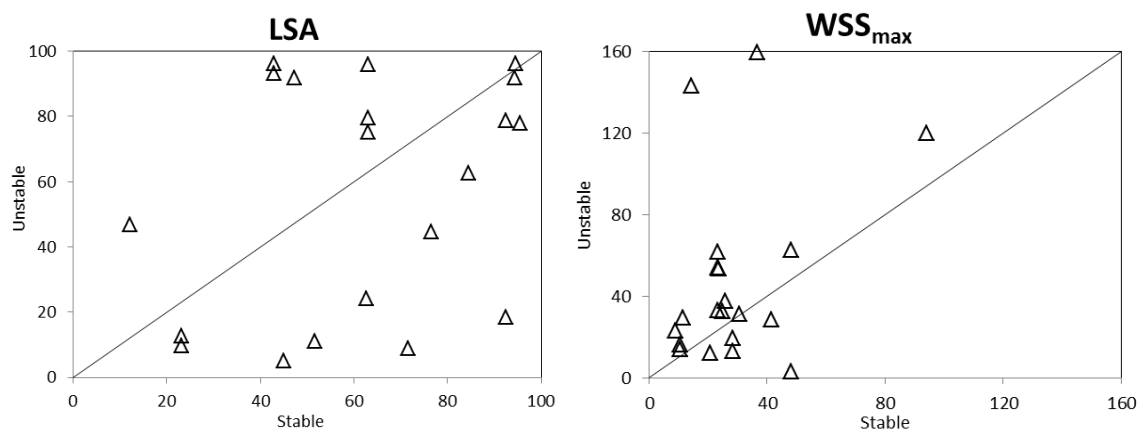
Figure 55: Comparison of LSA and WSS_{max}(Pa) in unstable aneurysms and their controls

Qualitative comparison of the flow patterns in the 20 unstable aneurysms and their stable counterparts is provided in subsequent figures. Streamtraces colored with velocity contours are used to depict the time-averaged flow behavior. Out of the 20 unstable cases, 6 had simple flow patterns with single vortices whereas 14 had complex flow patterns with multiple vortices in the aneurysm. Ten unstable cases were observed to have higher velocities in the aneurysm than their stable counterparts (Figure 56 - Figure 60) whereas 4 of them had lower aneurysmal velocities as compared to their stable matches (Figure 61-Figure 62). In 6 of the cases, the distribution of velocities appeared similar in between the two groups (Figure 63-Figure 65). In the group of aneurysms that went on to grow, both jet like flow (Figure 56) and slow oscillatory flow patterns (Figure 62) could be observed. These inconsistencies manifested themselves in the quantitative analysis where no hemodynamic index was found to be statistically different in between the two groups.

This study was designed to directly address the dilemma that clinicians face when a patient presents with an unruptured intracranial aneurysm. Using the information

available from the first scan of a patient, could hemodynamics be used to predict whether the aneurysm will grow or go on to rupture? This was the question that we sought to answer in this study. If this study population is representative of the general population, our results are not consistent with the hypothesis that hemodynamic based indices can be used to predict aneurysm instability.

Figure 56: Streamtraces with velocity contours (m/s) in 2 unstable ICA aneurysms (left) and their stable controls (right)

Figure 57: Streamtraces with velocity contours (m/s) in unstable Basilar and ICA
aneurysms (left) and their stable controls (right)

Figure 58: Streamtraces with velocity contours (m/s) in 2 unstable ICA aneurysms (left) and their stable controls (right)

Figure 59: Streamtraces with velocity contours (m/s) in unstable MCA and Ophth aneurysms (left) and their stable controls (right)

Figure 60: Streamtraces with velocity contours (m/s) in unstable ACA and PCOM aneurysms (left) and their stable controls (right)

Figure 61: Streamtraces with velocity contours (m/s) in unstable AComm aneurysms (left) and their stable controls (right)

Figure 62: Streamtraces with velocity contours (m/s) in unstable ICA and PComm
aneurysms (left) and their stable controls (right)
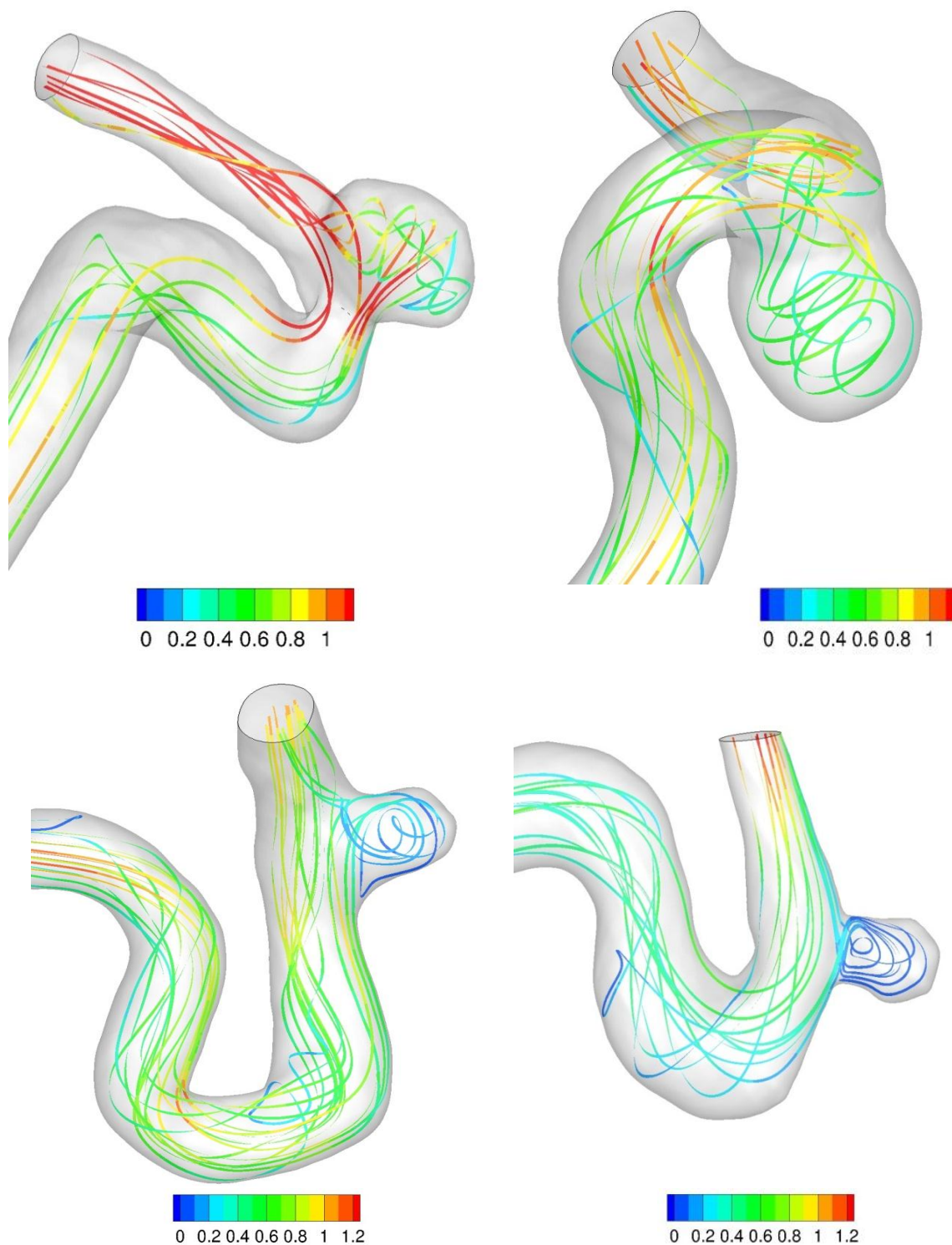
Figure 63: Streamtraces with velocity contours (m/s) in unstable ICA and SCA aneurysms (left) and their stable controls (right)
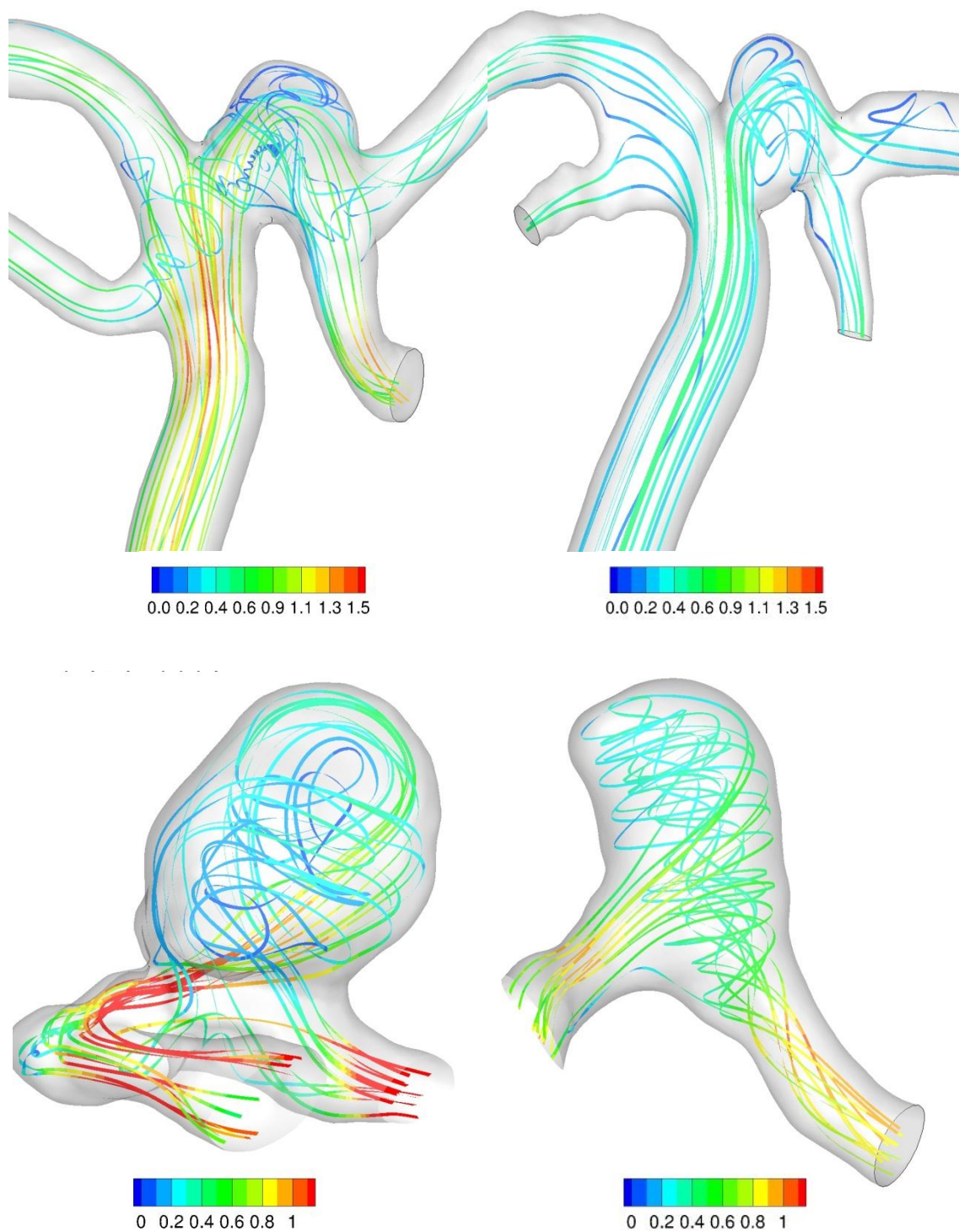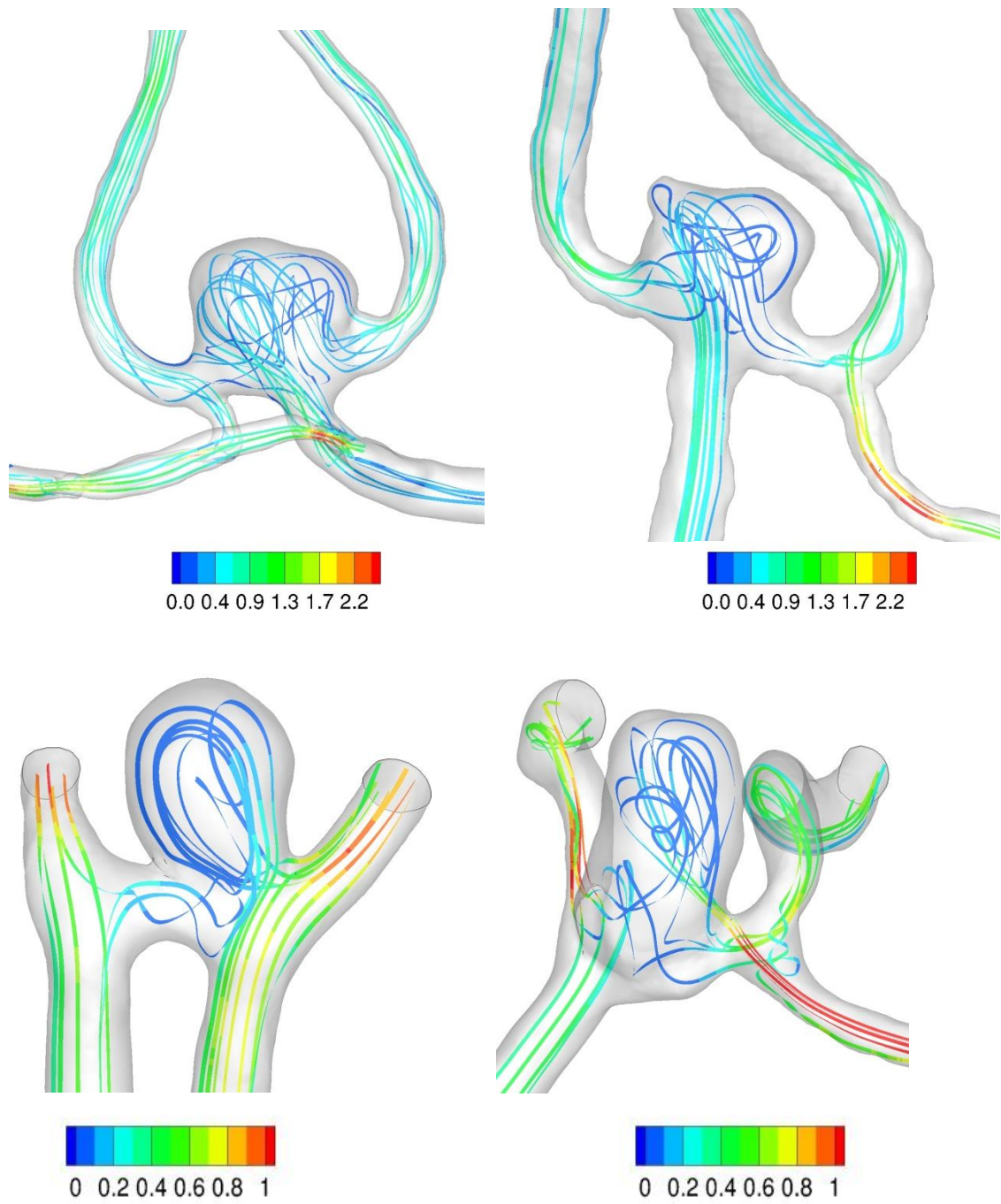
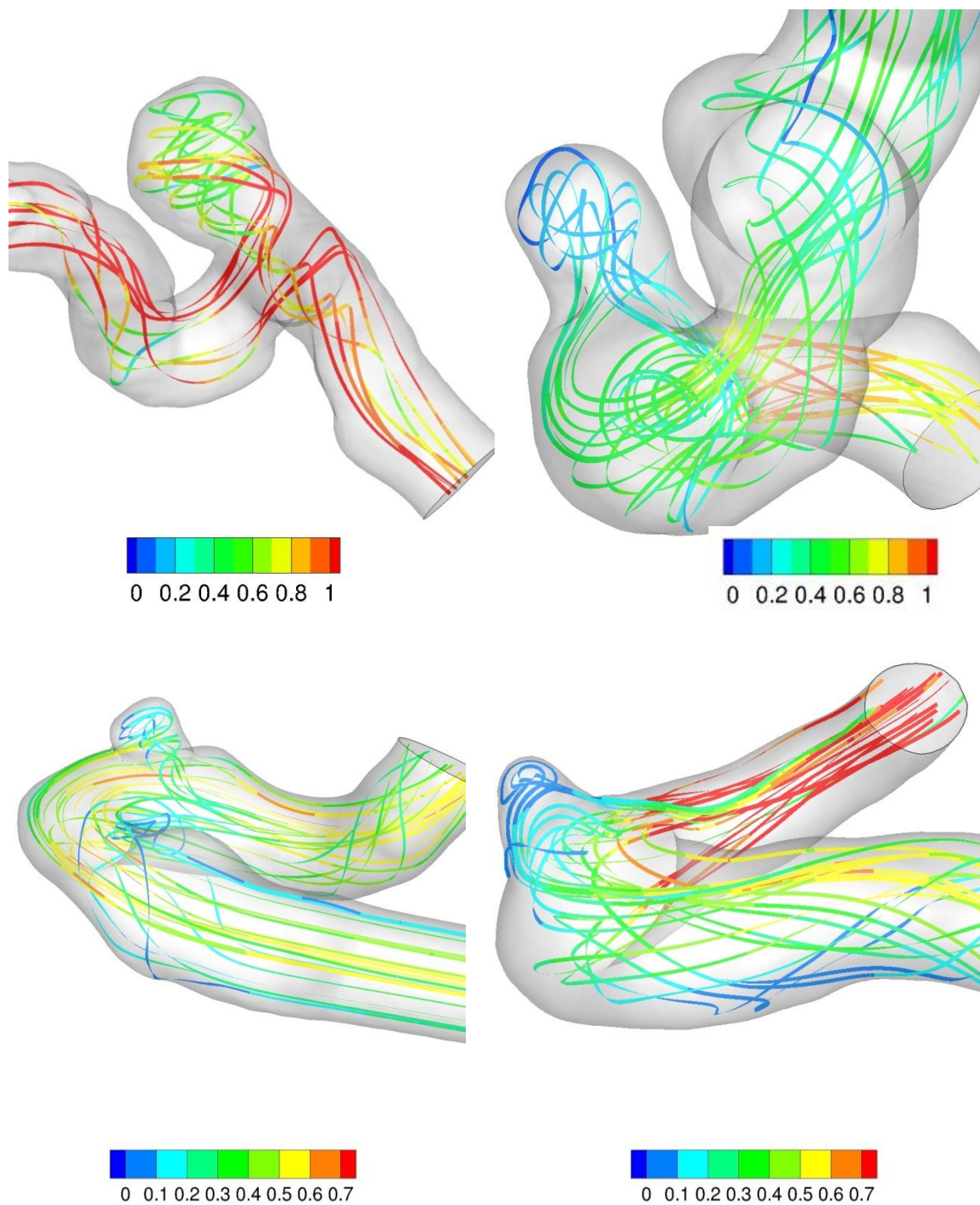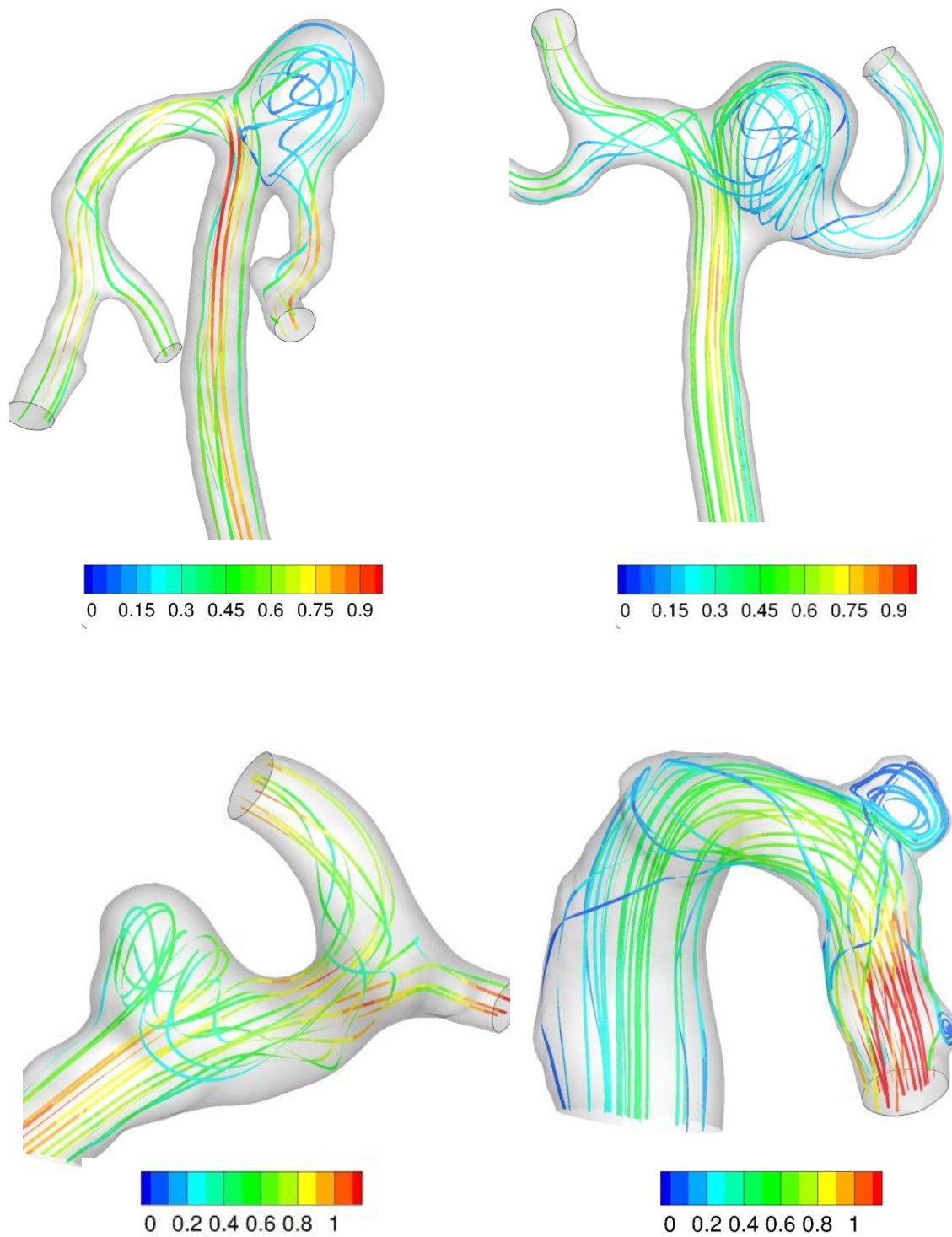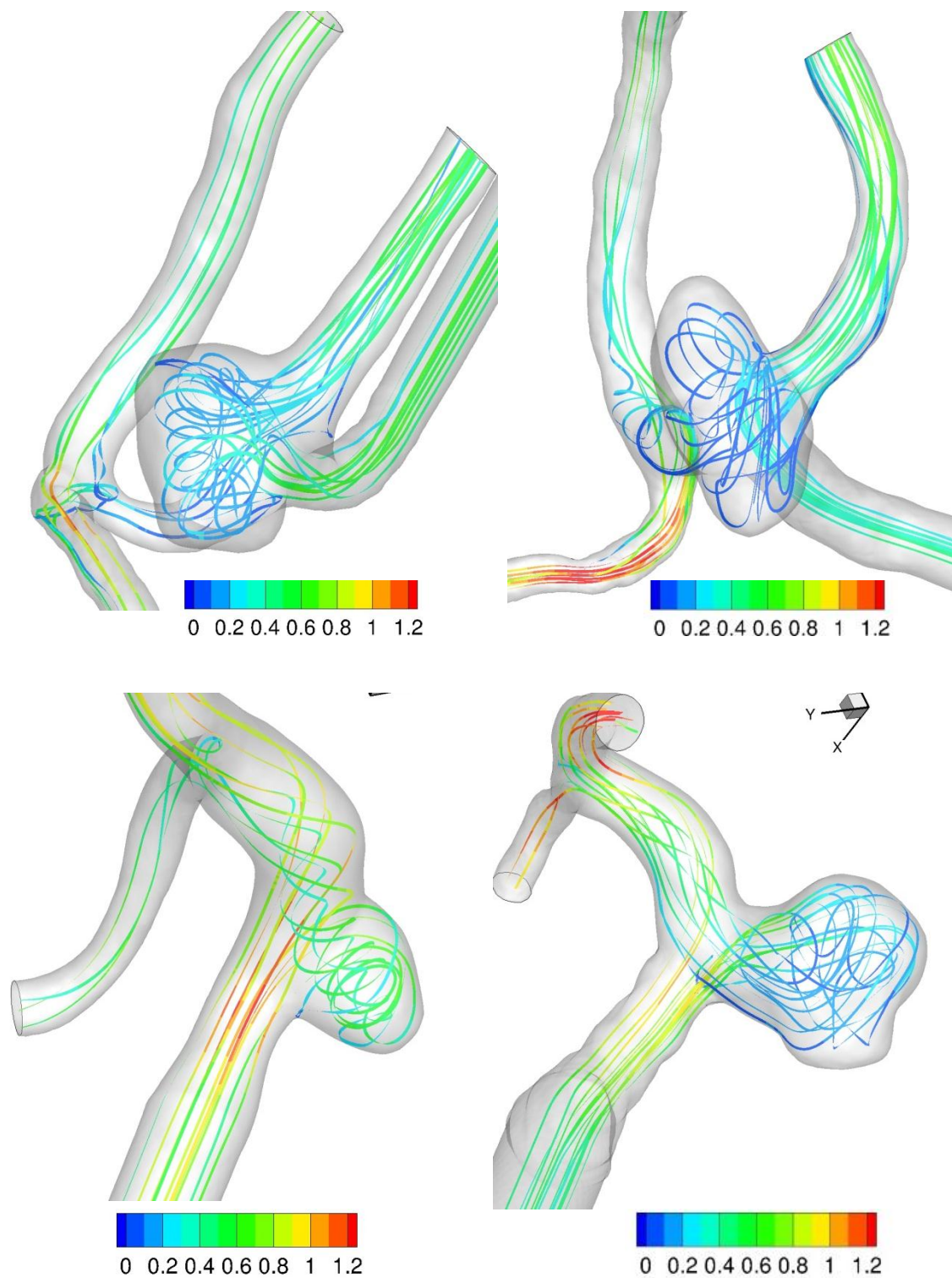Figure 64: Streamtraces with velocity contours (m/s) in unstable Acomm and ACA
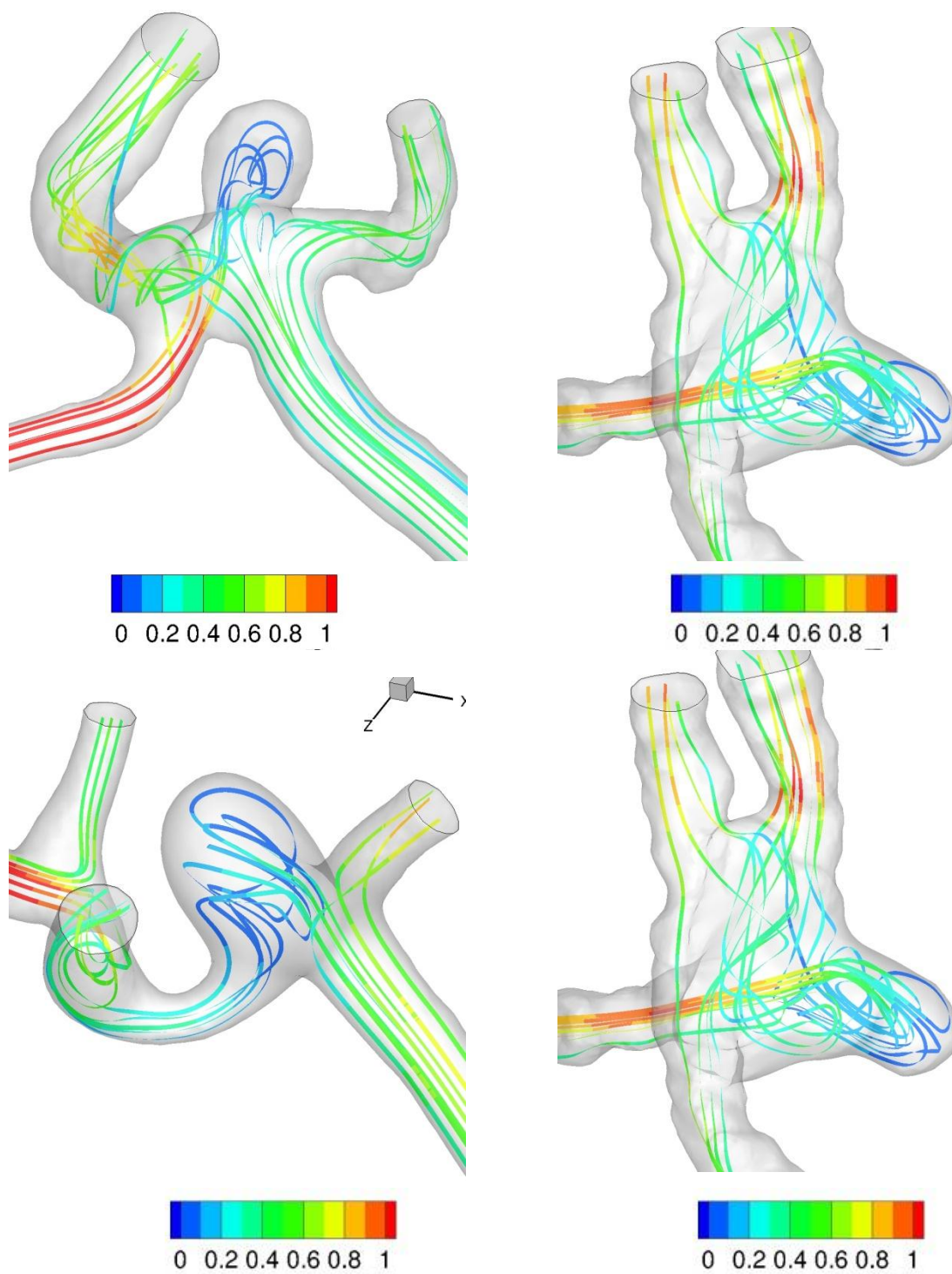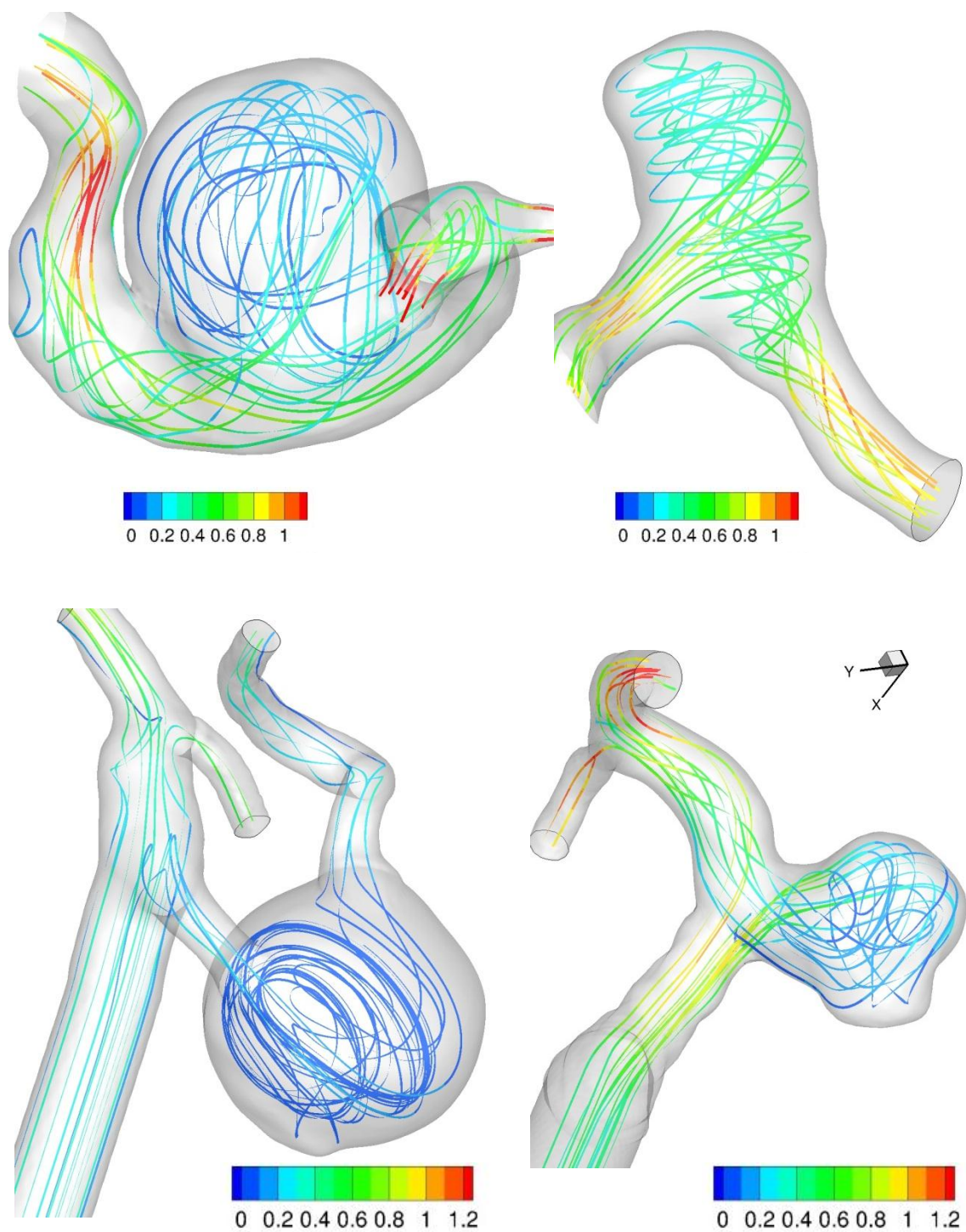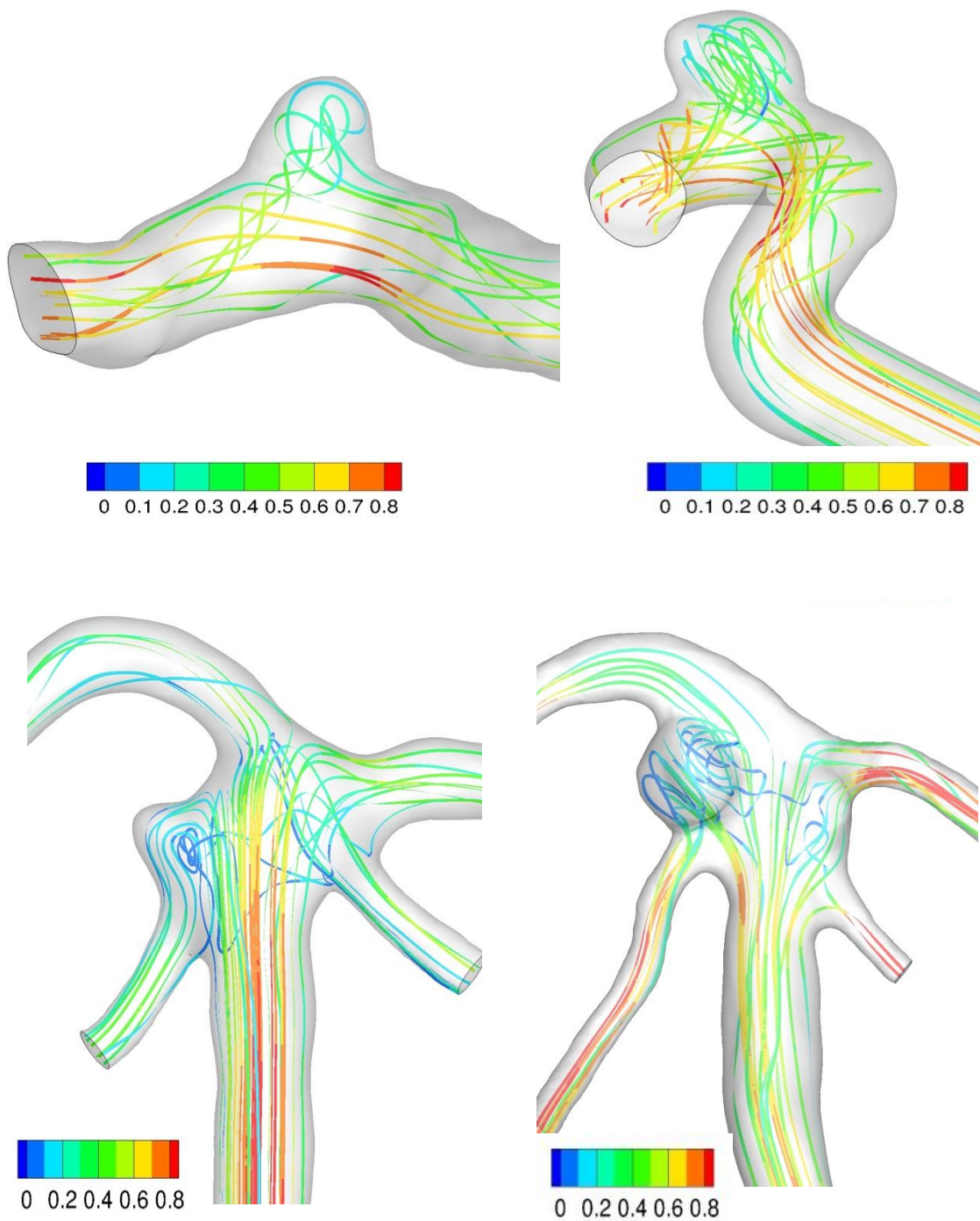aneurysms (left) and their stable controls (right)
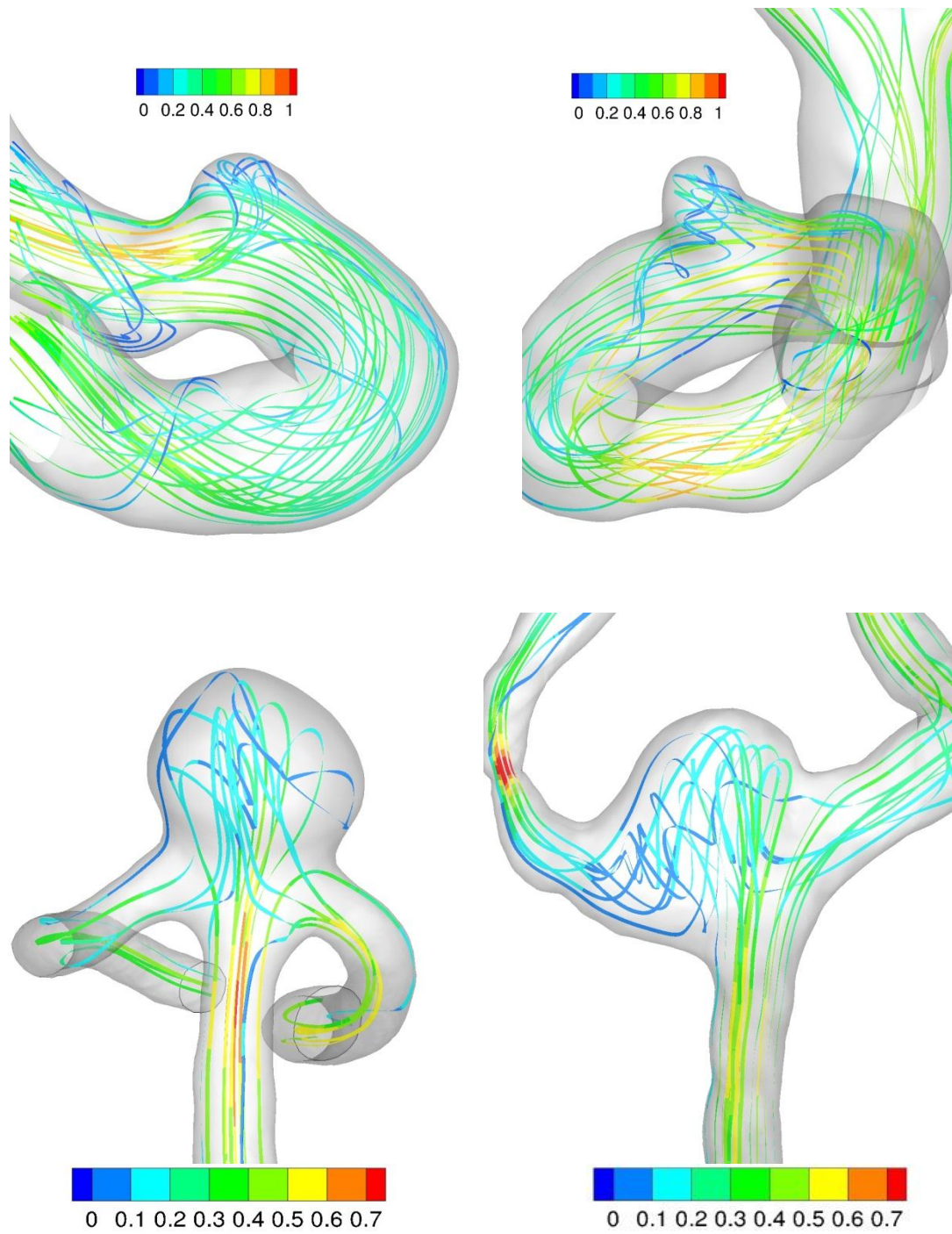
Figure 65: Streamtraces with velocity contours (m/s) in ICA and MCA aneurysms (left) and their stable controls (right)

Role of Modeling Choices

One of the objectives of this study was to assess the role of modeling choices, specifically boundary conditions, in the stratification of aneurysms based on hemodynamic indices. As a preliminary study, a subset of the total patient population was used. Although the results from the preliminary study clearly indicated similar stratification of the population based on hemodynamic indices computed from steady and pulsatile flow analysis, the sample size did not warrant confidence. Therefore, steady flow analyses were also performed for all the 198 study subjects along with their pulsatile flow analyses. Since, 5 of the steady flow simulations did not achieve convergence, the sample size of this study reduced to 193. Statistical metrics were used to compare the correlation between steady and pulsatile flow based indices. It was found that the indices calculated from steady flow analysis stratified aneurysms in the same order as their time-averaged pulsatile counterparts ($r > 0.95$ and $\rho > 0.95$). Slopes close to 1 indicate that even the time-averaged values of indices calculated from pulsatile flow analysis were identical to their steady flow counterparts. Perhaps use of a peak systolic or end diastolic time point for calculation of the pulsatile indices would alter the slope values, but the stratification order would remain same (Chapter 2). Only in the residence time computation, steady flow was found to overestimate the values as compared to pulsatile flow analysis ($k = 0.67$). However, it did so with significant consistency rendering a high r (0.97) and ρ (0.96).

Results obtained from this large sample size study reassert that if the only measured difference between patient specific simulations is in the geometry, a simpler and faster method of steady flow simulation can provide the same interpretation of the relative hemodynamic differences in the population as a pulsatile flow simulation does. Previously, Mantha et al. [66] identified common features of large scale flow patterns in 6 cerebral aneurysms using both steady and pulsatile flow simulations. Their results indicated that the basic flow pattern remains unchanged whether they use steady state or

pulsatile flow simulation. On similar lines, Geers et al.[46] also compared steady and transient simulations for 2 patient specific aneurysms and reported similarity in the hemodynamic environment obtained. Our results are consistent with those reported in the above studies.

<div align="center">Correlation between Morphometric and Hemodynamic

Indices</div>

Are the hemodynamic indices capturing unique characteristics of flow or are they merely proxies for the basic morphological characteristics? Answering this question can play an important role in prospective studies designed to test the hemodynamic-rupture correlation. Also, identifying the correlation between morphology and hemodynamics, if any, can help in evaluating factors responsible for aneurysm growth in a more direct way. Elimination of indices that provide redundant information can provide greater statistical power to studies testing the predictive capabilities of indices.

We tested the correlation between 25 hemodynamic indices that were a part of the longitudinal study and 4 aneurysm size indices (H, D_{max}, S and V) computed by Ramachandran et al. [17] for this population. Our results indicate that there exists no strong correlation between morphology and hemodynamics. Vortex length is the only hemodynamic index that showed a mild positive correlation to H and V. This correlation can be reasoned out as an aneurysm with a longer height will have more recirculation and hence more spiraling flow (Figure 66). Since VL captures the length of the centerline of this spiraling flow, it will also be greater. Ma et al.[65] determined the correlation between wall shear stress, pressure differential and particle residence time and aneurysm size indices. Results of this study are consistent with them.

Absence of any correlation between morphology and hemodynamics suggests that hemodynamic indices do provide unique information about the aneurysms. However, whether this information is clinically valuable or not is still not clear as the longitudinal

study provides no evidence that hemodynamic indices serve as prognostic indicators of rupture risk in intracranial aneurysms.
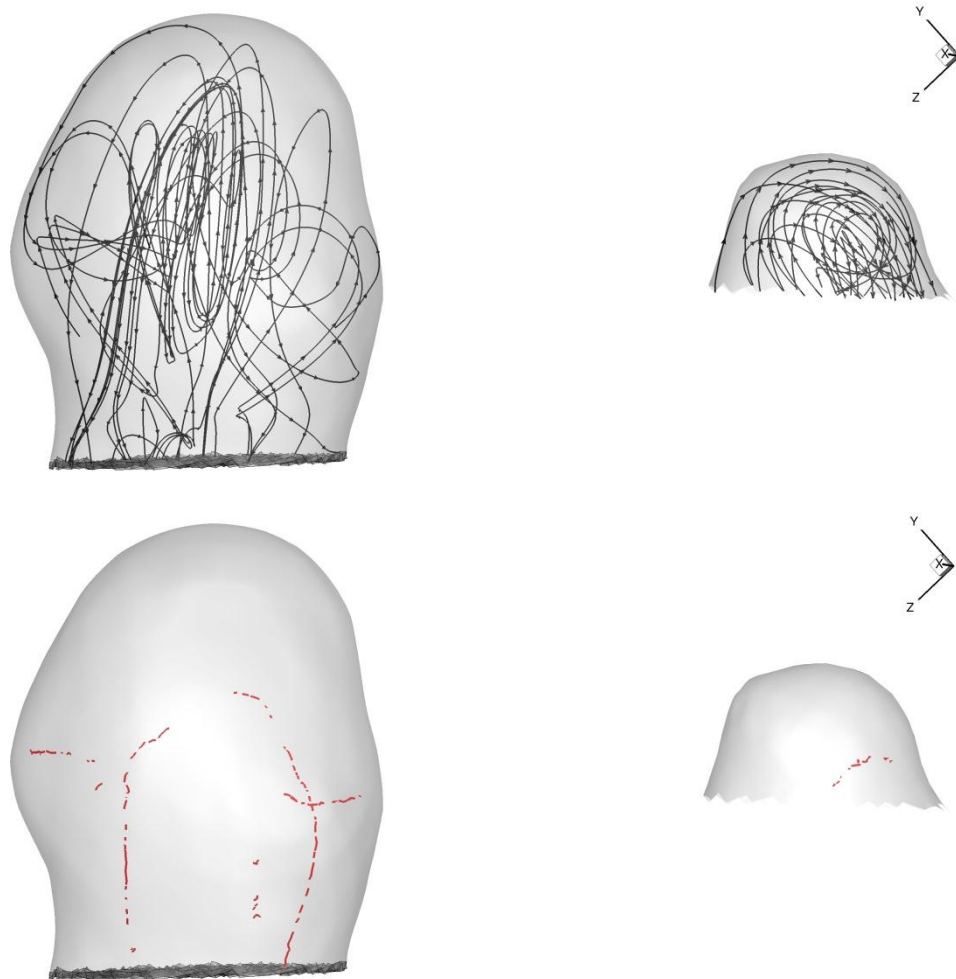
Figure 66: Streamlines and vortexcorelines for two aneurysms with different heights

Limitations

A few limitations of this work are presented below:

Study Population

The study population consists of aneurysms that are placed on a watchful waiting strategy by doctors. These are the aneurysms that are considered to be at lower rupture

risk by the doctors based on a gestalt assessment of the aneurysm morphology, asymptomatic behavior, patient history and treatment risk. Therefore, aneurysms in this population may be predisposed to have low growth or rupture risk.

CFD Analysis

In this study, population averaged boundary conditions were used to perform CFD simulations. Since in a large population study, it is difficult to obtain flow rates at a patient specific level, use of population averaged flow rate waveforms is a valid assumption. Over at the outlets, a constant pressure boundary condition was used. However, the total resistance offered by the distal vascular bed may be different for each outlet. Few other limitations of this that are common to CFD analyses are use of Newtonian fluid and rigid wall assumption. Although the value of hemodynamic indices may change due to these assumptions, the stratification of aneurysms would remain the same. Therefore, the scope of these limitations is reduced.

User Sensitivity

The data handling and segmentation of aneurysm images was performed by multiple users with different levels of experience. A protocol was developed to ensure consistency and reduce variability in the reconstruction of 3D models segmented by multiple users. However, a complete elimination of subjectivity was not possible. Also, the truncation lengths were different for some aneurysm models depending on the availability of vasculature. It could have resulted in hemodynamic differences in the aneurysm models. Set up of protocol to ensure availability of contiguous vasculature and truncation landmarks may help in minimizing differences in secondary flow effects.

Others

In this study, the aneurysms were isolated from their contiguous vasculature using cutting planes. However, this method is subjective and may introduce discrepancies in the

hemodynamic index calculations. Use of an automated isolation method may prove to be an efficient alternative. The study population may not be statistically powered as the choice of hemodynamic indices to be tested was made after patient recruitment.

Conclusion

Identifying factors responsible for aneurysm growth and its eventual rupture has been an area of considerable interest. Since the nature of blood flow pattern has been shown to affect aneurysm initiation, its role in aneurysm rupture is being widely studied. Previous studies have focused on analyzing differences between ruptured aneurysms and unruptured aneurysms. Although these studied provide valuable information about the disease, they do little in identifying those hemodynamic characteristics that are selectively found in aneurysms that go on to grow or rupture as compared to those that remain stable. The current study is the first that directly addresses the question: Can hemodynamics of an aneurysm when first presented be used to predict longitudinal growth risk? Results of this study are inconsistent with the hypothesis that hemodynamic indices of an unruptured aneurysm when it first presented are predictive of its longitudinal instability.

For future analysis, these hemodynamic indices could be estimated using a simpler method of steady flow analysis for an even larger population. A more stringent protocol should be laid out for image segmentation and CFD mesh generation process to reduce user-introduced inconsistencies. Automation in the isolation of aneurysms from the contiguous vasculature can limit the subjectivity involved in the use of cutting planes. Inclusion of patients that were chosen to be immediately treated by the clinicians in the study could provide additional valuable insights and eliminate selection bias to some extent.

REFERENCES

1.   Rinkel, G.J.E., M. Djibuti, A. Algra, and J. Van Gijn, *Prevalence and Risk of Rupture of Intracranial Aneurysms: A Systematic Review.* Stroke, 1998. **29**(1): p. 251-256.

2.   Ujiie, H., K. Sato, H. Onda, A. Oikawa, M. Kagawa, K. Takakura, and N. Kobayashi, *Clinical Analysis of Incidentally Discovered Unruptured Aneurysms.* Stroke, 1993. **24**(12): p. 1850-1856.

3.   Wiebers, D., *Unruptured Intracranial Aneurysms-Risk of Rupture and Risks of Surgical Intervention.* The New England Journal of Medicine, 1998. **339**(24): p. 1725-1733.

4.   Weir, B., *Unruptured Intracranial Aneurysms: A Review.* Journal of neurosurgery, 2002. **96**(1): p. 3-42.

5.   Wiebers, D.O., *Unruptured Intracranial Aneurysms: Natural History, Clinical Outcome, and Risks of Surgical and Endovascular Treatment.* The Lancet, 2003. **362**(9378): p. 103-110.

6.   Raaymakers, T.W.M., G.J.E. Rinkel, M. Limburg, and A. Algra, *Mortality and Morbidity of Surgery for Unruptured Intracranial Aneurysms: A Meta-Analysis.* Stroke, 1998. **29**(8): p. 1531-1538.

7.   Juvela, S., M. Porras, and K. Poussa, *Natural History of Unruptured Intracranial Aneurysms: Probability of and Risk Factors for Aneurysm Rupture.* Journal of neurosurgery, 2008. **108**(5): p. 1052-1060.

8.   Villablanca, J.P., R. Jahan, P. Hooshi, S. Lim, G. Duckwiler, A. Patel, J. Sayre, N. Martin, J. Frazee, and J. Bentson, *Detection and Characterization of Very Small Cerebral Aneurysms by Using 2d and 3d Helical Ct Angiography.* American journal of neuroradiology, 2002. **23**(7): p. 1187-1198.

9.   Ujiie, H., H. Tachibana, O. Hiramatsu, A.L. Hazel, T. Matsumoto, Y. Ogasawara, H. Nakajima, T. Hori, K. Takakura, and F. Kajiya, *Effects of Size and Shape (Aspect Ratio) on the Hemodynamics of Saccular Aneurysms: A Possible Index for Surgical Treatment of Intracranial Aneurysms.* Neurosurgery, 1999. **45**(1): p. 119.

10.   Dhar, S., M. Tremmel, J. Mocco, M. Kim, J. Yamamoto, A.H. Siddiqui, L.N. Hopkins, and H. Meng, *Morphology Parameters for Intracranial Aneurysm Rupture Risk Assessment.* Neurosurgery, 2008. **63**(2): p. 185.

11.   Beck, J., S. Rohde, M. El Beltagy, M. Zimmermann, J. Berkefeld, V. Seifert, and A. Raabe, *Difference in Configuration of Ruptured and Unruptured Intracranial Aneurysms Determined by Biplanar Digital Subtraction Angiography.* Acta neurochirurgica, 2003. **145**(10): p. 861-865.

12.   Raghavan, M.L., B. Ma, and R.E. Harbaugh, *Quantified Aneurysm Shape and Rupture Risk.* Journal of neurosurgery, 2005. **102**(2): p. 355-362.

13. Lauric, A. and M.I. Baharoglu, *Size Ratio Is a Poor Discriminant of Rupture Status Prone to Aneurysm-Type Distribution Bias.*

14. Lauric, A., M.I. Baharoglu, B.L. Gao, and A.M. Malek, *Incremental Contribution of Size Ratio as a Discriminant for Rupture Status in Cerebral Aneurysms: Comparison with Size, Height and Vessel Diameter.* Neurosurgery, 2011.

15. Xiang, J., S.K. Natarajan, M. Tremmel, D. Ma, J. Mocco, L.N. Hopkins, A.H. Siddiqui, E.I. Levy, and H. Meng, *Hemodynamic–Morphologic Discriminants for Intracranial Aneurysm Rupture.* Stroke, 2011. **42**(1): p. 144-152.

16. Ma, B., R.E. Harbaugh, and M.L. Raghavan, *Three-Dimensional Geometrical Characterization of Cerebral Aneurysms.* Annals of biomedical engineering, 2004. **32**(2): p. 264-273.

17. Ramachandran, M., *On the Role of Intracranial Aneurysm Morphology in Stable Versus Unstable Lesions.* 2012.

18. Steiger, H.J., R. Aaslid, S. Keller, and H.J. Reulen, *Strength, Elasticity and Viscoelastic Properties of Cerebral Aneurysms.* Heart and vessels, 1989. **5**(1): p. 41-46.

19. Toth, M., G. Nadasy, I. Nyary, T. Kerényi, M. Orosz, G. Molnárka, and E. Monos, *Sterically Inhomogenous Viscoelastic Behavior of Human Saccular Cerebral Aneurysms.* Journal of vascular research, 1998. **35**(5): p. 345-355.

20. Hademenos, G., T. Massoud, D. Valentino, G. Duckwiler, and F. Vinuela, *A Nonlinear Mathematical Model for the Development and Rupture of Intracranial Saccular Aneurysms.* Neurological research, 1994. **16**(5): p. 376.

21. Kyriacou, S. and J. Humphrey, *Influence of Size, Shape and Properties on the Mechanics of Axisymmetric Saccular Aneurysms.* Journal of biomechanics, 1996. **29**(8): p. 1015-1022.

22. Ma, B., J. Lu, R.E. Harbaugh, and M.L. Raghavan, *Nonlinear Anisotropic Stress Analysis of Anatomically Realistic Cerebral Aneurysms.* Journal of biomechanical engineering, 2007. **129**: p. 88.

23. Meng, H., Z. Wang, Y. Hoi, L. Gao, E. Metaxa, D.D. Swartz, and J. Kolega, *Complex Hemodynamics at the Apex of an Arterial Bifurcation Induces Vascular Remodeling Resembling Cerebral Aneurysm Initiation.* Stroke, 2007. **38**(6): p. 1924-1931.

24. Sforza, D.M., C.M. Putman, and J.R. Cebral, *Hemodynamics of Cerebral Aneurysms.* Annual review of fluid mechanics, 2009. **41**: p. 91.

25. Stehbens, W.E., *Etiology of Intracranial Berry Aneurysms.* Journal of neurosurgery, 1989. **70**(6): p. 823-831.

26. Malek, A.M., S.L. Alper, and S. Izumo, *Hemodynamic Shear Stress and Its Role in Atherosclerosis.* JAMA: the journal of the American Medical Association, 1999. **282**(21): p. 2035-2042.

27.   Shojima, M., M. Oshima, K. Takagi, R. Torii, M. Hayakawa, K. Katada, A. Morita, and T. Kirino, *Magnitude and Role of Wall Shear Stress on Cerebral Aneurysm Computational Fluid Dynamic Study of 20 Middle Cerebral Artery Aneurysms.* Stroke, 2004. **35**(11): p. 2500-2505.

28.   Cebral, J.R., M.A. Castro, J.E. Burgess, R.S. Pergolizzi, M.J. Sheridan, and C.M. Putman, *Characterization of Cerebral Aneurysms for Assessing Risk of Rupture by Using Patient-Specific Computational Hemodynamics Models.* American journal of neuroradiology, 2005. **26**(10): p. 2550-2559.

29.   Castro, M.A., C.M. Putman, M. Sheridan, and J. Cebral, *Hemodynamic Patterns of Anterior Communicating Artery Aneurysms: A Possible Association with Rupture.* American journal of neuroradiology, 2009. **30**(2): p. 297-302.

30.   Tremmel, M., S. Dhar, E.I. Levy, J. Mocco, and H. Meng, *Influence of Intracranial Aneurysm-to-Parent Vessel Size Ratio on Hemodynamics and Implication for Rupture: Results from a Virtual Experimental Study.* Neurosurgery, 2009. **64**(4): p. 622.

31.   Cebral, J.R., F. Mut, J. Weir, and C. Putman, *Quantitative Characterization of the Hemodynamic Environment in Ruptured and Unruptured Brain Aneurysms.* American journal of neuroradiology, 2011. **32**(1): p. 145-151.

32.   Jou, L.D., D. Lee, H. Morsi, and M. Mawad, *Wall Shear Stress on Ruptured and Unruptured Intracranial Aneurysms at the Internal Carotid Artery.* American journal of neuroradiology, 2008. **29**(9): p. 1761-1767.

33.   Qian, Y., T. Harada, K. Fukui, M. Umezu, H. Takao, and Y. Murayama, *Hemodynamic Analysis of Cerebral Aneurysm and Stenosed Carotid Bifurcation Using Computational Fluid Dynamics Technique.* Life System Modeling and Simulation, 2007: p. 292-299.

34.   Jou, L.D., G. Wong, B. Dispensa, M.T. Lawton, R.T. Higashida, W.L. Young, and D. Saloner, *Correlation between Lumenal Geometry Changes and Hemodynamics in Fusiform Intracranial Aneurysms.* American journal of neuroradiology, 2005. **26**(9): p. 2357-2363.

35.   Boussel, L., V. Rayz, C. McCulloch, A. Martin, G. Acevedo-Bolton, M. Lawton, R. Higashida, W.S. Smith, W.L. Young, and D. Saloner, *Aneurysm Growth Occurs at Region of Low Wall Shear Stress.* Stroke, 2008. **39**(11): p. 2997-3002.

36.   Raghavan, M.L., *Interactive Computer Model of Cerebral Vasculature*, in *Annual Meeting Biomedical Engineering Society*. 2009: Pittsburgh, PA.

37.   Ford, M.D., N. Alperin, S.H. Lee, D.W. Holdsworth, and D.A. Steinman, *Characterization of Volumetric Flow Rate Waveforms in the Normal Internal Carotid and Vertebral Arteries.* Physiological measurement, 2005. **26**: p. 477.

38.   Fahrig, R., H. Nikolov, A. Fox, and D. Holdsworth, *A Three-Dimensional Cerebrovascular Flow Phantom.* Medical physics, 1999. **26**: p. 1589.

39.   Catlett, C., *Teragrid: Analysis of Organization, System Architecture, and Middleware Enabling New Types of Applications.* HPC and Grids in Action Amsterdam, 2007(Advances in parallel computing series): p. 225-249.

40.   Mulder, G., A.C.B. Bogaerds, P. Rongen, and F.N. van de Vosse, *On Automated Analysis of Flow Patterns in Cerebral Aneurysms Based on Vortex Identification.* Journal of Engineering Mathematics, 2009. **64**(4): p. 391-401.

41.   Chong, M., A. Perry, and B. Cantwell, *A General Classification of Three-Dimensional Flow Fields.* Physics of Fluids, 1990. **2**: p. 408-420.

42.   Sujudi, D. and R. Haimes, *Identification of Swirling Flow in 3d Vector Fields*. 1995, Citeseer.

43.   Raschi, M., F. Mut, G. Byrne, C.M. Putman, S. Tateshima, F. Viñuela, T. Tanoue, K. Tanishita, and J.R. Cebral, *Cfd and Piv Analysis of Hemodynamics in a Growing Intracranial Aneurysm.* International Journal for Numerical Methods in Biomedical Engineering, 2012.

44.   Baharoglu, M.I., C.M. Schirmer, D.A. Hoit, B.L. Gao, and A.M. Malek, *Aneurysm Inflow-Angle as a Discriminant for Rupture in Sidewall Cerebral Aneurysms Morphometric and Computational Fluid Dynamic Analysis.* Stroke, 2010. **41**(7): p. 1423-1430.

45.   Ma, B., R. Harbaugh, J. Lu, and M. Raghavan. *Modeling the Geometry, Hemodynamics and Tissue Mechanics of Cerebral Aneurysms*. 2004: ASME.

46.   Geers, A., I. Larrabide, H. Morales, and A. Frangi. *Comparison of Steady-State and Transient Blood Flow Simulations of Intracranial Aneurysms*. 2010: IEEE.

47.   Speelman, L., E. Bosboom, G. Schurink, F. Hellenthal, J. Buth, M. Breeuwer, M. Jacobs, and F. van de Vosse, *Patient-Specific Aaa Wall Stress Analysis: 99-Percentile Versus Peak Stress.* European Journal of Vascular and Endovascular Surgery, 2008. **36**(6): p. 668-676.

48.   Cebral, J., F. Mut, M. Raschi, E. Scrivano, R. Ceratto, P. Lylyk, and C. Putman, *Aneurysm Rupture Following Treatment with Flow-Diverting Stents: Computational Hemodynamics Analysis of Treatment.* American journal of neuroradiology, 2011. **32**(1): p. 27-33.

49.   Fiorella, D., C. Sadasivan, H. Woo, and B. Lieber, *Regarding "Aneurysm Rupture Following Treatment with Flow-Diverting Stents: Computational Hemodynamics Analysis of Treatment".* American journal of neuroradiology, 2011. **32**(5): p. E95-E97.

50.   Jou, L.D., H. Morsi, H.M. Shaltoni, and M.E. Mawad, *Hemodynamics of Small Aneurysm Pairs at the Internal Carotid Artery.* Medical Engineering & Physics, 2012.

51.   Antiga, L., B. Ene-Iordache, and A. Remuzzi, *Computational Geometry for Patient-Specific Reconstruction and Meshing of Blood Vessels from Mr and Ct Angiography.* Medical Imaging, IEEE Transactions on, 2003. **22**(5): p. 674-684.

52.   Piccinelli, M., A. Veneziani, D.A. Steinman, A. Remuzzi, and L. Antiga, *A Framework for Geometric Analysis of Vascular Structures: Application to Cerebral Aneurysms.* Medical Imaging, IEEE Transactions on, 2009. **28**(8): p. 1141-1155.

53. Chandran, K.B., S.E. Rittgers, and A.P. Yoganathan, *Biofluid Mechanics: The Human Circulation*. 2007: CRC Press.

54. Gambit, G., *2.1 User Guide.* Fluent Inc.

55. Womersley, J., *Method for the Calculation of Velocity, Rate of Flow and Viscous Drag in Arteries When the Pressure Gradient Is Known.* The journal of physiology, 1955. **127**(3): p. 553-563.

56. Taylor, C.A., T.J.R. Hughes, and C.K. Zarins, *Finite Element Modeling of Blood Flow in Arteries.* Computer methods in applied mechanics and engineering, 1998. **158**(1): p. 155-196.

57. Torii, R., M. Oshima, T. Kobayashi, K. Takagi, and T.E. Tezduyar, *Fluid-Structure Interaction Modeling of Blood Flow and Cerebral Aneurysm: Significance of Artery and Aneurysm Shapes.* Computer methods in applied mechanics and engineering, 2009. **198**(45-46): p. 3613-3621.

58. Marzo, A., P. Singh, P. Reymond, N. Stergiopulos, U. Patel, and R. Hose, *Influence of Inlet Boundary Conditions on the Local Haemodynamics of Intracranial Aneurysms.* Computer Methods in Biomechanics and Biomedical Engineering, 2009. **12**(4): p. 431-444.

59. Fluent, F., *6.0 Udf Manual.* Fluent Inc., New Hampshire, 2001.

60. Oka, S. and M. Nakai, *Optimality Principle in Vascular Bifurcation.* Biorheology, 1987. **24**(6): p. 737.

61. Ferrandez, A., T. David, and M. Brown, *Numerical Models of Auto-Regulation and Blood Flow in the Cerebral Circulation.* Computer Methods in Biomechanics & Biomedical Engineering, 2002. **5**(1): p. 7-19.

62. Fluent, I., *Fluent 12.1. 4 Documentation.* User's guide, 2009.

63. Valencia, A., H. Morales, R. Rivera, E. Bravo, and M. Galvez, *Blood Flow Dynamics in Patient-Specific Cerebral Aneurysm Models: The Relationship between Wall Shear Stress and Aneurysm Area Index.* Medical Engineering & Physics, 2008. **30**(3): p. 329-340.

64. Takao, H., Y. Murayama, S. Otsuka, Y. Qian, A. Mohamed, S. Masuda, M. Yamamoto, and T. Abe, *Hemodynamic Differences between Unruptured and Ruptured Intracranial Aneurysms During Observation.* Stroke, 2012. **43**(5): p. 1436-1439.

65. Ma, B., *Modeling the Geometry, Hemodynamics and Tissue Mechanics of Cerebral Aneurysms*. 2005: THE UNIVERSITY OF IOWA.

66. Mantha, A.R., G. Benndorf, A. Hernandez, and R.W. Metcalfe, *Stability of Pulsatile Blood Flow at the Ostium of Cerebral Aneurysms.* Journal of biomechanics, 2009. **42**(8): p. 1081-1087.